

Friction Factor for Steady Periodically Developed Flow in Micro- and Mini-Channels with Arrays of Offset Strip Fins

A. Vangeffelen,^{1, 2, 3, a)} G. Buckinx,^{1, 2, 3} M. R. Vetrano,^{1, 3} and M. Baelmans^{1, 3}

¹⁾*Department of Mechanical Engineering, KU Leuven, Celestijnenlaan 300A, 3001 Leuven, Belgium*

²⁾*VITO, Boeretang 200, 2400 Mol, Belgium*

³⁾*EnergyVille, Thor Park, 3600 Genk, Belgium*

(Dated: 18 October 2021)

In this work, the friction factor for steady periodically developed flow through micro- and mini-channels with periodic arrays of offset strip fins is analyzed. The friction factor is studied numerically on a unit cell of the array for Reynolds numbers ranging from 1 to 600, and fin height-to-length ratios below 1. It is shown that the friction factor correlations from the literature, which primarily focus on larger conventional offset strip fin geometries in the transitional flow regime, do not predict the correct trends for laminar flow in micro- and mini-channels. Therefore, a new friction factor correlation for micro- and mini-channels with offset strip fin arrays is constructed from an extensive set of numerical simulations through a least-squares fitting procedure. The suitability of this new correlation is further supported by means of the Bayesian approach for parameter estimation and model validation. The correlation predicts an inversely linear relationship between the friction factor and the Reynolds number, in accordance with our observation that a strong inertia regime prevails over nearly the entire range of investigated Reynolds numbers. Yet, through a more detailed analysis, also the presence of a weak inertia regime and a transitional regime is identified, and the transitions from the strong inertia regime are quantified by means of two critical Reynolds numbers. Finally, the new correlation also incorporates the asymptotic trends that are observed for each geometrical parameter of the offset strip fin array, and whose origins are discussed from a physical perspective.

Key words: Offset Strip Fin, Friction Factor, Correlation, Periodically Developed Flow, Unit Cell, Strong Inertia Regime, Bayesian approach

^{a)}Electronic mail: arthur.vangeffelen@kuleuven.be.

I. INTRODUCTION

Over the last two decades, considerable research has been devoted to flow through micro- and mini-channels with a periodic array of solid fin structures (Refs. 1–4). Typically, micro-channels are defined as channels with the smallest dimension between $10\ \mu\text{m}$ and $200\ \mu\text{m}$, whereas for mini-channels, the smallest dimension ranges from $200\ \mu\text{m}$ to $3\ \text{mm}$ (Refs. 1). In particular, micro- and mini-channels with periodic arrays of offset strip fins have gained a lot of interest (Refs. 5–13). This is primarily due to the compactness this type of fin surface enables for heat transfer devices, which offers great potential in the ongoing trend towards higher power densities in many applications (Refs. 6 and 7). For example, micro-channels with a periodic array of offset strip fins have been applied for the cooling of microelectronic devices, such as high-performance processors and vertically stacked integrated circuit chips (Refs. 5–7, and 14). The reason is that they provide an effective means to cope with the increasing heat dissipation in these electronic devices as a result of their continuous miniaturization (Refs. 15). Additionally, mini-channels with offset strip fins are used in applications such as heat recuperators for compact gas turbines (Refs. 8 and 9), cryogenic heat exchangers for refrigeration and liquefaction (Refs. 10 and 11), and solar air heaters (Refs. 12 and 13). Here, the high thermal performance of offset strip fins allows for compact designs or small temperature differences between the two flows.

Due to the small dimensions, the flow inside micro- and mini-channels mostly remains in the laminar regime. It is characterized by a low to moderate Reynolds number, which typically lies between 10 and 500 (Refs. 5–14, 16, and 17). Inside arrays of offset strip fins, the flow exhibits a transition to vortex shedding in the wakes of the most downstream fins for Reynolds numbers between 350 and 750, depending on the geometrical parameters (Refs. 18–20). The onset point of this transition travels upstream in the channel as the Reynolds number is increased, until the oscillating flow breaks up and the flow becomes chaotic throughout the entire channel (Refs. 19 and 20). Similar observations have been made for plate channels with pin-fin arrays, in which the transition occurs at Reynolds numbers between 250 and 850 (Refs. 21 and 22). The flow regime inside micro- and mini-channels with offset strip fin arrays is therefore often steady.

In the past, the flow through periodic arrays of offset strip fins has been studied both experimentally and numerically (Refs. 18, 23–25). However, previous work mainly focuses on conventional channels with dimensions in the centimeter range, used for example in automotive radiators and

air coolers. As a consequence, most of the data in the literature only applies to the transitional and turbulent flow regime, but not to the steady flow regime at low to moderate Reynolds numbers, as encountered in micro- and mini-channels. Moreover, the available data mainly applies to offset strip fins with larger fin height-to-length ratios than those common in micro- and mini-channel applications (Refs. 5–14). Therefore, this work aims to study the pressure drop for flow through offset strip fin arrays in micro- and mini-channels.

The data from the literature consists to a large extent of pressure drop measurements over the array for different flow rates through the channel. These pressure drop measurements, often corrected for in- and outlet contractions, are frequently represented in the form of a friction factor, for which empirical correlations have been proposed. Tables I and II give a chronological overview of the different friction factor correlations for offset strip fins reported in the literature. In the literature, the friction factor has been defined as the average Fanning friction factor $f \triangleq \frac{\Delta P D_h}{2L \rho_f U_{\text{ref}}^2}$, which is based on the pressure drop ΔP measured over the flow length L . The overview further includes the adopted definition of the hydraulic diameter D_h and the range of Reynolds numbers $Re_{D_h} \triangleq \rho_f U_{\text{ref}} D_h / \mu_f$ based on this hydraulic diameter, as well as the ratio of fin height to fin length h/l considered in each study. The reference velocity U_{ref} equals the average bulk velocity based on the minimal cross-section area sh for all included correlations, with the exception of the correlation of Joshi and Webb, for which it is based on the surface area $(s-t)h$. Figure 1 displays the geometrical parameters of an array of offset strip fins with their conventional symbols: the fin thickness t , the fin height h , the lateral fin pitch s , and the fin length l . Typically, the lateral offset σ between successive fin rows is taken to be half of the lateral fin pitch: $\sigma = (s+t)/2$ (Refs. 18, 23–29). Figure 1 further presents a real example of an offset strip fin mini-channel which has been produced in-house by the laser powder bed fusion manufacturing technique (Refs. 30). Next, a short discussion on the studies from Tables I and II is given.

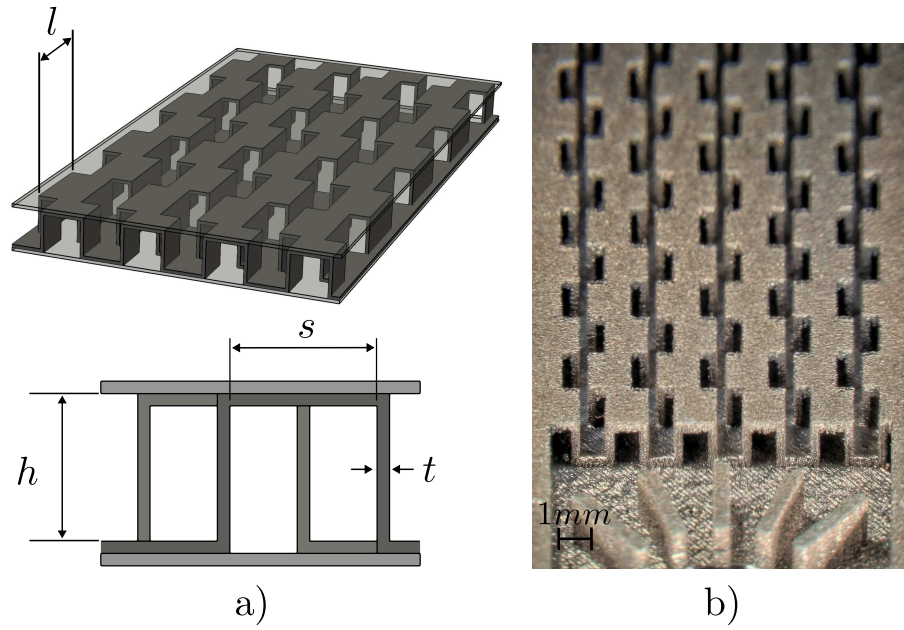


FIG. 1. Geometrical parameters of a periodic array of offset strip fins (a), example of a mini-channel with an array of periodic offset strip fins, fabricated in-house by the additive manufacturing technique of laser powder bed fusion (b)

TABLE I. Chronological list of flow correlation studies for offset strip fin channels

Researchers	Correlation	Re_{D_h}	h/l
Manson (1950)	For $Re_{D_h} \leq 3500$ $f = \begin{cases} 11.8(l/D_h)^{-1} Re_{D_h}^{-0.67} & \text{for } l/D_h \leq 3.5 \\ 11.8(3.5)^{-1} Re_{D_h}^{-0.67} & \text{for } l/D_h > 3.5 \end{cases}$	370-9020	4.8-7.9
	For $Re_{D_h} > 3500$ $f = \begin{cases} 0.38(l/D_h)^{-1} Re_{D_h}^{-0.24} & \text{for } l/D_h \leq 3.5 \\ 0.38(3.5)^{-1} Re_{D_h}^{-0.24} & \text{for } l/D_h > 3.5 \end{cases}$ where $D_h = 2sh/(s+h)$		
Wieting (1975)	For $Re_{D_h} \leq 1000$ $f = 7.661(l/D_h)^{-0.384} (s/h)^{-0.092} Re_{D_h}^{-0.712}$	120-50000	0.23-5.1
	For $Re_{D_h} > 2000$ $f = 1.136(l/D_h)^{-0.781} (t/D_h)^{0.534} Re_{D_h}^{-0.198}$ where $D_h = 2sh/(s+h)$		
Joshi & Webb (1987)	For $Re_{D_h} < Re^*$ $f = 8.12(l/D_h)^{-0.41} (s/h)^{-0.02} Re_{D_h}^{-0.74}$	120-50000	0.23-5.1
	For $Re_{D_h} > Re^* + 1000$ $f = 1.12(l/D_h)^{-0.65} (t/D_h)^{0.17} Re_{D_h}^{-0.36}$ where $Re^* = 257(l/s)^{1.23} (t/l)^{0.58} D_h$ $\times \left[t + 1.328 (Re_{D_h}/(lD_h))^{-0.5} \right]^{-1}$ $D_h = 2(s-t)h/((s+h) + ht/l)$		
Manglik & Bergles (1995)	$f = 9.6243(s/h)^{-0.1856} (t/l)^{0.3053} (t/s)^{-0.2659} Re_{D_h}^{-0.7422}$ $\times \left[1 + 7.669 \cdot 10^{-8} (s/h)^{0.920} (t/l)^{3.767} (t/s)^{0.236} Re_{D_h}^{4.429} \right]^{0.1}$ where $D_h = 4shl/(2(sl + hl + th) + ts)$	120-10000	0.23-5.1

TABLE II. Chronological list of flow correlation studies for offset strip fin channels (continued)

Researchers	Correlation	Re_{D_h}	h/l
	$f = 2.092(s/h)^{-0.739} (t/l)^{-0.78} (t/s)^{0.972} Re_{D_h}^{-0.281} (L/l)^{-0.497}$		
Dong, Chen et al. (2007)	where L the flow length $D_h = 2sh/(s+h)$	500-7500	0.91-2.3
	$f = 0.9415(2(s+t)/D_h)^{-1.052\alpha+6.161} (h/D_h)^{1.0540\alpha+2.057} \times (l/D_h)^{0.3388\alpha+0.4825} Re_{D_h}^{-0.06420} F$		
Guo, Qin et al. (2008)	where $F = 0.05166 - 0.4983/\alpha + 1.342/\alpha^2 - 1.002/\alpha^3 + 0.1254/Re_{D_h}^{0.5166}$ α is the flow angle of attack $D_h = 4V_{free}/A_{surface}$ V_{free} is the free flow volume $A_{surface}$ is the wetted surface area	20-400	1.9-2.9
	For $b < 0.2$ $f = \exp(7.91)(s/h)^{-0.159} (t/l)^{0.358} (t/s)^{-0.033} Re_{D_h}^{0.126\ln(Re_{D_h})-2.3}$		
	For $0.2 \leq b < 0.25$ $f = \exp(9.36)(s/h)^{-0.0025} (t/l)^{-0.0373} (t/s)^{1.85} Re_{D_h}^{0.142\ln(Re_{D_h})-2.39}$		
Kim, Lee et al. (2011)	For $0.25 \leq b < 0.3$ $f = \exp(5.58)(s/h)^{-0.36} (t/l)^{0.552} (t/s)^{-0.521} Re_{D_h}^{0.111\ln(Re_{D_h})-1.87}$	100-6000	0.046-10
	For $0.3 \leq b < 0.35$ $f = \exp(4.84)(s/h)^{-0.48} (t/l)^{0.347} (t/s)^{0.511} Re_{D_h}^{0.089\ln(Re_{D_h})-1.49}$		
	where $b = ((2s+2t)(h+t) - 2sh)/((2s+2t)(h+t))$ $D_h = 4shl/(2(sl+hl+th) + ts)$		

The first friction factor correlation was constructed by Manson (Refs. 27). It was based on experimental pressure drop measurements for nine different types of heat transfer surfaces, all consisting of periodic fin arrays, of which only three were offset strip fin geometries (Refs. 27). As it can be seen from the range of Reynolds numbers and fin height-to-length ratios in Table I, the experimental data in Manson's study is limited to flow regimes beyond the transition towards vortex shedding and to larger conventional fin geometries.

Following Manson's work, numerous other correlations have been constructed, for which the experimental pressure drop measurements of Kays and London served as the main source of data (Refs. 26). However, the database of Kays and London has limited applicability to micro- and mini-channels with offset strip fins, since only 13 of the 21 geometries in the database comply with $h/l \leq 1$. Moreover, less than 20% of the measurement points in the database relates to the steady laminar flow regime.

First, Wieting (Refs. 28) proposed a friction factor correlation for offset strip fins using the database of Kays and London, albeit without giving a consistent definition of the hydraulic diameter (Refs. 23). A second correlation based on the data of Kays and London was constructed by Joshi and Webb (Refs. 18), who also included data for two geometries of Walters (Refs. 31), another geometry of London and Shah (Refs. 32), as well as eight of their own geometries. Of these eight additional geometries, only one has a fin height-to-length ratio smaller than one. In total, less than 20% of Joshi and Webb's data points correspond to steady laminar flow conditions with $h/l \leq 1$. It must be remarked that Joshi and Webb also worked out a semi-analytical expression for the Reynolds number Re^* at which transition from a laminar to a turbulent flow regime occurs (see Table II).

A refit of the combined friction factor data of Kays and London, Walters, and London and Shah (Refs. 26, 31, and 32) was performed by Manglik and Bergles (Refs. 23). Manglik and Bergles' refitted correlation is perhaps the most widely used correlation for offset strip fins in conventional channels. One reason is that it is accurate to within a relative error of 20% with respect to the data considered in their work. Secondly, it also covers a wide range of Reynolds numbers with a single formula, without any partitioning around the transition point towards the turbulent flow regime. Considering that the underlying data comes from the previous studies, the refit of Manglik and Bergles has again limited applicability to micro- and mini-channels with offset strip fins.

For offset strip fin arrays in channels of a rather short length, the pressure drop over the entrance region has been included in the friction factor correlation of Dong, Chen et al. (Refs. 24) through

the ratio of the flow length L and the fin length l , as shown in Table II. To this end, pressure drop measurements were experimentally conducted for 16 different offset strip fin arrays containing 5 to 14 fins in the flow direction. Yet, since the experimental data was gathered for the transitional flow regime in fins with a relatively large height, as it can be seen in Table II, the validity of the latter study for the micro- and mini-channels considered in this work is still a question.

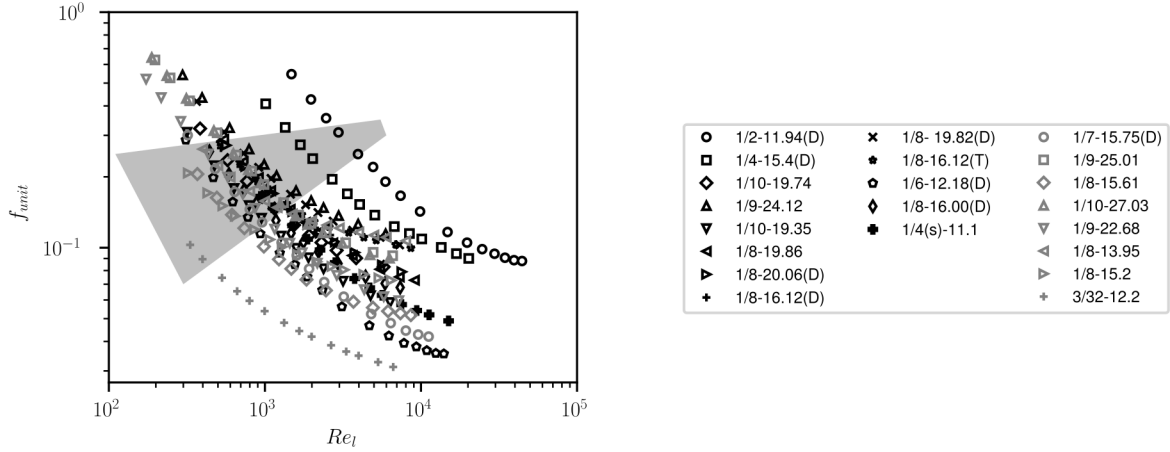
In contrast to the previous studies, a significant number of data points for the laminar flow regime have been incorporated in the friction factor correlation of Guo, Qin et al. (Refs. 29). The experimental study of Guo, Qin et al. introduced offset strip fin arrays having an inclined direction with respect to the flow, and was aimed at evaluating their performance for a novel design of, for instance, oil coolers (Refs. 33 and 34). To this end, the authors investigated the dependence of the pressure drop on the direction of the flow, i.e. the angle of attack, with respect to the fin orientation. Therefore, their data was gathered from experiments for 16 combinations of offset strip fin geometries and flow angles ranging from 0° to 90° . Unfortunately, in their work, neither an explicit definition of the hydraulic diameter nor a value of the fin thickness are given, so that the interpretation of their friction factor correlation remains ambiguous. Furthermore, only larger fin height-to-length ratios ($h/l > 1$) than common for micro- and mini-channels were included in their data set, as it is clear from Table II.

Finally, the only numerical study on the friction factor for arrays of offset strip fins has been conducted by Kim, Lee et al. (Refs. 25). In this study, the friction factor was computed from flow simulations on a three-dimensional domain consisting of an entire fin row spanning 68 fin lengths in the streamwise direction, under the assumption of lateral flow periodicity. However, as the numerical data from this study has not been published, it is unclear how many friction factor data points were included to cover the laminar flow regime. Furthermore, it seems that this study was rather focused on the turbulent flow regime, since the flow simulations were performed using the shear stress transport (SST) $k-\omega$ turbulence model to solve the flow equations for an incompressible Newtonian fluid. The empirical correlation constructed by Kim, Lee et al. is based on the numerical data for 39 different geometries, of which 30 have a fin height-to-length ratio h/l smaller than one. In particular, the correlation covers a large range of values for the so-called blockage ratio b , which is defined in Table II as the cross-section area blocked by the fins over the total cross-section area in the channel.

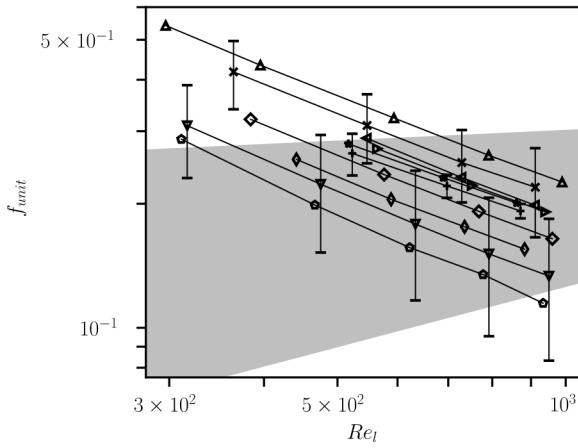
From the preceding literature review, we conclude that up to the present, the friction factor for the steady laminar flow regime in offset strip fin arrays as encountered in micro- and mini-channels is not well studied. After all, in total less than 50 pressure drop measurement points are available for the laminar regime in the entire literature. To support this conclusion graphically, almost all the experimental friction factor measurements in the literature, coming from the database of Kays and London (Refs. 26), are displayed in Figure 2(a). In this figure, the scarce measurement points for the laminar regime are located above the grey zone, which indicates the region of transitional flow. This region extends more or less over the Reynolds numbers Re_{D_h} between 350 and 750 (Refs. 18–20). The limited measurement points for geometries with a small ratio of fin height to fin length ($h/l < 1$) are indicated by the black markers, while those with $h/l > 1$ are indicated by the grey markers. In Figures 2(b) and 2(c) also the discrepancies between the data from Kays and London and the most commonly used correlations from the literature are shown by means of an error bar, at least over the Reynolds number range relevant for micro- and mini-channels (Refs. 26). These discrepancies are on an average as large as 20%, but become as large as 80% for a Reynolds number Re_l around 300.

Therefore, in this work, the friction factor for the steady laminar flow regime inside offset strip fin arrays is re-investigated numerically and correlated with respect to the geometrical fin parameters for micro- and mini-channel applications ($h/l < 1$). In these applications, the flow is expected to become periodically developed after a short distance from the inlet (Refs. 35). For that reason, the aim of this work is to quantify the friction factor for offset strip fins in the periodically developed flow regime. Since periodically developed flow can be simulated on a single unit cell of the fin array (Refs. 36), less computational resources are required than one would need for an analysis based on direct numerical simulation (DNS) of the entire flow in the channel.

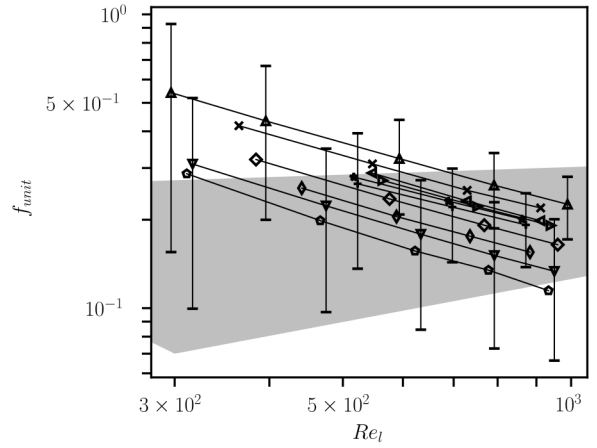
The remainder of this work is organized as follows. First, in Section II, the unit cell geometry, the periodically developed flow equations and the numerical procedure are discussed. In Section III, the friction factor is analyzed in the periodically developed regime for a large set of geometrical parameters and Reynolds numbers ranging from 1 to 600. Based on the dependence of the friction factor on the Reynolds number, three different flow regimes are identified in Section III E: the weak inertial flow regime, the strong inertial flow regime and the transitional flow regime. To mark the transition between these regimes, two critical Reynolds numbers are determined. A final friction factor correlation for periodically developed flow through offset strip fin arrays in micro- and mini-channels is presented in Section IV. Also its accuracy is evaluated with respect to our



a)



b)



c)

FIG. 2. Experimental friction factor data from Kays and London (Refs. 26) (a), discrepancies between the data of Kays and London and the friction factor correlation of Manglik and Bergles (Refs. 23) (b), discrepancies between the data of Kays and London and the friction factor correlation of Kim, Lee et al. (Refs. 25) (c); The black markers correspond to the geometries with $h/l < 1$, and the grey markers to those with $h/l > 1$. The grey zone indicates the region of transitional flow.

own data, as well as the experimental data from the literature.

II. UNIT CELL GEOMETRY AND PERIODICALLY DEVELOPED FLOW EQUATIONS

A. Geometry

The three-dimensional unit cell for the computation of the periodically developed flow through an offset strip fin array is depicted in Figure 3. The unit cell domain $\Omega_{unit} \subset \mathbb{R}^3$ exists of a fluid subdomain Ω_f , a solid subdomain Ω_s and their fluid-solid interface Γ_{fs} . The top plane Γ_t and bottom plane Γ_b , which are both part of the exterior boundary of the unit cell domain $\Gamma = \partial\Omega_{unit}$, correspond to the solid walls at the top and bottom of the channel. With respect to the normalized Cartesian vector basis $\{\mathbf{e}_j\}_{j=1,2,3}$, the unit cell domain is spanned by three lattice vectors: $\mathbf{l}_1 = l_1\mathbf{e}_1 = 2l\mathbf{e}_1$, $\mathbf{l}_2 = l_2\mathbf{e}_2 = 2(s+t)\mathbf{e}_2$ and $\mathbf{l}_3 = l_3\mathbf{e}_3 = (h+t)\mathbf{e}_3$.

Using the fin length l as the reference length, the following independent non-dimensional groups are selected to uniquely define the unit cell geometry: h/l , s/l and t/l . These non-dimensional parameters determine the unit cell's porosity as follows:

$$\varepsilon = \frac{(h/l)(s/l)}{[(h/l) + (t/l)][(s/l) + (t/l)]}. \quad (1)$$

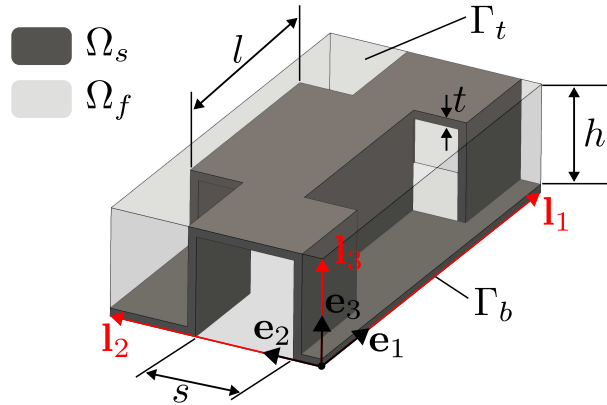


FIG. 3. Unit cell domain in an offset strip fin array

B. Periodically developed flow equations

For laminar periodically developed flow, the pressure field is composed of a component varying linearly with a constant gradient ∇P and a spatially periodic component p^* , which drive the

periodic velocity field \mathbf{u} (Refs. 36 and 37). Assuming constant material properties, the periodically developed flow field \mathbf{u} is the steady solution governed by the following time-dependent Navier-Stokes equations:

$$\begin{aligned} \nabla \cdot \mathbf{u} &= 0 && \text{in } \Omega_f, \\ \rho_f \frac{\partial \mathbf{u}}{\partial t} + \rho_f \nabla \cdot (\mathbf{u}\mathbf{u}) &= -\nabla p^* - \nabla P + \mu_f \nabla^2 \mathbf{u} && \text{in } \Omega_f, \end{aligned} \quad (2)$$

where

$$\begin{aligned} \mathbf{u}(\mathbf{x} + \mathbf{l}_j, t) &= \mathbf{u}(\mathbf{x}, t) && \text{in } \Omega_f, \\ p^*(\mathbf{x} + \mathbf{l}_j, t) &= p^*(\mathbf{x}, t) && \text{in } \Omega_f, \\ \mathbf{u}(\mathbf{x}, t) &= 0 && \text{in } \Gamma_{fs} \cup \Gamma_t \cup \Gamma_b, \\ \mathbf{u}(\mathbf{x}, 0) &= 0 && \text{in } \Omega_f, \\ p(\mathbf{x}, 0) &= 0 && \text{in } \Omega_f, \end{aligned} \quad (3)$$

for $j = \{1, 2\}$. Here, the no-slip condition is imposed at the fluid-solid interface Γ_{fs} , as well as at the top and bottom boundary Γ_t and Γ_b , respectively. The flow further exhibits periodicity with respect to the lattice vectors \mathbf{e}_1 and \mathbf{e}_2 . Given the periodically developed flow equations (2)-(3), a developed pressure gradient ∇P can be obtained for an imposed volume-averaged velocity vector $\langle \mathbf{u} \rangle$, which is defined as

$$\langle \mathbf{u} \rangle \triangleq \frac{1}{V_{unit}} \int_{\mathbf{r} \in \Omega_{unit}(\mathbf{x})} \mathbf{u}(\mathbf{r}, t) d\Omega(\mathbf{r}), \quad (4)$$

$$V_{unit} = \mathbf{l}_1 \cdot (\mathbf{l}_2 \times \mathbf{l}_3). \quad (5)$$

This relationship between ∇P and $\langle \mathbf{u} \rangle$ will be represented in non-dimensional form as a correlation between the friction factor, defined as

$$f_{unit} \triangleq \frac{\|\nabla P\| l}{2\rho_f \|\langle \mathbf{u} \rangle\|^2}, \quad (6)$$

and the Reynolds number, defined as

$$Re_l \triangleq \frac{\rho_f \|\langle \mathbf{u} \rangle\| l}{\mu_f}, \quad (7)$$

with $\|\cdot\|$ denoting the Euclidean vector norm. Note that the fin length l has been selected as the reference length for both the friction factor and Reynolds number, as opposed to the commonly used hydraulic diameter D_h . This choice of reference length is motivated by the fact that $\|\nabla P\| l$ corresponds to the constant pressure drop over each fin unit in the main flow direction, and the

argument that a Reynolds number based on the same, single reference length is easier to interpret than a Reynolds number based on two geometrical parameters like s and h . Besides, the actual hydraulic diameter for a channel containing a fin array is not a constant in the strict sense, since the cross-sectional area for the flow varies along the main flow direction.

When the periodically developed flow regime prevails over the largest part of the channel, the friction factor in equation 6 will be a good approximation for the total pressure drop over the entire channel. Furthermore, when the influence of the channel's side-wall on the flow can be neglected, $\|\langle \mathbf{u} \rangle\|$ will equal the bulk-average velocity through the channel, and hence directly determine the mass flow rate through the channel.

C. Numerical procedure

For solving the flow equations (2)-(3), the software package FEniCSLab has been employed, which was developed by G. Buckinx within the finite-element framework FEniCS (Refs. 38). The package FEniCSLab contains an object-oriented re-implementation of the parallel fractional-step solver of *Oasis* developed by Mortensen and Valen-Sendstad (Refs. 39) for the unsteady incompressible Navier-Stokes equations but has been modified to allow for variable time stepping and to solve for an imposed value of $\langle \mathbf{u} \rangle$.

A structured mesh has been used for the spatial discretization of the unit cell domain, with a number of grid cells equal to 48 along \mathbf{e}_1 , 26 to 108 along \mathbf{e}_2 , and 13 to 104 along \mathbf{e}_3 . This resulted in a total number of mesh cells between 127,088 and 4,066,816, depending on the geometrical parameters of the unit cell domain. The discretized velocity and pressure fields have been represented by continuous Galerkin tetrahedral elements of the second and first order, respectively. For the temporal discretization, a central difference scheme has been employed, while an implicit Crank-Nicolson scheme of the second order is used for the viscous term. A combination of an explicit Adam-Bashforth scheme and an implicit Crank-Nicolson scheme, both of the second order, has been selected for the discretization of the advective term, analogous to the flow solver of *Oasis* (Refs. 39).

The numerical discretization scheme has been validated through a mesh-independence study at the two largest Reynolds numbers, for the four lowest values of the unit cell's porosity. Stability for the time-stepping scheme was ensured by limiting the local Courant–Friedrichs–Lewy number in each mesh cell to a value below 0.9. As time-convergence criterion, the requirement that the

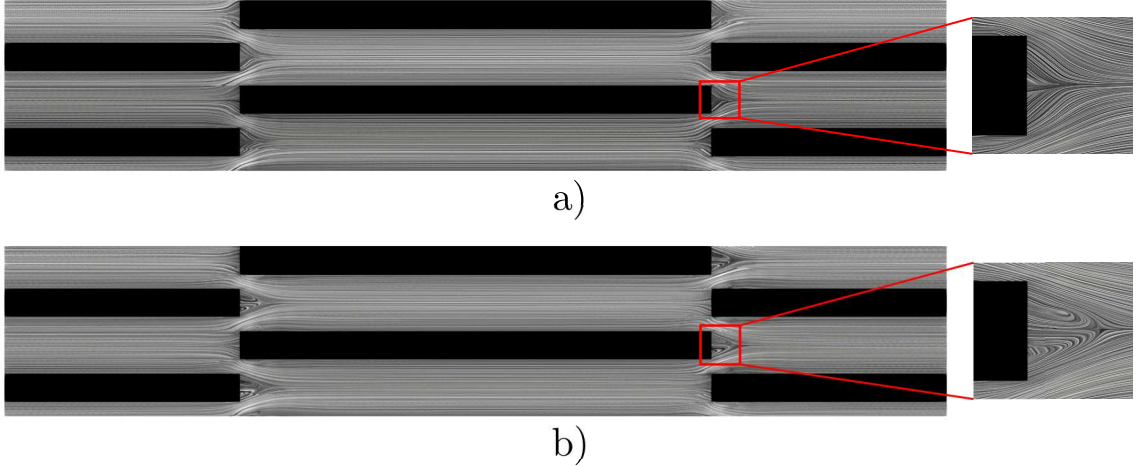


FIG. 4. Example of flow pattern visualization by Line Integral Convolution (LIC) in a cross-section mid-plane spanned by \mathbf{e}_1 and \mathbf{e}_2 for $Re_l = 100$ (a) and $Re_l = 400$ (b) when $t/l = 0.06$, $h/l = 0.48$, $s/l = 0.12$

L^2 -norm of each of the dimensionless velocity components $u_i/\|\langle \mathbf{u} \rangle\|$ is smaller than 10^{-6} was chosen, next to the requirement that the relative change in friction factor is smaller than 10^{-6} . By means of the Richardson extrapolation method and the grid convergence index (Refs. 40 and 41), this mesh-refinement study has indicated that the relative discretization error on the computed friction factor does not exceed 1%.

As an example of the flow field inside a unit cell, the detailed flow patterns observed in the mid-plane of the unit cell spanned by \mathbf{e}_1 and \mathbf{e}_2 at a Reynolds number of 100 and 400 are shown in Figure 4. The growth of a wake with symmetrical recirculation zones at the fin's trailing edge can be seen for an increasing Reynolds number Re_l .

III. FRICTION FACTOR FOR PERIODICALLY DEVELOPED FLOW

In order to investigate the relationship between f_{unit} and Re_l , we consider the case where the volume-averaged velocity vector is parallel to the offset strip fins and thus aligned with the unit vector \mathbf{e}_1 . In that case, also the pressure gradient ∇P and \mathbf{e}_1 are aligned. For our study, we have selected the values of the geometrical parameters and the Reynolds number in accordance with the applications of offset strip fin arrays in micro- and mini-channels (Refs. 5–13), as enlisted in Table III. These values of the geometrical parameters result in a porosity ε ranging from 0.44 to 0.97. The resulting total of 2765 data points for the friction factor f_{unit} , obtained by solving the

periodically developed flow equations for 275 different geometries, are tabulated in Appendix A. In the following subsections, the influence of the Reynolds number on the friction factor, as well as that of each geometrical parameter, are discussed.

TABLE III. Adopted values for the Reynolds number and the geometrical parameters for our study of the friction factor for periodically developed flow.

Re_l	1, 10, 15, 25, 35, 50, 75, 100, 150, 200, 300, 400, 600
h/l	0.12, 0.16, 0.20, 0.24, 0.28, 0.32, 0.40, 0.48, 0.56, 0.68, 1.00
s/l	0.12, 0.16, 0.20, 0.24, 0.28, 0.32, 0.40, 0.48
t/l	0.01, 0.02, 0.04, 0.06

A. The influence of the Reynolds number Re_l on the friction factor

Figure 5 shows the dependence of the friction factor on the Reynolds number for various combinations of geometrical parameters. It can be observed that this dependence is well captured by an inversely linear relationship of the form

$$f_{unit} \simeq ARe_l^{-1} + B, \quad (8)$$

where the parameters A and B are only a function of the unit cell geometry. The exponent of the Reynolds number has been confirmed to effectively equal -1 with a standard deviation of 0.02 by means of a log-linear regression analysis of all the friction factor data from this work. For each unit cell geometry from table III, it was found that the correlation form (8) captures the variation of the friction factor with the Reynolds number within an average and maximum relative error of 0.8% and 8%, respectively.

In the correlation form (8), the term ARe_l^{-1} may be interpreted as originating from Darcy's law, which predicts a linear relationship between the pressure gradient and the volume-averaged velocity: $\|\nabla P\| \sim \mu_f A \|\langle \mathbf{u} \rangle\|$. On the other hand, the constant B in (8) may be regarded as originating from Forchheimer's correction $\rho_f B \|\langle \mathbf{u} \rangle\|^2$ to Darcy's law, which is quadratic in the volume-averaged velocity (Refs. 42–46). According to this interpretation, the correlation form (8) reflects that periodically developed flow through an array of offset strip fins exhibits a regime of strong

inertia, which is similar to the one encountered in steady laminar flows through porous media at low to moderate Reynolds numbers (Refs. 47 and 48). In this regime of strong inertia within offset strip fins, the relationship between the pressure gradient and the volume-averaged velocity deviates only slightly from the linear relationship predicted by Darcy’s law since the Forchheimer correction term remains relatively small, as illustrated in Figure 5. Our observation that the Forchheimer coefficient B has a limited contribution to the friction factor over the entire range of Reynolds numbers investigated here, is in agreement with the pressure drop measurements reported for other micro- and mini-channels applications (Refs. 5–14).

Although the assumption in (8) that the Forchheimer correction term scales quadratically with the volume-averaged velocity, leads to accurate friction factor correlations for our data (see Section IV), and is supported by similar findings for flows through porous media and micro- and mini-channels, a more detailed analysis actually reveals a more complex dependence on the volume-averaged velocity. This more detailed analysis is discussed in Section III E. Here, we first compare the accuracy of the correlation form (8) for our data with respect to the correlations proposed in the literature.

In Figure 6, the friction factor correlations from the literature (see Tables I and II) are compared with the friction factor data from this work for a single geometry. Despite the fact that only a single geometry has been selected for comparison, this figure is also representative of the accuracy with which the correlations from the literature capture our data for other geometries. We clarify that the correlations from the literature, which are based on f and Re , have been converted to our definitions of f_{unit} and Re_l , using the definitions for f and Re specified in Section I.

As shown in Figure 6, the friction factor correlations of Wieting, Joshi and Webb, and Manglik and Bergles (Refs. 18, 23, and 28) display a dependence on the Reynolds number of the form $f \sim Re^{-0.7}$, in contrast to the inversely linear relationship (8) that we observed. Likely, the reason for this different exponent is that the largest part of the friction factor data used by the former authors covers the transitional and turbulent regime. It is known that towards the turbulent regime, the friction losses scale with $\|\langle \mathbf{u} \rangle\|^e$ with $e > 1$, so that $f \sim Re^k$ with $k > -1$ (Refs. 43). As a result, the friction factor correlations of the former authors underestimate our friction factor data in the laminar regime with an average relative error of 20% and a maximum relative error of 80% for a Reynolds number near 1. An even larger underestimation of our data is apparent with respect to the study of Dong, Chen et al. (Refs. 24), who observed that $f \sim Re^{-0.281}$. This can be explained by the fact that the validity range of their correlation was limited to a lowest Reynolds number

equal to 500 (see Table II). In contrast, in the numerical study of Kim, Lee et al. (Refs. 25) also lower values of the Reynolds number were included in the data set. However, according to Kim, Lee et al., the friction factor scales approximately as $f \sim Re^{0.1 \ln(Re) - 2}$. It can be seen from Figure 6 that the latter empirical correlation results in a significant overestimation of our friction factor data at Reynolds numbers Re_l below 300, with a difference going up to a factor of one hundred as the Reynolds number decreases.

The previous discussion thus shows that the correlations from the literature do not predict the appropriate scaling of the friction factor with the Reynolds number for steady laminar periodically developed flow in micro- and mini-channels.

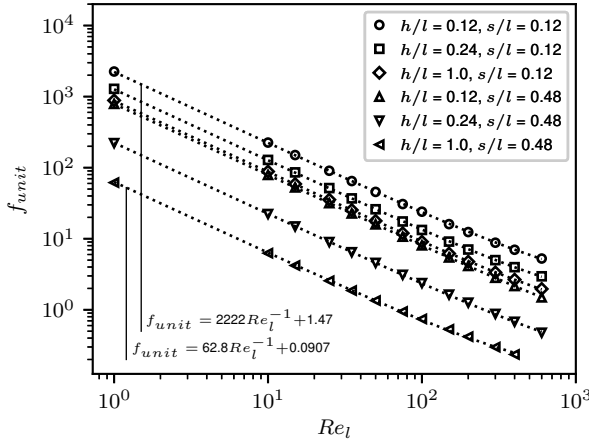


FIG. 5. Influence of the Reynolds number on the friction factor for steady periodically developed flow, when $t/l = 0.04$

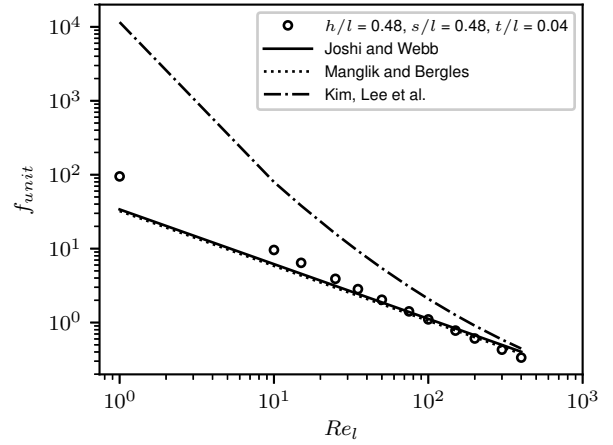


FIG. 6. A comparison between the friction factor correlations from the literature with the data from this work for steady periodically developed flow at low Reynolds numbers, when $t/l = 0.04$, $h/l = 0.48$, $s/l = 0.48$

B. The influence of the fin height-to-length ratio h/l on the friction factor

From the data in Figure 7, the influence of the fin height-to-length ratio h/l on the friction factor in the steady periodically developed flow regime can be observed. For low values of h/l , this friction factor becomes proportional to $(h/l)^{-2}$ according to our data. This is analogous to

the friction factor for developed flow between two parallel plates (Refs. 49), as the viscous forces on the top and bottom plate become the main contribution to the pressure drop for fins of a small height. On the contrary, for high values of h/l , the friction factor becomes independent of the fin height-to-length ratio. This can be explained by the fact that, as the relative fin height h/l increases, the area of the fin sides increases, while the area of the top and bottom plate in contact with the flow remains the same. Therefore, the total pressure drop will mainly originate from the total drag (i.e. viscous drag and form drag) at the fin sides, when h/l increases. Since the area of the fin sides depends on the relative fin pitch s/l , the relative fin thickness t/l of the fins, as well as the relative fin height h/l , one would expect h/l to still influence the friction factor. However, when h/l increases, the flow field around the fin sides also becomes more two-dimensional, as its variation along the direction \mathbf{e}_2 diminishes, so that eventually the drag at the fin sides is no longer affected by the relative fin height h/l .

Based on the discussed trends, the dependence of the friction factor on the height-to-length ratio may be captured through a correlation of the form

$$f_{unit} \simeq A \left(\frac{h}{l} \right)^{-2} + B, \quad (9)$$

where the parameters A and B depend on the Reynolds number Re_l , as well as the remaining geometrical parameters. The latter correlation form shows a good qualitative agreement with our data, when the parameters A and B are determined through a least-squares fitting. As one can see in Figure 7, the correlation form (9) has an average and maximum relative error of 1% and 6%, respectively.

Figure 7 also shows that the shift between the two asymptotic trends $f_{unit} \sim (h/l)^{-2}$ and $f_{unit} \sim (h/l)^0$ is significantly influenced by the fin pitch-to-length ratio s/l , because the aspect ratio s/h dictates the relative contribution of the friction on the top and bottom plate to the overall friction factor. Therefore, the trend $f_{unit} \sim (h/l)^0$ is more dominant when s/l becomes smaller.

In the literature, the influence of the fin height relative to the fin length has been incorporated in the friction factor both in an implicit and explicit way. Implicitly, the fin height-to-length ratio h/l affects the Reynolds number Re , as the fin height h appears in the expression for the hydraulic diameter. Explicitly, the influence of the fin height-to-length ratio has been included in the friction factor correlation through a factor $(h/l)^e$ such that $f_{unit} \sim (h/l)^e g(Re)$, where $g(Re)$ is a function of the Reynolds number Re and the exponent e lies between 0.02 and 2. In the correlations based on the experimental data of Kays and London (Refs. 18, 23, and 28), the resulting effective exponent

E , such that $f_{unit} \sim (h/l)^E$, lies between -1.3 and -1.5 for low fin height-to-length ratios.

Hence, it is clear that the correlations from the literature, which have been obtained for the larger h/l ratios common in conventional channels, do not respect the correct trend for the small h/l values that are encountered in micro- and mini-channels. As a consequence, the accuracy of the correlations from the literature rapidly diminishes when h/l decreases because small h/l values tend to fall outside the validity range of these correlations. In Figure 8 it is shown that the incorrect scaling of the correlations from the literature with h/l results in an underestimation of our friction factor data in the laminar regime. Even if the correlations from the literature are rescaled with a constant to minimize the difference with our data and to account for incorrect scaling for other parameters, we still observe an average relative error of 30% and a maximum relative error up to 65% for h/l near 0.1.

In addition, it should be noted that from the more recent numerically determined correlation of Kim, Lee, et al. (Refs. 25), no continuous scaling laws for the variation of f_{unit} with h/l could be derived, since the latter correlation depends on the fin porosity, and thus also the fin height-to-length ratio, in a discontinuous way. Finally, we remark that for all correlations from the literature, the friction factor still increases with h/l for large fin height-to-length ratios, which is contradicted by our observation that f_{unit} becomes independent of h/l in that case.

C. The influence of the fin pitch-to-length ratio s/l on the friction factor

Figure 9 displays the influence of the fin pitch-to-length ratio s/l on the friction factor in the steady periodically developed flow regime. It can be seen that as s/l approaches the fin thickness t/l , the friction factor approaches infinity because the channel becomes blocked. The influence of the fin pitch-to-length ratio s/l on f_{unit} is therefore best analyzed via the factor $(s-t)/l$. As illustrated in Figure 9, the friction factor is quite accurately expressed as a function of $(s-t)/l$ by correlations of the form

$$f_{unit} \simeq A \left(\frac{s}{l} - \frac{t}{l} \right)^k + B, \quad (10)$$

where A and B depend on the Reynolds number Re_l , as well as h/l and t/l . The negative exponent k , which ensures that $f_{unit} \rightarrow \infty$ for $s \rightarrow t$, can be taken as approximately constant over a wide range of Reynolds numbers, and over relatively broad intervals of h/l and t/l . For instance, for $Re_l \in (1, 600)$, $t/l \in (0.01, 0.02)$ and $h/l \in (0.5, 1)$, the previous correlation form holds within a

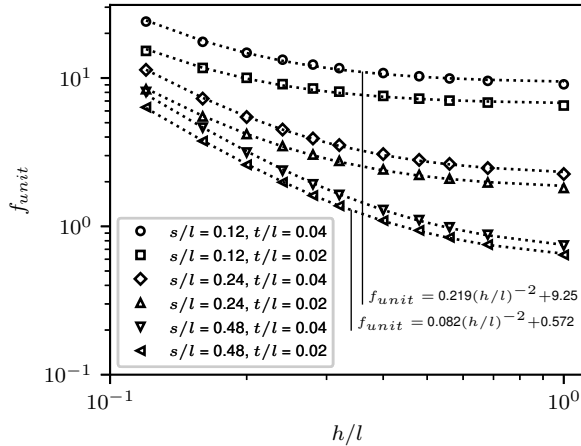


FIG. 7. Influence of the fin height-to-length ratio on the friction factor for steady periodically developed flow, when $Re_l = 100$

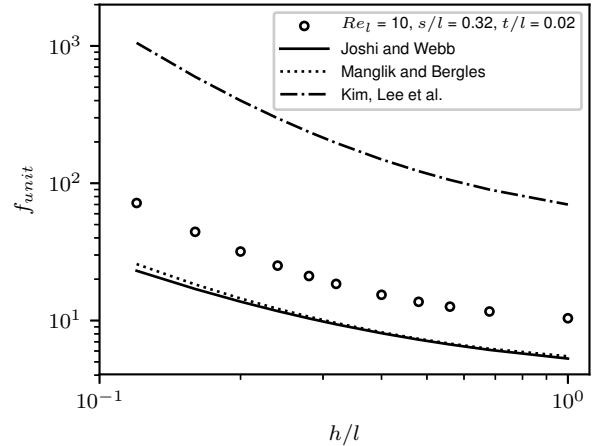


FIG. 8. A comparison between the friction factor correlations from the literature with the data from this work for steady periodically developed flow at small fin heights, when $Re_l = 10$, $t/l = 0.02$, $s/l = 0.32$

relative error of 5% when $k = -1.69$. Yet, the exponent k in (10) is not a constant over the entire set of our friction factor data.

The proposed correlation form (10) predicts that for high values of s/l , the friction factor becomes independent of the fin pitch-to-length ratio s/l . This is in agreement with our data, as it can be seen in Figure 9. The reason is that in that case, the overall pressure gradient stems primarily from the friction forces on the top and bottom plate of the channel, which are primarily dependent on the fin height-to-length ratio, so that $f_{unit} \sim (h/l)^{-2}$ as discussed in the previous subsection. As this trend originates from a reduced contribution of the total drag at the fin sides to the pressure gradient, its manifestation is greatly influenced by the relative fin height h/l , which is illustrated in Figure 9 for a few geometries. More specifically, for smaller values of h/l , the trend $f_{unit} \sim (s/l - t/l)^0$ will become more dominant.

Similar to the fin height-to-length ratio, the influence of the fin pitch-to-length ratio on the friction factor is usually incorporated in the correlations from the literature through a formula of the form $f \sim (s/l)^k$ for some negative exponent k . Of the correlations listed in Tables I and II, Joshi and Webb's correlation (Refs. 18) is the only one which accounts for the limit that the friction factor becomes infinite when $s - t$ approaches zero. This limit, however, is incorporated

implicitly in the definition of the friction factor, via a hydraulic diameter $D_h \sim (s - t)$ and a reference velocity $U_{ref} \sim (s - t)^{-1}$, which give rise to an infinitely large pressure drop when the fin pitch s approaches the fin thickness t . On the other hand, for small fin pitch-to-length ratios, i.e. $s/l < 0.25$, the correlation of Joshi and Webb (Refs. 18) overestimates the friction factor by 5% to 75%. Also the other correlations deviate within the same order of magnitude, albeit they typically show an underestimation, which is as much as 75% for $s/l > 0.4$. This is illustrated in Figure 10. Again, these errors have been determined after rescaling the correlations from the literature with a constant, to minimize the deviation from our data and compensate for the wrong scaling with other parameters. For larger values of s/l , the friction factor still depends on the fin pitch-to-length ratio according to all correlations from Tables I and II. Most notably, this is the case for the correlation of Kim, Lee et al. (Refs. 25), as shown in Figure 10. Their correlation significantly underestimates the friction factor up to 70% for s/l near 0.5. Furthermore, this correlation predicts a discontinuous dependence of the friction factor on the fin pitch-to-length ratio due to its piecewise dependence on the fin porosity.

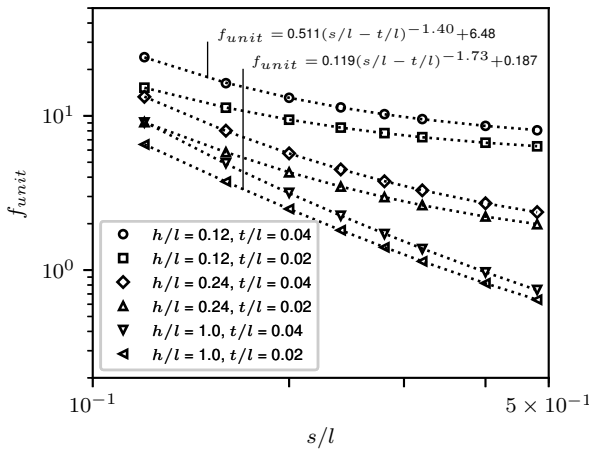


FIG. 9. Influence of the fin pitch-to-length ratio on the friction factor for steady periodically developed flow, when $Re_l = 100$

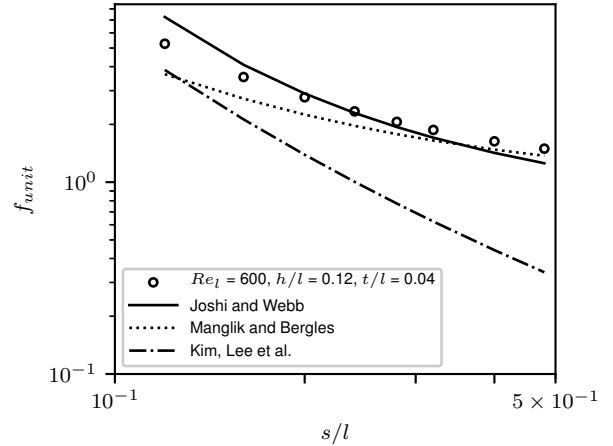


FIG. 10. A comparison between the friction factor correlations from the literature with the data from this work for steady periodically developed flow at small fin heights, when $Re_l = 600$, $t/l = 0.04$, $h/l = 0.12$

D. The influence of the fin thickness-to-length ratio t/l on the friction factor

The final geometrical parameter is the fin thickness-to-length ratio t/l , whose influence on the friction factor is shown in Figure 11. In this figure, it can be seen that when the fin thickness-to-length ratio t/l goes to zero, the friction factor becomes independent of t/l . This can be explained from the fact that the form drag over the fin sides, which are normal to the main flow direction e_1 and which give the fin its thickness t , mainly results from the presence of the wakes behind the fin (see Figure 4). So, for small fin thicknesses, these wakes become small as well, and the contribution of the corresponding form drag force on f_{unit} becomes negligible. This has been observed by quantifying the contribution of the viscous and form drag to the overall pressure gradient for various fin thicknesses. Obviously, Figure 11 demonstrates again that when t/l approaches the fin pitch-to-length ratio s/l , the friction factor increases to infinity, as described already in the previous subsection.

A closer inspection of our friction factor data has revealed that, in good approximation, the friction factor depends on t/l through a relationship of the form

$$f_{unit} \simeq A \left(\frac{t}{l} \right)^n + B. \quad (11)$$

Here, n is a positive constant, while A and B are assumed to represent functions of the Reynolds number Re_l , as well as h/l and s/l , or $(s-t)/l$. In Figure 11, curves for f_{unit} versus t/l have been fitted according to the form (11). It can be observed that the positive exponent n can not be considered a constant over all the friction factor data. However, n can be approximated by a constant over separate ranges of the Reynolds number Re_l . For example, for $Re_l \in (1, 200)$ and all values of s/l and h/l included in this work, the correlation form (11) results in a relative error below 5% with our data when $n = 0.84$.

In order that the proposed form (11) for the friction factor respects the asymptotic trend that f_{unit} becomes independent of t/l for $t/l \rightarrow 0$, B can only be a function s/l , but not $(s-t)/l$. On the other hand, the form (11) is only compatible with the previously proposed form (10) for the dependence of f_{unit} on $(s-t)/l$, if $A \sim (s/l - t/l)^e$ with $e < 0$.

For virtually all friction factor correlations, the latter restrictions on the form (11) are violated, as these correlations are based on the assumption that $f_{unit} \sim (t/l)^n$. Only the correlation of Joshi and Webb (Refs. 18) accounts for the observation that friction factor becomes independent of t/l for small fin thickness values. All other correlations listed in Tables I and II predict an asymptotic

behaviour of the form $f_{unit} \sim (t/l)^n$ with n between 0.03-0.3 for $t/l \rightarrow 0$. This results in an underestimation of the friction factor by approximately 20% for $t/l < 0.02$, after rescaling the correlation with a constant to exclude the wrong scaling with other parameters. For the correlation of Kim, Lee et al. (Refs. 25), the friction factor does not depend on the fin thickness-to-length ratio in a continuous manner, since its mathematical relationship to t/l is expressed through a discontinuous piecewise function of the porosity, as depicted in Figure 12.

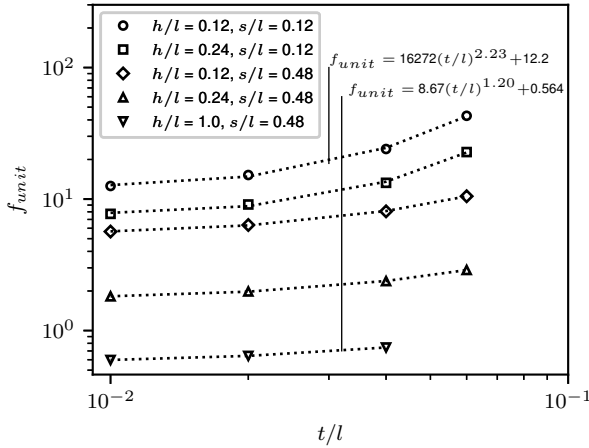


FIG. 11. Influence of the fin thickness-to-length ratio on the friction factor for steady periodically developed flow, when $Re_l = 100$

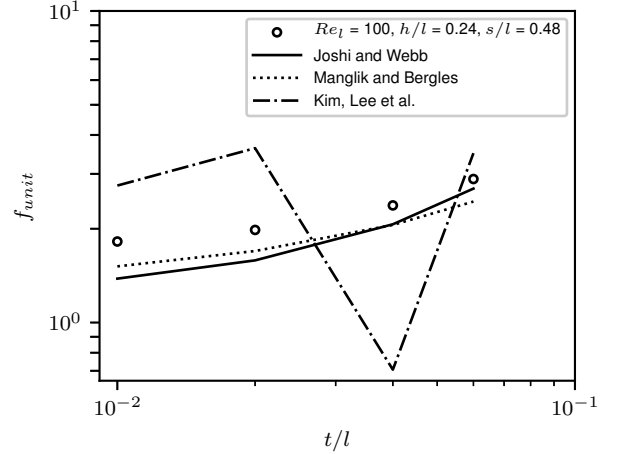


FIG. 12. A comparison between the friction factor correlations from the literature with the data from this work for steady periodically developed flow at small fin heights, when $Re_l = 100$, $h/l = 0.24$, $s/l = 0.48$

E. The influence of the critical Reynolds number

Although the correlation form (8) accurately captures our friction factor data for periodically developed flow in offset strip fin arrays in micro- and mini-channels, it is actually an approximation from a physical point of view. The reason is that the assumption that the Forchheimer correction term scales quadratically with the magnitude of the volume-averaged velocity only holds for the strong inertia regime, as discussed in Subsection III A. Nevertheless, the following more detailed analysis of our friction factor data reveals that also a so-called weak inertia regime (Refs. 47, 48, 50, and 51) occurs in offset strip fin arrays at very low Reynolds numbers. In the weak inertia

regime, the Forchheimer correction term is known to display a cubic dependence on the magnitude of the volume-averaged velocity, so that $f_{unit} = ARe_l^{-1} + CRe_l$ instead of $f_{unit} = ARe_l^{-1} + B$.

In Figure 13, the existence of both a strong and weak inertia regime has been visualized by plotting the Forchheimer correction term ($f_{unit}Re_l - A$) with respect to the Reynolds number Re_l . To this end, the parameter A was determined for each unit cell geometry by fitting the relation $f_{unit} = ARe_l^{-1}$ through the friction factor data points in the lower Reynolds number range. This range is determined by the values of Re_l where f_{unit} can be approximated by ARe_l^{-1} within an accuracy of 1%, for some constant value of A .

The strong inertia regime, which justifies the theoretical validity of (8), extends over the Reynolds number range $Re_l \in (Re_{l,ws}, Re_{l,st})$ in Figure 13. The two critical Reynolds numbers $Re_{l,ws}$ and $Re_{l,st}$ mark the transition from the weak inertia regime to the strong inertia regime and the transition from the strong inertia regime to the transitional regime, respectively. Both correspond to the values of Re_l at which the correction term ($f_{unit}Re_l - A$) deviates 5% from the linear dependence ($f_{unit}Re_l - A$) $\simeq BRe_l + C$, as in the study (Ref. 48). In the strong inertia regime, the constant C is found to be small with respect to A for all the geometries in this work. This confirms the expected purely quadratic dependence of the Forchheimer correction term on the magnitude of the volume-averaged velocity in this regime.

The weak inertia regime in Figure 13, which is characterized by ($f_{unit}Re_l - A$) $\simeq DRe_l^2 + F$, is found for $Re_l \in (0, Re_{l,ws})$. Also, the constant F remains small relative to A , which confirms a pure cubic relation between the Forchheimer correction term and $\|\langle \mathbf{u} \rangle\|$ in this regime. Furthermore, at higher Reynolds numbers, $Re_l > Re_{l,st}$, a transitional flow regime can be recognized in Figure 13. For Reynolds numbers in the transitional flow regime, the periodically developed flow equations (2) have time-dependent, chaotic flow solutions on a unit cell. Therefore, the friction factor in the transitional regime is actually defined based on the ensemble-averaged pressure gradient $\|\overline{\nabla P}\|$ instead of $\|\nabla P\|$, as a constant $\langle \mathbf{u} \rangle$ was imposed. Nevertheless, it still remains a question whether these chaotic flow solutions are representative of the complete flow through a finite fin array in a channel (Ref. 52). In any case, our friction factor data indicates that in the transitional regime, the correction ($f_{unit}Re_l - A$) can be captured by a quadratic dependence of the Reynolds number, comparable to the weak inertia regime. This is in agreement with the study of Lasseux et al. (Ref. 48).

Figure 14 depicts the critical Reynolds number $Re_{l,ws}$ as a function of the fin pitch-to-length ratio s/l . A monotonous decrease of $Re_{l,ws}$ can be observed for increasing s/l . This figure also

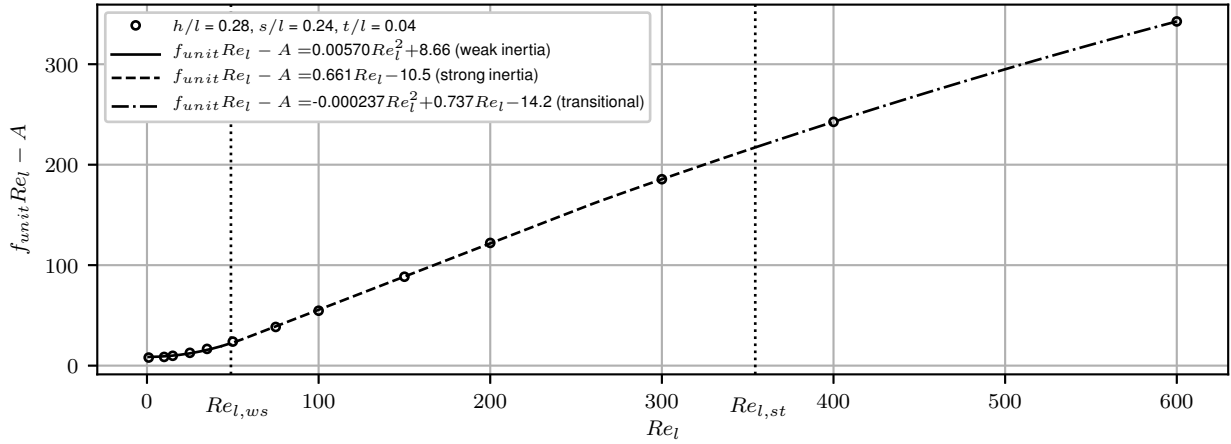


FIG. 13. Distinction between the flow regimes based on the Forchheimer correction term for steady periodically developed flow, when $h/l = 0.28$, $s/l = 0.24$, $t/l = 0.04$

shows that no significant influence of the fin height-to-length ratio h/l and fin thickness-to-length ratio t/l on the critical Reynolds number $Re_{l,ws}$ has been found.

The critical Reynolds number $Re_{l,st}$ is shown in Figures 15 and 16. It can be seen that for a higher value of the fin height-to-length ratio h/l , transition tends to occur at a lower Reynolds number. However, as illustrated in Figure 15, for fin height-to-length ratios larger than 0.4, $Re_{l,st}$ becomes independent of h/l . This can again be observed in Figure 16, which also shows that the fin pitch-to-length ratio s/l has an inverse relationship with $Re_{l,st}$. Finally, we add that the fin thickness-to-length ratio t/l has been found to have no significant influence on the critical Reynolds number $Re_{l,st}$.

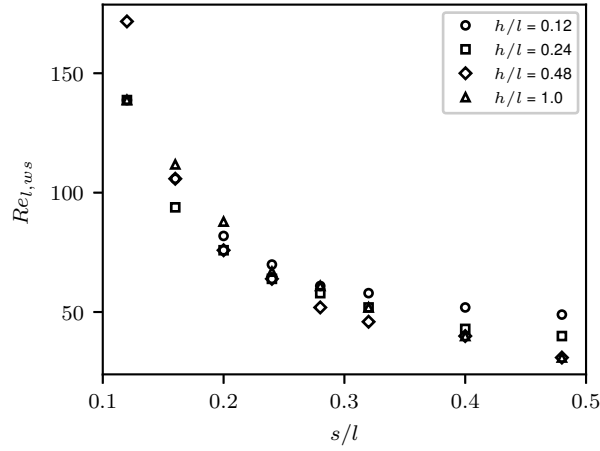


FIG. 14. Critical Reynolds number representing the transition of the weak inertia regime towards the strong inertia regime, when $t/l = 0.02$

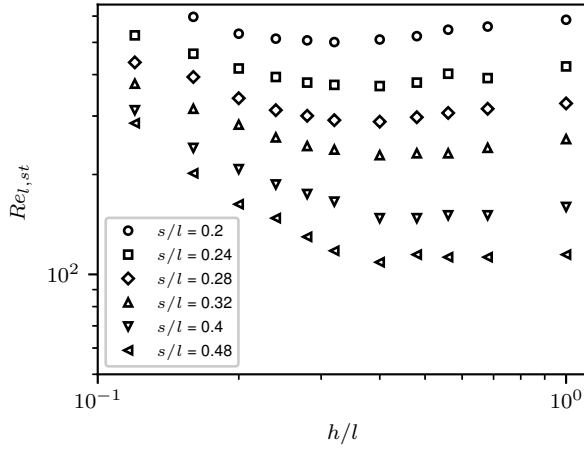


FIG. 15. Critical Reynolds number representing the transition of the weak inertia regime towards the strong inertia regime, when $t/l = 0.02$

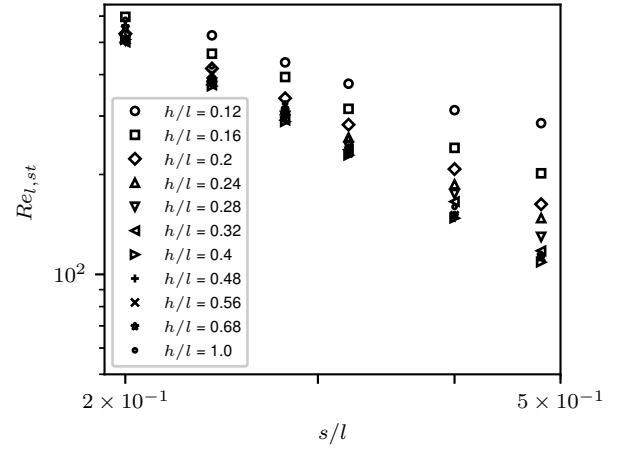


FIG. 16. Critical Reynolds number representing the transition of the strong inertia regime towards the transitional regime, when $t/l = 0.02$

The previous figures indicate the Reynolds number range over which a direct proportionality between the correction $(f_{unit}Re_l - A)$ and BRe_l is valid from a physical perspective. However, from a practical perspective, the correlation form (8) is able to accurately capture the periodically developed friction factor data for offset strip fin arrays in micro- and mini-channels.

IV. FRICTION FACTOR CORRELATION

A. Fitting approach

To obtain an accurate friction factor correlation for steady periodically developed flow through offset strip fin arrays in micro- and mini-channels, several heuristically constructed candidate correlations, all respecting the forms (8)-(11), were fitted to the friction factor data from this work. For the fitting procedure, two methods were applied. First, a non-linear least-squares optimization method based on the trust region reflective algorithm (Refs. 53) was used to find the *optimal* parameter values for each candidate correlation. Secondly, the Bayesian approach for parameter estimation and model validation (Refs. 54) was used to find the *most likely* parameter values for each candidate correlation. The Bayesian approach was also employed to quantify the so-called *log-evidence* for each candidate correlation, which is a statistical measure for its ability to capture the data. Finally, the candidate correlation and the fitting parameters leading to the highest relative accuracy and highest log-evidence with respect to our friction factor data were selected. We remark that for this final correlation, which is discussed in the next subsection, the *optimal* and *most likely* parameter values were found to be equal within their significant digits.

For an explanation on how the most likely parameters and log-evidence of each candidate correlation were quantified via the Bayesian approach, we refer in the first place to the relevant literature as e.g. in (Refs. 54). For the sake of transparency, we do clarify that, given a certain correlation model \mathcal{M} , the Bayesian approach allows for the computation of the joint probability density function of the fitting parameters $\boldsymbol{\theta}$, and thus their most likely value, having observed a given data set \mathcal{D} of friction factor values. This joint probability density function, or so-called posterior, has been calculated as

$$\mathcal{P}(\boldsymbol{\theta}|\mathcal{D}, \mathcal{M}) = \frac{\mathcal{L}(\mathcal{D}|\boldsymbol{\theta}, \mathcal{M}) \mathcal{P}(\boldsymbol{\theta}|\mathcal{M})}{\mathcal{P}(\mathcal{D}|\mathcal{M})}. \quad (12)$$

In this equation, the likelihood $\mathcal{L}(\mathcal{D}|\boldsymbol{\theta}, \mathcal{M})$ is the probability density function of observing the data \mathcal{D} for the given fitting parameters $\boldsymbol{\theta}$. It thus represents the correlation error, which we assume to have distribution equal to the multiplication of different Gaussian distributions for every data point \mathcal{D}_i , similar to (Refs. 54), each with a mean of 0 and a standard deviation of $0.01\mathcal{D}_i$. The prior $\mathcal{P}(\boldsymbol{\theta}|\mathcal{M})$ is the probability density function of the fitting parameters $\boldsymbol{\theta}$ prior to observing the data \mathcal{D} and depends on the mathematical constraints of the correlation model. For our study, this probability density function for each fitting parameter θ_i has been assumed to be uniform

since any a priori information regarding the fitting parameters is absent. Finally, the evidence $\mathcal{P}(\mathcal{D}|\mathcal{M})$ is the probability to observe the data \mathcal{D} regardless of the fitting parameter values θ and is computed through the expression $\mathcal{P}(\mathcal{D}|\mathcal{M}) = \int \mathcal{L}(\mathcal{D}|\theta, \mathcal{M}) \mathcal{P}(\theta|\mathcal{M}) d\theta$. The log-evidence $\log[\mathcal{P}(\mathcal{D}|\mathcal{M})]$ thus provides a quantitative measure for the suitability of the correlation model \mathcal{M} to represent the given data. Therefore, it has been used to compare the different candidate correlations models for the friction factor. As a last remark, we add that the Laplace approximation was introduced for the computation of the evidence, which means that the posterior is assumed to have a Gaussian distribution. This is true for a large number of data samples of independent and identically distributed fitting parameters (Refs. 54), as it is the case in this study.

B. Fitting result

By evaluating several heuristically constructed candidate correlations through the former fitting procedures, the following correlation for the friction factor in the steady periodically developed flow regime was obtained:

$$f_{unit} = c_0 Re_l^{-1} + c_1,$$

with

$$\begin{aligned} c_0 &= [23.5(s/l - t/l)^{-0.83} + 14.9](t/l)^{0.84}(h/l)^{-2} \\ &\quad + 13.0(s/l - t/l)^{-1.69} + 6.0(h/l)^{-2}, \\ c_1 &= 56.5(s/l - t/l)^{-1.34}(t/l)^{2.94}(h/l)^{-1.08} \\ &\quad + 0.0355(s/l - t/l)^{-0.83}. \end{aligned} \tag{13}$$

For the friction factor data in this work, this final correlation results in an average relative error of 2%. Its maximal relative error is below 4%, 5% and 8% for respectively 90%, 95%, 99% of the data points. Besides having the highest accuracy, the correlation form (13) resulted in the largest log-evidence value of all the considered candidate correlations. For example, regarding the dependence of the friction factor on the Reynolds number, the form $f_{unit} = c_0 Re_l^{-1} + c_1$ resulted in a log-evidence values 10 times larger than that of the form $f_{unit} = c_0 Re_l^e$, which is typically used in the literature (see Tables I and II). Furthermore, through the joint probability density function obtained from the Bayesian approach, the standard deviations of all the exponents in expression (13) are observed to remain below 1% of the exponent value. This confirms the uniqueness of all the exponent values and the prevention of over-fitting the data, which was further reflected in the high log-evidence value of the presented correlation form.

As an illustration of the correlation's accuracy for the friction factor data from this work, it has been compared with a selection of data points in Figure 17. In Figure 18, the presented correlation (13) is compared with the experimental friction factor data from Kays and London (Refs. 26). It can be seen that below a Reynolds number Re_l of 600, the relative difference between our correlation and the data from Kays and London, indicated by the error bars, remains smaller than 10%, and even decreases at lower Re_l , for all geometries with $h/l < 1$. Taking into account that the experimental uncertainty on the friction factor and the Reynolds number from (Refs. 26) are equal to 5% and 2% respectively, this relative difference falls well within our correlation's accuracy. We note that the grey zone in this last figure indicates again the expected region of transitional flow according to (Refs. 18–20).

The correlation (13) is consistent with our observation that the assumption of a strong inertia regime (8) is justified over almost the entire range of Reynolds numbers studied in this work, i.e. $Re_l = 1 - 600$. Yet, it also incorporates all the trends (8)-(11) which describe the influence of the geometrical parameters, as discussed in Section III.

Regarding the influence of the fin height-to-length ratio, the final correlation respects the asymptotic trends $f_{unit} \sim (h/l)^{-2}$ for $h/l \rightarrow 0$ and $f_{unit} \sim (h/l)^0$ for $h/l \rightarrow \infty$. Due to the inclusion of the term $(h/l)^{-1.08}$ in the coefficient c_1 , both of these asymptotic trends have been matched for intermediate values of h/l . Furthermore, in the first coefficient c_0 , the term $6.0(h/l)^{-2}$ corresponds to the friction factor for fully-developed flow between parallel plates: $f_{unit}(h/l) = 6[Re_l(h/l)]^{-1}$. This is considered the asymptotic value of the friction factor that is recovered when the fin height-to-length ratio h/l and the fin thickness-to-length ratio t/l approach zero.

Regarding the influence of the fin pitch-to-length, it is clear that the limit $f_{unit} \rightarrow \infty$ for $s \rightarrow t$ has been incorporated as well. After all, the four different exponents for the term $(s/l - t/l)$, which have been included for an accurate fit over the entire range of s/l values from this work, are all negative. Moreover, in accordance with our observations, the correlation (13) becomes independent of the fin pitch-to-length ratio as s/l increases.

Finally, the presented relation for f_{unit} also becomes independent of the fin thickness-to-length ratio as t/l decreases. For larger values of t/l , two different exponents for the term (t/l) account for the influence of the thickness-to-length ratio over different Reynolds number ranges.

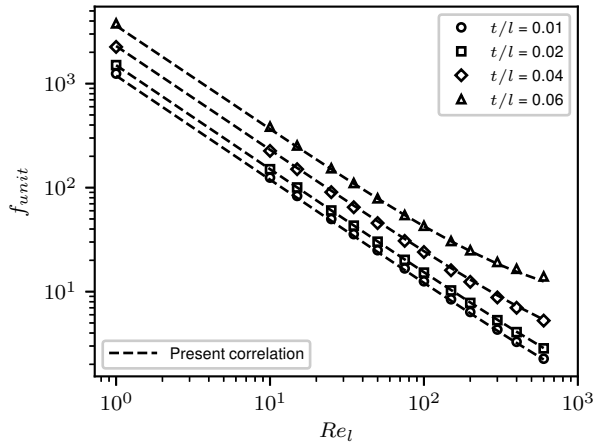


FIG. 17. A comparison between the final friction factor correlation with data from this work for steady periodically developed flow at small fin heights, when $h/l = 0.12$, $s/l = 0.12$

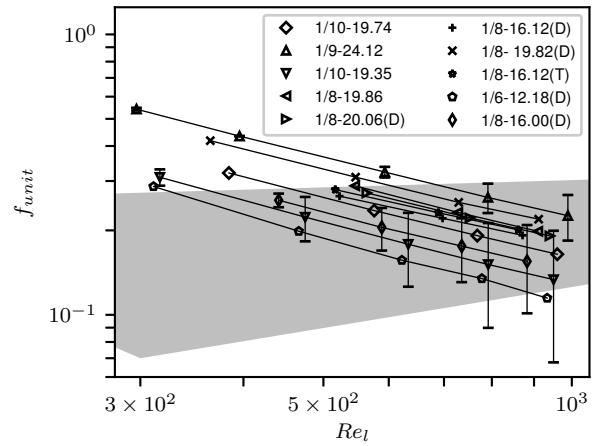


FIG. 18. Discrepancies between the final friction factor correlation and the data from Kays and London (Refs. 26), where the grey zone indicates the region of transitional flow

V. CONCLUSIONS

The friction factor for steady laminar periodically developed flow through offset strip fins arrays in micro- and mini-channels has been examined in the present study. The friction factor data was collected by solving numerically the periodically developed flow equations on a unit cell of the fin array. To this end, more than 2765 flow simulations have been carried out.

It was found that the friction factor correlations in the literature generally cover applications of offset strip fins in larger conventional channels, so that very few data points in the laminar flow regime were considered. Therefore, they do not respect the correct asymptotic behaviour of the friction factor for low to moderate Reynolds numbers and result in deviations of 20%-80% and more for the laminar regime in micro- and mini-channels. Neither do they consider the asymptotic trends and limits observed for small and large values of the fin height, pitch and thickness relative to the fin length.

To overcome these discrepancies, a new correlation has been presented for the periodically developed friction factor, whose maximal relative error is below 8% with respect to our data. This new correlation was obtained through a least-square fitting procedure, though its suitability was further analyzed by means of the Bayesian approach for parameter estimation.

The new correlation scales inversely linear with the Reynolds number, in agreement with our observation that a strong inertia regime prevails over nearly the entire range of Reynolds numbers up to 600. Nevertheless, a closer look at the dependence of the friction factor on the Reynolds number has revealed that also a regime of weak inertia occurs at low Reynolds numbers. In contrast, a transitional regime occurs at higher Reynolds numbers. The transitions from the strong inertia regime have been characterized by two critical Reynolds numbers in this work. Both critical Reynolds numbers are found to decrease monotonously with the fin pitch and to be independent of the fin thickness. Furthermore, the transition from the weak inertia regime to the strong inertia regime was shown to be independent of the fin height. Yet, the transition from the strong inertia regime towards the transitional regime occurs at lower Reynolds numbers for larger fin heights.

Finally, the presented new correlation incorporates all the observed trends for variations in the geometrical parameters of the offset strip fin array. First, the correlation predicts that the friction factor becomes proportional to the inverse square of the fin height for small fin heights, analogous to fully-developed flow between two parallel plates. Secondly, it predicts that the pressure gradient approaches infinity as the fin pitch becomes equal to the fin thickness. Additionally, the correlation

respects the observation that the friction factor becomes independent of the fin height, fin pitch, and fin thickness for large fin heights, large fin pitches, and small fin thicknesses, respectively.

VI. CONTRIBUTIONS

The computational algorithms and software framework for the periodic flow equations were implemented and validated by G. Buckinx. All flow simulations and post-processing calculations were performed by A. Vangeffelen. The interpretation of the results was done by A. Vangeffelen, with input from G. Buckinx regarding the existing literature. A. Vangeffelen and G. Buckinx wrote the paper with input from M. Baelmans and M. R. Vetrano.

VII. ACKNOWLEDGEMENTS

This work was partly funded by the Research Foundation — Flanders (FWO) through G. Buckinx's post-doctoral project grant 12Y2919N, and by the Flemish Institute for Technological Research (VITO) through A. Vangeffelen's Ph.D. grant 1810603.

Appendix A: Periodically developed friction factor data

	t/l	h/l	s/l	ϵ	Re_l	f_{unit}
1	0.01	0.12	0.12	0.85207	1	1247.6
2	0.01	0.12	0.12	0.85207	10	124.78
3	0.01	0.12	0.12	0.85207	15	83.228
4	0.01	0.12	0.12	0.85207	25	49.968
5	0.01	0.12	0.12	0.85207	35	35.711
6	0.01	0.12	0.12	0.85207	50	25.019
7	0.01	0.12	0.12	0.85207	75	16.718
8	0.01	0.12	0.12	0.85207	100	12.573
9	0.01	0.12	0.12	0.85207	150	8.438
10	0.01	0.12	0.12	0.85207	200	6.3758
11	0.01	0.12	0.12	0.85207	300	4.3183
12	0.01	0.12	0.12	0.85207	400	3.2914
13	0.01	0.12	0.12	0.85207	600	2.2649
14	0.01	0.12	0.16	0.86878	50	18.956
15	0.01	0.12	0.16	0.86878	100	9.5407
16	0.01	0.12	0.16	0.86878	300	3.2945
17	0.01	0.12	0.16	0.86878	400	2.5164
18	0.01	0.12	0.16	0.86878	600	1.7368
19	0.01	0.12	0.2	0.87912	50	16.075
20	0.01	0.12	0.2	0.87912	100	8.0957
21	0.01	0.12	0.2	0.87912	300	2.7976
22	0.01	0.12	0.2	0.87912	400	2.1359
23	0.01	0.12	0.2	0.87912	600	1.4704
24	0.01	0.12	0.24	0.88615	50	14.448
25	0.01	0.12	0.24	0.88615	100	7.276
26	0.01	0.12	0.24	0.88615	300	2.5093
27	0.01	0.12	0.24	0.88615	400	1.9123
28	0.01	0.12	0.24	0.88615	600	1.3101
29	0.01	0.12	0.28	0.89125	50	13.419
30	0.01	0.12	0.28	0.89125	100	6.7552
31	0.01	0.12	0.28	0.89125	300	2.3222
32	0.01	0.12	0.28	0.89125	400	1.7657
33	0.01	0.12	0.28	0.89125	600	1.204
34	0.01	0.12	0.32	0.8951	50	12.715
35	0.01	0.12	0.32	0.8951	100	6.3974
36	0.01	0.12	0.32	0.8951	300	2.1915
37	0.01	0.12	0.32	0.8951	400	1.6629
38	0.01	0.12	0.32	0.8951	600	1.1296
39	0.01	0.12	0.4	0.90056	50	11.819
40	0.01	0.12	0.4	0.90056	100	5.9403
41	0.01	0.12	0.4	0.90056	300	2.0226
42	0.01	0.12	0.4	0.90056	400	1.5301
43	0.01	0.12	0.4	0.90056	600	1.0343
44	0.01	0.12	0.48	0.90424	50	11.276
45	0.01	0.12	0.48	0.90424	100	5.662
46	0.01	0.12	0.48	0.90424	300	1.9196
47	0.01	0.12	0.48	0.90424	400	1.4494
48	0.01	0.12	0.48	0.90424	600	0.97691
49	0.01	0.16	0.12	0.86878	10	96.924
50	0.01	0.16	0.12	0.86878	50	19.448
51	0.01	0.16	0.12	0.86878	100	9.7831
52	0.01	0.16	0.12	0.86878	300	3.3829
53	0.01	0.16	0.12	0.86878	400	2.5875
54	0.01	0.16	0.12	0.86878	600	1.7918
55	0.01	0.16	0.16	0.88581	10	68.309
56	0.01	0.16	0.16	0.88581	50	13.722
57	0.01	0.16	0.16	0.88581	100	6.9243
58	0.01	0.16	0.16	0.88581	300	2.4254
59	0.01	0.16	0.16	0.88581	400	1.8651
60	0.01	0.16	0.16	0.88581	600	1.302
61	0.01	0.16	0.2	0.89636	50	11.034
62	0.01	0.16	0.2	0.89636	100	5.5804
63	0.01	0.16	0.2	0.89636	300	1.9683
64	0.01	0.16	0.2	0.89636	400	1.5164
65	0.01	0.16	0.2	0.89636	600	1.0586
66	0.01	0.16	0.24	0.90353	50	9.54
67	0.01	0.16	0.24	0.90353	100	4.8305
68	0.01	0.16	0.24	0.90353	300	1.7064
69	0.01	0.16	0.24	0.90353	400	1.313
70	0.01	0.16	0.24	0.90353	600	0.91203
71	0.01	0.16	0.28	0.90872	50	8.6117
72	0.01	0.16	0.28	0.90872	100	4.3619
73	0.01	0.16	0.28	0.90872	300	1.5373
74	0.01	0.16	0.28	0.90872	400	1.1794
75	0.01	0.16	0.28	0.90872	600	0.81418
76	0.01	0.16	0.32	0.91266	10	39.674
77	0.01	0.16	0.32	0.91266	50	7.987
78	0.01	0.16	0.32	0.91266	100	4.0448
79	0.01	0.16	0.32	0.91266	300	1.4191
80	0.01	0.16	0.32	0.91266	400	1.0854

	t/l	h/l	s/l	ϵ	Re_l	f_{unit}
81	0.01	0.16	0.32	0.91266	600	0.74508
82	0.01	0.16	0.4	0.91822	10	35.822
83	0.01	0.16	0.4	0.91822	50	7.2088
84	0.01	0.16	0.4	0.91822	100	3.6456
85	0.01	0.16	0.4	0.91822	300	1.2661
86	0.01	0.16	0.4	0.91822	400	0.96344
87	0.01	0.16	0.4	0.91822	600	0.65636
88	0.01	0.16	0.48	0.92197	10	33.553
89	0.01	0.16	0.48	0.92197	50	6.7477
90	0.01	0.16	0.48	0.92197	100	3.407
91	0.01	0.16	0.48	0.92197	300	1.1733
92	0.01	0.16	0.48	0.92197	400	0.88991
93	0.01	0.16	0.48	0.92197	600	0.60347
94	0.01	0.2	0.12	0.87912	10	83.77
95	0.01	0.2	0.12	0.87912	50	16.815
96	0.01	0.2	0.12	0.87912	100	8.4631
97	0.01	0.2	0.12	0.87912	300	2.9366
98	0.01	0.2	0.12	0.87912	400	2.25
99	0.01	0.2	0.12	0.87912	600	1.5631
100	0.01	0.2	0.16	0.89636	10	56.137
101	0.01	0.2	0.16	0.89636	50	11.286
102	0.01	0.2	0.16	0.89636	100	5.7057
103	0.01	0.2	0.16	0.89636	300	2.0171
104	0.01	0.2	0.16	0.89636	400	1.5574
105	0.01	0.2	0.16	0.89636	600	1.0947
106	0.01	0.2	0.2	0.90703	100	4.4164
107	0.01	0.2	0.2	0.90703	300	1.5824
108	0.01	0.2	0.2	0.90703	400	1.2267
109	0.01	0.2	0.2	0.90703	600	0.86449
110	0.01	0.2	0.24	0.91429	50	7.2746
111	0.01	0.2	0.24	0.91429	100	3.7025
112	0.01	0.2	0.24	0.91429	300	1.3356
113	0.01	0.2	0.24	0.91429	400	1.0354
114	0.01	0.2	0.24	0.91429	600	0.72633
115	0.01	0.2	0.28	0.91954	50	6.3953
116	0.01	0.2	0.28	0.91954	100	3.2605
117	0.01	0.2	0.28	0.91954	300	1.1769
118	0.01	0.2	0.28	0.91954	400	0.90983
119	0.01	0.2	0.28	0.91954	600	0.63383
120	0.01	0.2	0.32	0.92352	50	5.8098
121	0.01	0.2	0.32	0.92352	100	2.9641
122	0.01	0.2	0.32	0.92352	300	1.066
123	0.01	0.2	0.32	0.92352	400	0.82093
124	0.01	0.2	0.32	0.92352	600	0.56812
125	0.01	0.2	0.4	0.92915	50	5.0896
126	0.01	0.2	0.4	0.92915	100	2.5949
127	0.01	0.2	0.4	0.92915	300	0.92136
128	0.01	0.2	0.4	0.92915	400	0.70489
129	0.01	0.2	0.4	0.92915	600	0.48325
130	0.01	0.2	0.48	0.93294	50	4.6695
131	0.01	0.2	0.48	0.93294	100	2.376
132	0.01	0.2	0.48	0.93294	300	0.83315
133	0.01	0.2	0.48	0.93294	400	0.63461
134	0.01	0.2	0.48	0.93294	600	0.43258
135	0.01	0.24	0.12	0.88615	50	15.332
136	0.01	0.24	0.12	0.88615	100	7.7188
137	0.01	0.24	0.12	0.88615	300	2.6827
138	0.01	0.24	0.12	0.88615	400	2.0573
139	0.01	0.24	0.12	0.88615	600	1.4316
140	0.01	0.24	0.16	0.90353	50	9.9428
141	0.01	0.24	0.16	0.90353	100	5.032
142	0.01	0.24	0.16	0.90353	300	1.7888
143	0.01	0.24	0.16	0.90353	400	1.3846
144	0.01	0.24	0.16	0.90353	600	0.97739
145	0.01	0.24	0.2	0.91429	50	7.426
146	0.01	0.24	0.2	0.91429	100	3.7783
147	0.01	0.24	0.2	0.91429	300	1.3684
148	0.01	0.24	0.2	0.91429	400	1.0653
149	0.01	0.24	0.2	0.91429	600	0.75543
150	0.01	0.24	0.24	0.9216	50	6.0404
151	0.01	0.24	0.24	0.9216	100	3.0872
152	0.01	0.24	0.24	0.9216	300	1.1315
153	0.01	0.24	0.24	0.9216	400	0.88179
154	0.01	0.24	0.24	0.9216	600	0.62286
155	0.01	0.24	0.28	0.9269	50	5.1902
156	0.01	0.24	0.28	0.9269	100	2.6617
157	0.01	0.24	0.28	0.9269	300	0.97976
158	0.01	0.24	0.28	0.9269	400	0.76165
159	0.01	0.24	0.28	0.9269	600	0.53414
160	0.01	0.24	0.32	0.93091	50	4.627

	t/l	h/l	s/l	ϵ	Re_l	f_{unit}
161	0.01	0.24	0.32	0.93091	100	2.3777
162	0.01	0.24	0.32	0.93091	300	0.87368
163	0.01	0.24	0.32	0.93091	400	0.67645
164	0.01	0.24	0.32	0.93091	600	0.47101
165	0.01	0.24	0.4	0.93659	50	3.9402
166	0.01	0.24	0.4	0.93659	100	2.0269
167	0.01	0.24	0.4	0.93659	300	0.7349
168	0.01	0.24	0.4	0.93659	400	0.56465
169	0.01	0.24	0.4	0.93659	600	0.38907
170	0.01	0.24	0.48	0.94041	50	3.5444
171	0.01	0.24	0.48	0.94041	100	1.82
172	0.01	0.2				

	t/l	h/l	s/l	ϵ	Re_l	f_{unit}
241	0.01	0.32	0.28	0.93626	400	0.60934
242	0.01	0.32	0.28	0.93626	600	0.43117
243	0.01	0.32	0.32	0.94031	50	3.4448
244	0.01	0.32	0.32	0.94031	100	1.7909
245	0.01	0.32	0.32	0.94031	300	0.6784
246	0.01	0.32	0.32	0.94031	400	0.52905
247	0.01	0.32	0.32	0.94031	600	0.37162
248	0.01	0.32	0.4	0.94605	50	2.7956
249	0.01	0.32	0.4	0.94605	100	1.4618
250	0.01	0.32	0.4	0.94605	300	0.54758
251	0.01	0.32	0.4	0.94605	400	0.42339
252	0.01	0.32	0.4	0.94605	600	0.29414
253	0.01	0.32	0.48	0.94991	50	2.4267
254	0.01	0.32	0.48	0.94991	100	1.2691
255	0.01	0.32	0.48	0.94991	300	0.46652
256	0.01	0.32	0.48	0.94991	400	0.35856
257	0.01	0.32	0.48	0.94991	600	0.24734
258	0.01	0.4	0.12	0.90056	50	12.939
259	0.01	0.4	0.12	0.90056	100	6.5152
260	0.01	0.4	0.12	0.90056	300	2.2662
261	0.01	0.4	0.12	0.90056	400	1.7394
262	0.01	0.4	0.12	0.90056	600	1.213
263	0.01	0.4	0.16	0.91822	50	7.8656
264	0.01	0.4	0.16	0.91822	300	1.4273
265	0.01	0.4	0.16	0.91822	400	1.1086
266	0.01	0.4	0.16	0.91822	600	0.78792
267	0.01	0.4	0.2	0.92915	50	5.5027
268	0.01	0.4	0.2	0.92915	100	2.8107
269	0.01	0.4	0.2	0.92915	300	1.0356
270	0.01	0.4	0.2	0.92915	400	0.81217
271	0.01	0.4	0.2	0.92915	600	0.58256
272	0.01	0.4	0.24	0.93659	50	4.2038
273	0.01	0.4	0.24	0.93659	100	2.1661
274	0.01	0.4	0.24	0.93659	300	0.8176
275	0.01	0.4	0.24	0.93659	400	0.64375
276	0.01	0.4	0.24	0.93659	600	0.46107
277	0.01	0.4	0.28	0.94197	50	3.4106
278	0.01	0.4	0.28	0.94197	300	0.67956
279	0.01	0.4	0.28	0.94197	400	0.53444
280	0.01	0.4	0.28	0.94197	600	0.38105
281	0.01	0.4	0.32	0.94605	50	2.8887
282	0.01	0.4	0.32	0.94605	300	0.58365
283	0.01	0.4	0.32	0.94605	400	0.45723
284	0.01	0.4	0.32	0.94605	600	0.32437
285	0.01	0.4	0.4	0.95181	50	2.2609
286	0.01	0.4	0.4	0.95181	300	0.45813
287	0.01	0.4	0.4	0.95181	400	0.35623
288	0.01	0.4	0.4	0.95181	600	0.25244
289	0.01	0.4	0.48	0.9557	300	0.38037
290	0.01	0.4	0.48	0.9557	400	0.29469
291	0.01	0.4	0.48	0.9557	600	0.21544
292	0.01	0.48	0.12	0.90424	10	61.939
293	0.01	0.48	0.12	0.90424	50	12.438
294	0.01	0.48	0.12	0.90424	300	2.1783
295	0.01	0.48	0.12	0.90424	600	1.1665
296	0.01	0.48	0.16	0.92197	300	1.3541
297	0.01	0.48	0.16	0.92197	400	1.0524
298	0.01	0.48	0.16	0.92197	600	0.74893
299	0.01	0.48	0.2	0.93294	300	0.9703
300	0.01	0.48	0.2	0.93294	400	0.76206
301	0.01	0.48	0.2	0.93294	600	0.54815
302	0.01	0.48	0.24	0.94041	50	3.8659
303	0.01	0.48	0.24	0.94041	300	0.75716
304	0.01	0.48	0.24	0.94041	400	0.59756
305	0.01	0.48	0.24	0.94041	600	0.42998
306	0.01	0.48	0.28	0.94581	50	3.089
307	0.01	0.48	0.28	0.94581	300	0.6226
308	0.01	0.48	0.28	0.94581	600	0.3521
309	0.01	0.48	0.32	0.94991	50	2.5782
310	0.01	0.48	0.32	0.94991	300	0.52926
311	0.01	0.48	0.32	0.94991	600	0.29746
312	0.01	0.48	0.4	0.9557	300	0.4075
313	0.01	0.48	0.4	0.9557	600	0.23161
314	0.01	0.48	0.48	0.9596	100	0.87006
315	0.01	0.48	0.48	0.9596	300	0.33238
316	0.01	0.56	0.12	0.90688	10	60.269
317	0.01	0.56	0.12	0.90688	50	12.103
318	0.01	0.56	0.12	0.90688	300	2.119
319	0.01	0.56	0.12	0.90688	600	1.1348
320	0.01	0.56	0.16	0.92466	50	7.1894

	t/l	h/l	s/l	ϵ	Re_l	f_{unit}
321	0.01	0.56	0.16	0.92466	300	1.3052
322	0.01	0.56	0.16	0.92466	600	0.723
323	0.01	0.56	0.2	0.93567	300	0.9274
324	0.01	0.56	0.2	0.93567	600	0.52568
325	0.01	0.56	0.24	0.94316	50	3.6514
326	0.01	0.56	0.24	0.94316	300	0.7179
327	0.01	0.56	0.24	0.94316	600	0.40964
328	0.01	0.56	0.28	0.94858	50	2.887
329	0.01	0.56	0.28	0.94858	300	0.58588
330	0.01	0.56	0.28	0.94858	600	0.33361
331	0.01	0.56	0.32	0.95268	50	2.3846
332	0.01	0.56	0.32	0.95268	300	0.4945
333	0.01	0.56	0.32	0.95268	600	0.28103
334	0.01	0.56	0.4	0.95849	300	0.37561
335	0.01	0.56	0.4	0.95849	600	0.2261
336	0.01	0.56	0.48	0.96241	300	0.30274
337	0.01	0.68	0.12	0.9097	10	58.583
338	0.01	0.68	0.12	0.9097	50	11.77
339	0.01	0.68	0.12	0.9097	300	2.059
340	0.01	0.68	0.12	0.9097	600	1.1027
341	0.01	0.68	0.16	0.92754	300	1.2567
342	0.01	0.68	0.16	0.92754	600	0.69659
343	0.01	0.68	0.2	0.93858	50	4.6768
344	0.01	0.68	0.2	0.93858	300	0.88513
345	0.01	0.68	0.2	0.93858	600	0.50269
346	0.01	0.68	0.24	0.94609	300	0.67959
347	0.01	0.68	0.28	0.95152	300	0.55041
348	0.01	0.68	0.28	0.95152	600	0.31608
349	0.01	0.68	0.32	0.95564	300	0.46122
350	0.01	0.68	0.32	0.95564	600	0.26674
351	0.01	0.68	0.4	0.96147	300	0.34564
352	0.01	0.68	0.48	0.96539	300	0.27821
353	0.01	1.0	0.12	0.91394	10	56.219
354	0.01	1.0	0.12	0.91394	300	1.9747
355	0.01	1.0	0.12	0.91394	600	1.0573
356	0.01	1.0	0.16	0.93186	300	1.1895
357	0.01	1.0	0.16	0.93186	600	0.66003
358	0.01	1.0	0.2	0.94295	300	0.82734
359	0.01	1.0	0.2	0.94295	600	0.47163
360	0.01	1.0	0.24	0.9505	300	0.62794
361	0.01	1.0	0.24	0.9505	600	0.36349
362	0.01	1.0	0.28	0.95596	600	0.29453
363	0.01	1.0	0.32	0.9601	600	0.25783
364	0.01	1.0	0.48	0.96989	100	0.59787
365	0.01	1.0	0.48	0.96989	300	0.23716
366	0.02	0.12	0.12	0.73469	1	1506.1
367	0.02	0.12	0.12	0.73469	10	150.37
368	0.02	0.12	0.12	0.73469	15	100.36
369	0.02	0.12	0.12	0.73469	25	60.284
370	0.02	0.12	0.12	0.73469	35	43.103
371	0.02	0.12	0.12	0.73469	50	30.223
372	0.02	0.12	0.12	0.73469	75	20.224
373	0.02	0.12	0.12	0.73469	100	15.237
374	0.02	0.12	0.12	0.73469	150	10.265
375	0.02	0.12	0.12	0.73469	200	7.7876
376	0.02	0.12	0.12	0.73469	300	5.3145
377	0.02	0.12	0.12	0.73469	400	4.0805
378	0.02	0.12	0.12	0.73469	600	2.8496
379	0.02	0.12	0.16	0.7619	1	1113.6
380	0.02	0.12	0.16	0.7619	10	111.31
381	0.02	0.12	0.16	0.7619	15	74.27
382	0.02	0.12	0.16	0.7619	25	44.612
383	0.02	0.12	0.16	0.7619	35	31.902
384	0.02	0.12	0.16	0.7619	50	22.379
385	0.02	0.12	0.16	0.7619	75	14.988
386	0.02	0.12	0.16	0.7619	100	11.301
387	0.02	0.12	0.16	0.7619	150	7.6235
388	0.02	0.12	0.16	0.7619	200	5.7891
389	0.02	0.12	0.16	0.7619	300	3.9572
390	0.02	0.12	0.16	0.7619	400	3.0417
391	0.02	0.12	0.16	0.7619	600	2.1263
392	0.02	0.12	0.2	0.77922	1	929.63
393	0.02	0.12	0.2	0.77922	10	92.946
394	0.02	0.12	0.2	0.77922	15	62.007
395	0.02	0.12	0.2	0.77922	25	37.246
396	0.02	0.12	0.2	0.77922	35	26.638
397	0.02	0.12	0.2	0.77922	50	18.69
398	0.02	0.12	0.2	0.77922	75	12.521
399	0.02	0.12	0.2	0.77922	100	9.4428
400	0.02	0.12	0.2	0.77922	150	6.3709

	t/l	h/l	s/l	ϵ	Re_l	f_{unit}
401	0.02	0.12	0.2	0.77922	200	4.8374
402	0.02	0.12	0.2	0.77922	300	3.3046
403	0.02	0.12	0.2	0.77922	400	2.537
404	0.02	0.12	0.2	0.77922	600	1.7647
405	0.02	0.12	0.24	0.79121	1	826.61
406	0.02	0.12	0.24	0.79121	10	82.654
407	0.02	0.12	0.24	0.79121	15	55.136
408	0.02	0.12	0.24	0.79121	25	33.118
409	0.02	0.12	0.24	0.79121	35	23.686
410	0.02	0.12	0.24	0.79121	50	16.62
411	0.02	0.12	0.24			

	<i>t/l</i>	<i>h/l</i>	<i>s/l</i>	ϵ	<i>Re_l</i>	<i>f_{unit}</i>
481	0.02	0.16	0.12	0.7619	400	3.1639
482	0.02	0.16	0.12	0.7619	600	2.2245
483	0.02	0.16	0.16	0.79012	1	794.63
484	0.02	0.16	0.16	0.79012	10	79.417
485	0.02	0.16	0.16	0.79012	15	53.002
486	0.02	0.16	0.16	0.79012	25	31.848
487	0.02	0.16	0.16	0.79012	35	22.783
488	0.02	0.16	0.16	0.79012	50	15.992
489	0.02	0.16	0.16	0.79012	75	10.724
490	0.02	0.16	0.16	0.79012	100	8.0993
491	0.02	0.16	0.16	0.79012	150	5.4836
492	0.02	0.16	0.16	0.79012	200	4.18
493	0.02	0.16	0.16	0.79012	300	2.8784
494	0.02	0.16	0.16	0.79012	400	2.2271
495	0.02	0.16	0.16	0.79012	600	1.5735
496	0.02	0.16	0.2	0.80808	1	628.38
497	0.02	0.16	0.2	0.80808	10	62.818
498	0.02	0.16	0.2	0.80808	15	41.92
499	0.02	0.16	0.2	0.80808	25	25.193
500	0.02	0.16	0.2	0.80808	35	18.028
501	0.02	0.16	0.2	0.80808	50	12.663
502	0.02	0.16	0.2	0.80808	75	8.5017
503	0.02	0.16	0.2	0.80808	100	6.4279
504	0.02	0.16	0.2	0.80808	150	4.3606
505	0.02	0.16	0.2	0.80808	200	3.3294
506	0.02	0.16	0.2	0.80808	300	2.2983
507	0.02	0.16	0.2	0.80808	400	1.7805
508	0.02	0.16	0.2	0.80808	600	1.256
509	0.02	0.16	0.24	0.82051	1	536.82
510	0.02	0.16	0.24	0.82051	10	53.675
511	0.02	0.16	0.24	0.82051	15	35.816
512	0.02	0.16	0.24	0.82051	25	21.527
513	0.02	0.16	0.24	0.82051	35	15.408
514	0.02	0.16	0.24	0.82051	50	10.827
515	0.02	0.16	0.24	0.82051	75	7.2733
516	0.02	0.16	0.24	0.82051	100	5.5019
517	0.02	0.16	0.24	0.82051	150	3.7348
518	0.02	0.16	0.24	0.82051	200	2.8524
519	0.02	0.16	0.24	0.82051	300	1.9681
520	0.02	0.16	0.24	0.82051	400	1.5218
521	0.02	0.16	0.24	0.82051	600	1.0669
522	0.02	0.16	0.28	0.82963	1	480.35
523	0.02	0.16	0.28	0.82963	10	48.035
524	0.02	0.16	0.28	0.82963	15	32.051
525	0.02	0.16	0.28	0.82963	25	19.265
526	0.02	0.16	0.28	0.82963	35	13.791
527	0.02	0.16	0.28	0.82963	50	9.6918
528	0.02	0.16	0.28	0.82963	75	6.512
529	0.02	0.16	0.28	0.82963	100	4.9261
530	0.02	0.16	0.28	0.82963	150	3.3482
531	0.02	0.16	0.28	0.82963	200	2.5512
532	0.02	0.16	0.28	0.82963	300	1.7558
533	0.02	0.16	0.28	0.82963	400	1.353
534	0.02	0.16	0.28	0.82963	600	0.94135
535	0.02	0.16	0.32	0.8366	1	442.64
536	0.02	0.16	0.32	0.8366	10	44.267
537	0.02	0.16	0.32	0.8366	15	29.536
538	0.02	0.16	0.32	0.8366	25	17.753
539	0.02	0.16	0.32	0.8366	35	12.709
540	0.02	0.16	0.32	0.8366	50	8.9315
541	0.02	0.16	0.32	0.8366	75	6.0002
542	0.02	0.16	0.32	0.8366	100	4.5375
543	0.02	0.16	0.32	0.8366	150	3.0764
544	0.02	0.16	0.32	0.8366	200	2.3448
545	0.02	0.16	0.32	0.8366	300	1.6082
546	0.02	0.16	0.32	0.8366	400	1.2348
547	0.02	0.16	0.32	0.8366	600	0.85383
548	0.02	0.16	0.4	0.84656	1	396.09
549	0.02	0.16	0.4	0.84656	10	39.615
550	0.02	0.16	0.4	0.84656	15	26.429
551	0.02	0.16	0.4	0.84656	25	15.885
552	0.02	0.16	0.4	0.84656	35	11.37
553	0.02	0.16	0.4	0.84656	50	7.9882
554	0.02	0.16	0.4	0.84656	75	5.3624
555	0.02	0.16	0.4	0.84656	100	4.0512
556	0.02	0.16	0.4	0.84656	150	2.7396
557	0.02	0.16	0.4	0.84656	200	2.0816
558	0.02	0.16	0.4	0.84656	300	1.4183
559	0.02	0.16	0.4	0.84656	400	1.0827
560	0.02	0.16	0.4	0.84656	600	0.74196

	<i>t/l</i>	<i>h/l</i>	<i>s/l</i>	ϵ	<i>Re_l</i>	<i>f_{unit}</i>
561	0.02	0.16	0.48	0.85333	1	368.81
562	0.02	0.16	0.48	0.85333	10	36.887
563	0.02	0.16	0.48	0.85333	15	24.608
564	0.02	0.16	0.48	0.85333	25	14.787
565	0.02	0.16	0.48	0.85333	35	10.582
566	0.02	0.16	0.48	0.85333	50	7.4317
567	0.02	0.16	0.48	0.85333	75	4.9843
568	0.02	0.16	0.48	0.85333	100	3.7615
569	0.02	0.16	0.48	0.85333	150	2.5373
570	0.02	0.16	0.48	0.85333	200	1.9228
571	0.02	0.16	0.48	0.85333	300	1.304
572	0.02	0.16	0.48	0.85333	400	0.99168
573	0.02	0.16	0.48	0.85333	600	0.67583
574	0.02	0.2	0.12	0.77922	1	988.26
575	0.02	0.2	0.12	0.77922	10	98.699
576	0.02	0.2	0.12	0.77922	15	65.903
577	0.02	0.2	0.12	0.77922	25	39.605
578	0.02	0.2	0.12	0.77922	35	28.323
579	0.02	0.2	0.12	0.77922	50	19.868
580	0.02	0.2	0.12	0.77922	75	13.303
581	0.02	0.2	0.12	0.77922	100	10.032
582	0.02	0.2	0.12	0.77922	150	6.774
583	0.02	0.2	0.12	0.77922	200	5.152
584	0.02	0.2	0.12	0.77922	300	3.5345
585	0.02	0.2	0.12	0.77922	400	2.7258
586	0.02	0.2	0.12	0.77922	600	1.9195
587	0.02	0.2	0.16	0.80808	1	648.13
588	0.02	0.2	0.16	0.80808	10	64.765
589	0.02	0.2	0.16	0.80808	15	43.231
590	0.02	0.2	0.16	0.80808	25	25.984
591	0.02	0.2	0.16	0.80808	35	18.592
592	0.02	0.2	0.16	0.80808	50	13.055
593	0.02	0.2	0.16	0.80808	75	8.762
594	0.02	0.2	0.16	0.80808	100	6.6239
595	0.02	0.2	0.16	0.80808	150	4.495
596	0.02	0.2	0.16	0.80808	200	3.4344
597	0.02	0.2	0.16	0.80808	300	2.3752
598	0.02	0.2	0.16	0.80808	400	1.8444
599	0.02	0.2	0.16	0.80808	600	1.313
600	0.02	0.2	0.2	0.82645	1	491.15
601	0.02	0.2	0.2	0.82645	10	49.412
602	0.02	0.2	0.2	0.82645	15	32.769
603	0.02	0.2	0.2	0.82645	25	19.701
604	0.02	0.2	0.2	0.82645	35	14.104
605	0.02	0.2	0.2	0.82645	50	9.9146
606	0.02	0.2	0.2	0.82645	75	6.6679
607	0.02	0.2	0.2	0.82645	100	5.0514
608	0.02	0.2	0.2	0.82645	150	3.4411
609	0.02	0.2	0.2	0.82645	200	2.6382
610	0.02	0.2	0.2	0.82645	300	1.8345
611	0.02	0.2	0.2	0.82645	400	1.4295
612	0.02	0.2	0.2	0.82645	600	1.0158
613	0.02	0.2	0.24	0.83916	1	405.28
614	0.02	0.2	0.24	0.83916	10	40.521
615	0.02	0.2	0.24	0.83916	15	27.046
616	0.02	0.2	0.24	0.83916	25	16.265
617	0.02	0.2	0.24	0.83916	35	11.65
618	0.02	0.2	0.24	0.83916	50	8.1964
619	0.02	0.2	0.24	0.83916	75	5.5205
620	0.02	0.2	0.24	0.83916	100	4.1879
621	0.02	0.2	0.24	0.83916	150	2.8598
622	0.02	0.2	0.24	0.83916	200	2.1964
623	0.02	0.2	0.24	0.83916	300	1.53
624	0.02	0.2	0.24	0.83916	400	1.1915
625	0.02	0.2	0.24	0.83916	600	0.84244
626	0.02	0.2	0.28	0.84848	1	352.78
627	0.02	0.2	0.28	0.84848	10	35.279
628	0.02	0.2	0.28	0.84848	15	23.547
629	0.02	0.2	0.28	0.84848	25	14.164
630	0.02	0.2	0.28	0.84848	35	10.149
631	0.02	0.2	0.28	0.84848	50	7.1443
632	0.02	0.2	0.28	0.84848	75	4.8162
633	0.02	0.2	0.28	0.84848	100	3.6563
634	0.02	0.2	0.28	0.84848	150	2.4991
635	0.02	0.2	0.28	0.84848	200	1.9198
636	0.02	0.2	0.28	0.84848	300	1.3552
637	0.02	0.2	0.28	0.84848	400	1.0366
638	0.02	0.2	0.28	0.84848	600	0.72728
639	0.02	0.2	0.32	0.85561	1	318.06
640	0.02	0.2	0.32	0.85561	10	31.811

	<i>t/l</i>	<i>h/l</i>	<i>s/l</i>	ϵ	<i>Re_l</i>	<i>f_{unit}</i>
641	0.02	0.2	0.32	0.85561	15	21.233
642	0.02	0.2	0.32	0.85561	25	12.774
643	0.02	0.2	0.32	0.85561	35	9.1544
644	0.02	0.2	0.32	0.85561	50	6.4465
645	0.02	0.2	0.32	0.85561	75	4.3474
646	0.02	0.2	0.32	0.85561	100	3.301
647	0.02	0.2	0.32	0.85561	150	2.2557
648	0.02	0.2	0.32	0.85561	200	1.7312
649	0.02	0.2	0.32	0.85561	300	1.1998
650	0.02	0.2	0.32	0.85561	400	0.9276
651	0.02	0.2	0.32	0.85561	600	0.64638
652	0.02	0.2	0.4	0.8658	1	275.81

	<i>t/l</i>	<i>h/l</i>	<i>s/l</i>	ϵ	<i>Re_l</i>	<i>f_{unit}</i>
721	0.02	0.24	0.24	0.85207	35	9.6209
722	0.02	0.24	0.24	0.85207	50	6.7756
723	0.02	0.24	0.24	0.85207	75	4.573
724	0.02	0.24	0.24	0.85207	100	3.477
725	0.02	0.24	0.24	0.85207	150	2.3849
726	0.02	0.24	0.24	0.85207	200	1.8392
727	0.02	0.24	0.24	0.85207	300	1.2898
728	0.02	0.24	0.24	0.85207	400	1.0093
729	0.02	0.24	0.24	0.85207	600	0.71831
730	0.02	0.24	0.28	0.86154	1	284.13
731	0.02	0.24	0.28	0.86154	10	28.415
732	0.02	0.24	0.28	0.86154	15	18.971
733	0.02	0.24	0.28	0.86154	25	11.419
734	0.02	0.24	0.28	0.86154	35	8.188
735	0.02	0.24	0.28	0.86154	50	5.7726
736	0.02	0.24	0.28	0.86154	75	3.9027
737	0.02	0.24	0.28	0.86154	100	2.9721
738	0.02	0.24	0.28	0.86154	150	2.0437
739	0.02	0.24	0.28	0.86154	200	1.5782
740	0.02	0.24	0.28	0.86154	300	1.1064
741	0.02	0.24	0.28	0.86154	400	0.86335
742	0.02	0.24	0.28	0.86154	600	0.60958
743	0.02	0.24	0.32	0.86878	1	251.1
744	0.02	0.24	0.32	0.86878	10	25.117
745	0.02	0.24	0.32	0.86878	15	16.77
746	0.02	0.24	0.32	0.86878	25	10.098
747	0.02	0.24	0.32	0.86878	35	7.2443
748	0.02	0.24	0.32	0.86878	50	5.1112
749	0.02	0.24	0.32	0.86878	75	3.4596
750	0.02	0.24	0.32	0.86878	100	2.6369
751	0.02	0.24	0.32	0.86878	150	1.8148
752	0.02	0.24	0.32	0.86878	200	1.4009
753	0.02	0.24	0.32	0.86878	300	0.97899
754	0.02	0.24	0.32	0.86878	400	0.76064
755	0.02	0.24	0.32	0.86878	600	0.53283
756	0.02	0.24	0.4	0.87912	1	211.26
757	0.02	0.24	0.4	0.87912	10	21.138
758	0.02	0.24	0.4	0.87912	15	14.115
759	0.02	0.24	0.4	0.87912	25	8.5024
760	0.02	0.24	0.4	0.87912	35	6.1032
761	0.02	0.24	0.4	0.87912	50	4.3091
762	0.02	0.24	0.4	0.87912	75	2.9187
763	0.02	0.24	0.4	0.87912	100	2.2246
764	0.02	0.24	0.4	0.87912	150	1.5279
765	0.02	0.24	0.4	0.87912	200	1.175
766	0.02	0.24	0.4	0.87912	300	0.81367
767	0.02	0.24	0.4	0.87912	400	0.62714
768	0.02	0.24	0.4	0.87912	600	0.43456
769	0.02	0.24	0.48	0.88615	1	188.65
770	0.02	0.24	0.48	0.88615	10	18.879
771	0.02	0.24	0.48	0.88615	15	12.606
772	0.02	0.24	0.48	0.88615	25	7.5946
773	0.02	0.24	0.48	0.88615	35	5.4528
774	0.02	0.24	0.48	0.88615	50	3.849
775	0.02	0.24	0.48	0.88615	75	2.605
776	0.02	0.24	0.48	0.88615	100	1.9826
777	0.02	0.24	0.48	0.88615	150	1.3557
778	0.02	0.24	0.48	0.88615	200	1.0377
779	0.02	0.24	0.48	0.88615	300	0.71297
780	0.02	0.24	0.48	0.88615	400	0.54647
781	0.02	0.24	0.48	0.88615	600	0.37595
782	0.02	0.28	0.12	0.8	1	837.25
783	0.02	0.28	0.12	0.8	10	83.57
784	0.02	0.28	0.12	0.8	15	55.818
785	0.02	0.28	0.12	0.8	25	33.555
786	0.02	0.28	0.12	0.8	35	24
787	0.02	0.28	0.12	0.8	50	16.837
788	0.02	0.28	0.12	0.8	75	11.274
789	0.02	0.28	0.12	0.8	100	8.5014
790	0.02	0.28	0.12	0.8	150	5.7418
791	0.02	0.28	0.12	0.8	200	4.3689
792	0.02	0.28	0.12	0.8	300	3
793	0.02	0.28	0.12	0.8	400	2.3159
794	0.02	0.28	0.12	0.8	600	1.6333
795	0.02	0.28	0.16	0.82963	1	518.27
796	0.02	0.28	0.16	0.82963	10	51.77
797	0.02	0.28	0.16	0.82963	15	34.567
798	0.02	0.28	0.16	0.82963	25	20.783
799	0.02	0.28	0.16	0.82963	35	14.874
800	0.02	0.28	0.16	0.82963	50	10.448

	<i>t/l</i>	<i>h/l</i>	<i>s/l</i>	ϵ	<i>Re_l</i>	<i>f_{unit}</i>
801	0.02	0.28	0.16	0.82963	75	7.0172
802	0.02	0.28	0.16	0.82963	100	5.3095
803	0.02	0.28	0.16	0.82963	150	3.6102
804	0.02	0.28	0.16	0.82963	200	2.764
805	0.02	0.28	0.16	0.82963	300	1.9186
806	0.02	0.28	0.16	0.82963	400	1.495
807	0.02	0.28	0.16	0.82963	600	1.0666
808	0.02	0.28	0.2	0.84848	1	371.43
809	0.02	0.28	0.2	0.84848	10	37.12
810	0.02	0.28	0.2	0.84848	15	24.784
811	0.02	0.28	0.2	0.84848	25	14.91
812	0.02	0.28	0.2	0.84848	35	10.678
813	0.02	0.28	0.2	0.84848	50	7.5133
814	0.02	0.28	0.2	0.84848	75	5.0626
815	0.02	0.28	0.2	0.84848	100	3.8439
816	0.02	0.28	0.2	0.84848	150	2.6308
817	0.02	0.28	0.2	0.84848	200	2.0256
818	0.02	0.28	0.2	0.84848	300	1.4193
819	0.02	0.28	0.2	0.84848	400	1.1129
820	0.02	0.28	0.2	0.84848	600	0.79913
821	0.02	0.28	0.24	0.86154	1	291.43
822	0.02	0.28	0.24	0.86154	10	29.137
823	0.02	0.28	0.24	0.86154	15	19.455
824	0.02	0.28	0.24	0.86154	25	11.709
825	0.02	0.28	0.24	0.86154	35	8.3947
826	0.02	0.28	0.24	0.86154	50	5.9164
827	0.02	0.28	0.24	0.86154	75	3.999
828	0.02	0.28	0.24	0.86154	100	3.0456
829	0.02	0.28	0.24	0.86154	150	2.096
830	0.02	0.28	0.24	0.86154	200	1.6208
831	0.02	0.28	0.24	0.86154	300	1.142
832	0.02	0.28	0.24	0.86154	400	0.89665
833	0.02	0.28	0.24	0.86154	600	0.64016
834	0.02	0.28	0.28	0.87111	1	242.82
835	0.02	0.28	0.28	0.87111	10	24.284
836	0.02	0.28	0.28	0.87111	15	16.217
837	0.02	0.28	0.28	0.87111	25	9.766
838	0.02	0.28	0.28	0.87111	35	7.0076
839	0.02	0.28	0.28	0.87111	50	4.9463
840	0.02	0.28	0.28	0.87111	75	3.352
841	0.02	0.28	0.28	0.87111	100	2.5589
842	0.02	0.28	0.28	0.87111	150	1.7676
843	0.02	0.28	0.28	0.87111	200	1.3704
844	0.02	0.28	0.28	0.87111	300	0.96623
845	0.02	0.28	0.28	0.87111	400	0.75679
846	0.02	0.28	0.28	0.87111	600	0.53676
847	0.02	0.28	0.32	0.87843	1	210.9
848	0.02	0.28	0.32	0.87843	10	21.098
849	0.02	0.28	0.32	0.87843	15	14.091
850	0.02	0.28	0.32	0.87843	25	8.4905
851	0.02	0.28	0.32	0.87843	35	6.0969
852	0.02	0.28	0.32	0.87843	50	4.3089
853	0.02	0.28	0.32	0.87843	75	2.9258
854	0.02	0.28	0.32	0.87843	100	2.2373
855	0.02	0.28	0.32	0.87843	150	1.5485
856	0.02	0.28	0.32	0.87843	200	1.201
857	0.02	0.28	0.32	0.87843	300	0.84445
858	0.02	0.28	0.32	0.87843	400	0.65859
859	0.02	0.28	0.32	0.87843	600	0.46355
860	0.02	0.28	0.4	0.88889	1	171.61
861	0.02	0.28	0.4	0.88889	10	17.271
862	0.02	0.28	0.4	0.88889	15	11.538
863	0.02	0.28	0.4	0.88889	25	6.958
864	0.02	0.28	0.4	0.88889	35	5.0017
865	0.02	0.28	0.4	0.88889	50	3.5404
866	0.02	0.28	0.4	0.88889	75	2.4088
867	0.02	0.28	0.4	0.88889	100	1.8438
868	0.02	0.28	0.4	0.88889	150	1.2751
869	0.02	0.28	0.4	0.88889	200	0.98538
870	0.02	0.28	0.4	0.88889	300	0.6863
871	0.02	0.28	0.4	0.88889	400	0.53069
872	0.02	0.28	0.4	0.88889	600	0.36964
873	0.02	0.28	0.48	0.896	1	150.4
874	0.02	0.28	0.48	0.896	10	15.116
875	0.02	0.28	0.48	0.896	15	10.099
876	0.02	0.28	0.48	0.896	25	6.0931
877	0.02	0.28	0.48	0.896	35	4.382
878	0.02	0.28	0.48	0.896	50	3.1032
879	0.02	0.28	0.48	0.896	75	2.111
880	0.02	0.28	0.48	0.896	100	1.6138

	<i>t/l</i>	<i>h/l</i>	<i>s/l</i>	ϵ	<i>Re_l</i>	<i>f_{unit}</i>
881	0.02	0.28	0.48	0.896	150	1.1109
882	0.02	0.28	0.48	0.896	200	0.85398
883	0.02	0.28	0.48	0.896	300	0.58954
884	0.02	0.28	0.48	0.896	400	0.45314
885	0.02	0.28	0.48	0.896	600	0.31297
886	0.02	0.32	0.12	0.80672	1	797.26
887	0.02	0.32	0.12	0.80672	10	79.558
888	0.02	0.32	0.12	0.80672	15	53.144
889	0.02	0.32	0.12	0.80672	25	31.952
890	0.02	0.32	0.12	0.80672	35	22.854
891	0.02	0.32	0.12	0.80672	50	16.034
892	0.02	0.32	0.12	0.8067		

	t/l	h/l	s/l	ϵ	Re_l	f_{unit}
961	0.02	0.32	0.32	0.88581	300	0.75552
962	0.02	0.32	0.32	0.88581	400	0.59083
963	0.02	0.32	0.32	0.88581	600	0.41741
964	0.02	0.32	0.4	0.89636	1	146.68
965	0.02	0.32	0.4	0.89636	10	14.768
966	0.02	0.32	0.4	0.89636	15	9.869
967	0.02	0.32	0.4	0.89636	25	5.9579
968	0.02	0.32	0.4	0.89636	35	4.2886
969	0.02	0.32	0.4	0.89636	50	3.0426
970	0.02	0.32	0.4	0.89636	75	2.0784
971	0.02	0.32	0.4	0.89636	100	1.5968
972	0.02	0.32	0.4	0.89636	150	1.1107
973	0.02	0.32	0.4	0.89636	200	0.86165
974	0.02	0.32	0.4	0.89636	300	0.60285
975	0.02	0.32	0.4	0.89636	400	0.46745
976	0.02	0.32	0.4	0.89636	600	0.32646
977	0.02	0.32	0.48	0.90353	1	126.06
978	0.02	0.32	0.48	0.90353	10	12.682
979	0.02	0.32	0.48	0.90353	15	8.4775
980	0.02	0.32	0.48	0.90353	25	5.1229
981	0.02	0.32	0.48	0.90353	35	3.6907
982	0.02	0.32	0.48	0.90353	50	2.6216
983	0.02	0.32	0.48	0.90353	75	1.792
984	0.02	0.32	0.48	0.90353	100	1.3755
985	0.02	0.32	0.48	0.90353	150	0.95243
986	0.02	0.32	0.48	0.90353	200	0.73472
987	0.02	0.32	0.48	0.90353	300	0.50922
988	0.02	0.32	0.48	0.90353	400	0.39243
989	0.02	0.32	0.48	0.90353	600	0.27188
990	0.02	0.4	0.12	0.81633	1	746.23
991	0.02	0.4	0.12	0.81633	10	74.433
992	0.02	0.4	0.12	0.81633	15	49.73
993	0.02	0.4	0.12	0.81633	25	29.906
994	0.02	0.4	0.12	0.81633	35	21.392
995	0.02	0.4	0.12	0.81633	50	15.008
996	0.02	0.4	0.12	0.81633	75	10.047
997	0.02	0.4	0.12	0.81633	100	7.5778
998	0.02	0.4	0.12	0.81633	150	5.1146
999	0.02	0.4	0.12	0.81633	200	3.8906
1000	0.02	0.4	0.12	0.81633	300	2.6712
1001	0.02	0.4	0.12	0.81633	400	2.0644
1002	0.02	0.4	0.12	0.81633	600	1.4557
1003	0.02	0.4	0.16	0.84656	1	444.13
1004	0.02	0.4	0.16	0.84656	10	44.342
1005	0.02	0.4	0.16	0.84656	15	29.614
1006	0.02	0.4	0.16	0.84656	25	17.811
1007	0.02	0.4	0.16	0.84656	35	12.749
1008	0.02	0.4	0.16	0.84656	50	8.9603
1009	0.02	0.4	0.16	0.84656	75	6.0158
1010	0.02	0.4	0.16	0.84656	100	4.553
1011	0.02	0.4	0.16	0.84656	150	3.0978
1012	0.02	0.4	0.16	0.84656	200	2.3734
1013	0.02	0.4	0.16	0.84656	300	1.6492
1014	0.02	0.4	0.16	0.84656	400	1.2871
1015	0.02	0.4	0.16	0.84656	600	0.92169
1016	0.02	0.4	0.2	0.8658	1	305.31
1017	0.02	0.4	0.2	0.8658	10	30.502
1018	0.02	0.4	0.2	0.8658	15	20.37
1019	0.02	0.4	0.2	0.8658	25	12.258
1020	0.02	0.4	0.2	0.8658	35	8.7827
1021	0.02	0.4	0.2	0.8658	50	6.1823
1022	0.02	0.4	0.2	0.8658	75	4.1699
1023	0.02	0.4	0.2	0.8658	100	3.1692
1024	0.02	0.4	0.2	0.8658	150	2.1734
1025	0.02	0.4	0.2	0.8658	200	1.6779
1026	0.02	0.4	0.2	0.8658	300	1.1802
1027	0.02	0.4	0.2	0.8658	400	0.92888
1028	0.02	0.4	0.2	0.8658	600	0.66975
1029	0.02	0.4	0.24	0.87912	1	229.77
1030	0.02	0.4	0.24	0.87912	10	22.967
1031	0.02	0.4	0.24	0.87912	15	15.341
1032	0.02	0.4	0.24	0.87912	25	9.2386
1033	0.02	0.4	0.24	0.87912	35	6.6277
1034	0.02	0.4	0.24	0.87912	50	4.6767
1035	0.02	0.4	0.24	0.87912	75	3.1678
1036	0.02	0.4	0.24	0.87912	100	2.4182
1037	0.02	0.4	0.24	0.87912	150	1.672
1038	0.02	0.4	0.24	0.87912	200	1.2988
1039	0.02	0.4	0.24	0.87912	300	0.92147
1040	0.02	0.4	0.24	0.87912	400	0.72757

	t/l	h/l	s/l	ϵ	Re_l	f_{unit}
1041	0.02	0.4	0.24	0.87912	600	0.52412
1042	0.02	0.4	0.28	0.88889	1	182.01
1043	0.02	0.4	0.28	0.88889	10	18.394
1044	0.02	0.4	0.28	0.88889	15	12.289
1045	0.02	0.4	0.28	0.88889	25	7.4079
1046	0.02	0.4	0.28	0.88889	35	5.3218
1047	0.02	0.4	0.28	0.88889	50	3.7644
1048	0.02	0.4	0.28	0.88889	75	2.5612
1049	0.02	0.4	0.28	0.88889	100	1.9633
1050	0.02	0.4	0.28	0.88889	150	1.3666
1051	0.02	0.4	0.28	0.88889	200	1.0663
1052	0.02	0.4	0.28	0.88889	300	0.75904
1053	0.02	0.4	0.28	0.88889	400	0.59864
1054	0.02	0.4	0.28	0.88889	600	0.42813
1055	0.02	0.4	0.32	0.89636	1	152.6
1056	0.02	0.4	0.32	0.89636	10	15.398
1057	0.02	0.4	0.32	0.89636	15	10.291
1058	0.02	0.4	0.32	0.89636	25	6.2099
1059	0.02	0.4	0.32	0.89636	35	4.4676
1060	0.02	0.4	0.32	0.89636	50	3.1679
1061	0.02	0.4	0.32	0.89636	75	2.1641
1062	0.02	0.4	0.32	0.89636	100	1.6646
1063	0.02	0.4	0.32	0.89636	150	1.1642
1064	0.02	0.4	0.32	0.89636	200	0.91038
1065	0.02	0.4	0.32	0.89636	300	0.64729
1066	0.02	0.4	0.32	0.89636	400	0.50825
1067	0.02	0.4	0.32	0.89636	600	0.36056
1068	0.02	0.4	0.4	0.90703	1	117.24
1069	0.02	0.4	0.4	0.90703	10	11.818
1070	0.02	0.4	0.4	0.90703	15	7.9042
1071	0.02	0.4	0.4	0.90703	25	4.7796
1072	0.02	0.4	0.4	0.90703	35	3.4479
1073	0.02	0.4	0.4	0.90703	50	2.4618
1074	0.02	0.4	0.4	0.90703	75	1.6874
1075	0.02	0.4	0.4	0.90703	100	1.3035
1076	0.02	0.4	0.4	0.90703	150	0.9143
1077	0.02	0.4	0.4	0.90703	200	0.71317
1078	0.02	0.4	0.4	0.90703	300	0.50269
1079	0.02	0.4	0.4	0.90703	400	0.39111
1080	0.02	0.4	0.4	0.90703	600	0.27453
1081	0.02	0.4	0.48	0.91429	1	97.474
1082	0.02	0.4	0.48	0.91429	10	9.8217
1083	0.02	0.4	0.48	0.91429	15	6.5723
1084	0.02	0.4	0.48	0.91429	25	3.9819
1085	0.02	0.4	0.48	0.91429	35	2.8784
1086	0.02	0.4	0.48	0.91429	50	2.0555
1087	0.02	0.4	0.48	0.91429	75	1.4165
1088	0.02	0.4	0.48	0.91429	100	1.0945
1089	0.02	0.4	0.48	0.91429	150	0.76454
1090	0.02	0.4	0.48	0.91429	200	0.59291
1091	0.02	0.4	0.48	0.91429	300	0.41353
1092	0.02	0.4	0.48	0.91429	400	0.32002
1093	0.02	0.4	0.48	0.91429	600	0.2234
1094	0.02	0.48	0.12	0.82286	1	715.1
1095	0.02	0.48	0.12	0.82286	10	71.306
1096	0.02	0.48	0.12	0.82286	15	47.644
1097	0.02	0.48	0.12	0.82286	25	28.656
1098	0.02	0.48	0.12	0.82286	35	20.5
1099	0.02	0.48	0.12	0.82286	50	14.379
1100	0.02	0.48	0.12	0.82286	75	9.6314
1101	0.02	0.48	0.12	0.82286	100	7.2615
1102	0.02	0.48	0.12	0.82286	150	4.9029
1103	0.02	0.48	0.12	0.82286	200	3.7261
1104	0.02	0.48	0.12	0.82286	300	2.5578
1105	0.02	0.48	0.12	0.82286	400	1.9777
1106	0.02	0.48	0.12	0.82286	600	1.3945
1107	0.02	0.48	0.16	0.85333	1	419.87
1108	0.02	0.48	0.16	0.85333	10	41.908
1109	0.02	0.48	0.16	0.85333	15	27.991
1110	0.02	0.48	0.16	0.85333	25	16.837
1111	0.02	0.48	0.16	0.85333	35	12.052
1112	0.02	0.48	0.16	0.85333	50	8.4665
1113	0.02	0.48	0.16	0.85333	75	5.6866
1114	0.02	0.48	0.16	0.85333	100	4.3031
1115	0.02	0.48	0.16	0.85333	150	2.9288
1116	0.02	0.48	0.16	0.85333	200	2.2422
1117	0.02	0.48	0.16	0.85333	300	1.5612
1118	0.02	0.48	0.16	0.85333	400	1.2196
1119	0.02	0.48	0.16	0.85333	600	0.87344
1120	0.02	0.48	0.2	0.87273	1	284.41

	t/l	h/l	s/l	ϵ	Re_l	f_{unit}
1121	0.02	0.48	0.2	0.87273	10	28.408
1122	0.02	0.48	0.2	0.87273	15	18.974
1123	0.02	0.48	0.2	0.87273	25	11.419
1124	0.02	0.48	0.2	0.87273	35	8.1822
1125	0.02	0.48	0.2	0.87273	50	5.7599
1126	0.02	0.48	0.2	0.87273	75	3.8849
1127	0.02	0.48	0.2	0.87273	100	2.9536
1128	0.02	0.48	0.2	0.87273	150	2.0272
1129	0.02	0.48	0.2	0.87273	200	1.5657
1130	0.02	0.48	0.2	0.87273	300	1.1032
1131	0.02	0.48				

	t/l	h/l	s/l	ϵ	Re_l	f_{unit}
1201	0.02	0.56	0.12	0.82759	35	19.899
1202	0.02	0.56	0.12	0.82759	50	13.959
1203	0.02	0.56	0.12	0.82759	75	9.3444
1204	0.02	0.56	0.12	0.82759	100	7.0443
1205	0.02	0.56	0.12	0.82759	150	4.7545
1206	0.02	0.56	0.12	0.82759	200	3.6153
1207	0.02	0.56	0.12	0.82759	300	2.4811
1208	0.02	0.56	0.12	0.82759	400	1.9158
1209	0.02	0.56	0.12	0.82759	600	1.3537
1210	0.02	0.56	0.16	0.85824	1	403.89
1211	0.02	0.56	0.16	0.85824	10	40.302
1212	0.02	0.56	0.16	0.85824	15	26.922
1213	0.02	0.56	0.16	0.85824	25	16.195
1214	0.02	0.56	0.16	0.85824	35	11.593
1215	0.02	0.56	0.16	0.85824	50	8.1438
1216	0.02	0.56	0.16	0.85824	75	5.4691
1217	0.02	0.56	0.16	0.85824	100	4.1397
1218	0.02	0.56	0.16	0.85824	150	2.8143
1219	0.02	0.56	0.16	0.85824	200	2.1559
1220	0.02	0.56	0.16	0.85824	300	1.5018
1221	0.02	0.56	0.16	0.85824	400	1.174
1222	0.02	0.56	0.16	0.85824	600	0.84312
1223	0.02	0.56	0.2	0.87774	1	270.93
1224	0.02	0.56	0.2	0.87774	10	27.056
1225	0.02	0.56	0.2	0.87774	15	18.072
1226	0.02	0.56	0.2	0.87774	25	10.877
1227	0.02	0.56	0.2	0.87774	35	7.7942
1228	0.02	0.56	0.2	0.87774	50	5.4867
1229	0.02	0.56	0.2	0.87774	75	3.7003
1230	0.02	0.56	0.2	0.87774	100	2.8135
1231	0.02	0.56	0.2	0.87774	150	1.9313
1232	0.02	0.56	0.2	0.87774	200	1.4922
1233	0.02	0.56	0.2	0.87774	300	1.0507
1234	0.02	0.56	0.2	0.87774	400	0.82875
1235	0.02	0.56	0.2	0.87774	600	0.60164
1236	0.02	0.56	0.24	0.89125	1	198.69
1237	0.02	0.56	0.24	0.89125	10	19.854
1238	0.02	0.56	0.24	0.89125	15	13.264
1239	0.02	0.56	0.24	0.89125	25	7.9905
1240	0.02	0.56	0.24	0.89125	35	5.7337
1241	0.02	0.56	0.24	0.89125	50	4.047
1242	0.02	0.56	0.24	0.89125	75	2.7429
1243	0.02	0.56	0.24	0.89125	100	2.0959
1244	0.02	0.56	0.24	0.89125	150	1.4512
1245	0.02	0.56	0.24	0.89125	200	1.1294
1246	0.02	0.56	0.24	0.89125	300	0.80451
1247	0.02	0.56	0.24	0.89125	400	0.63844
1248	0.02	0.56	0.24	0.89125	600	0.46207
1249	0.02	0.56	0.28	0.90115	1	153.15
1250	0.02	0.56	0.28	0.90115	10	15.486
1251	0.02	0.56	0.28	0.90115	15	10.349
1252	0.02	0.56	0.28	0.90115	25	6.2419
1253	0.02	0.56	0.28	0.90115	35	4.4866
1254	0.02	0.56	0.28	0.90115	50	3.1762
1255	0.02	0.56	0.28	0.90115	75	2.1645
1256	0.02	0.56	0.28	0.90115	100	1.6619
1257	0.02	0.56	0.28	0.90115	150	1.1609
1258	0.02	0.56	0.28	0.90115	200	0.90958
1259	0.02	0.56	0.28	0.90115	300	0.65155
1260	0.02	0.56	0.28	0.90115	400	0.51575
1261	0.02	0.56	0.28	0.90115	600	0.37111
1262	0.02	0.56	0.32	0.90872	1	124.95
1263	0.02	0.56	0.32	0.90872	10	12.626
1264	0.02	0.56	0.32	0.90872	15	8.4414
1265	0.02	0.56	0.32	0.90872	25	5.0985
1266	0.02	0.56	0.32	0.90872	35	3.6717
1267	0.02	0.56	0.32	0.90872	50	2.6079
1268	0.02	0.56	0.32	0.90872	75	1.7868
1269	0.02	0.56	0.32	0.90872	100	1.3785
1270	0.02	0.56	0.32	0.90872	150	0.96953
1271	0.02	0.56	0.32	0.90872	200	0.76161
1272	0.02	0.56	0.32	0.90872	300	0.54522
1273	0.02	0.56	0.32	0.90872	400	0.43013
1274	0.02	0.56	0.32	0.90872	600	0.30739
1275	0.02	0.56	0.4	0.91954	1	91.206
1276	0.02	0.56	0.4	0.91954	10	9.2115
1277	0.02	0.56	0.4	0.91954	15	6.1699
1278	0.02	0.56	0.4	0.91954	25	3.7361
1279	0.02	0.56	0.4	0.91954	35	2.7017
1280	0.02	0.56	0.4	0.91954	50	1.9314

	t/l	h/l	s/l	ϵ	Re_l	f_{unit}
1281	0.02	0.56	0.4	0.91954	75	1.336
1282	0.02	0.56	0.4	0.91954	100	1.038
1283	0.02	0.56	0.4	0.91954	150	0.73476
1284	0.02	0.56	0.4	0.91954	200	0.57688
1285	0.02	0.56	0.4	0.91954	300	0.40968
1286	0.02	0.56	0.4	0.91954	400	0.32066
1287	0.02	0.56	0.4	0.91954	600	0.22688
1288	0.02	0.56	0.48	0.9269	1	72.399
1289	0.02	0.56	0.48	0.9269	10	7.3123
1290	0.02	0.56	0.48	0.9269	15	4.9002
1291	0.02	0.56	0.48	0.9269	25	2.9799
1292	0.02	0.56	0.48	0.9269	35	2.1633
1293	0.02	0.56	0.48	0.9269	50	1.5549
1294	0.02	0.56	0.48	0.9269	75	1.0823
1295	0.02	0.56	0.48	0.9269	100	0.84276
1296	0.02	0.56	0.48	0.9269	150	0.59483
1297	0.02	0.56	0.48	0.9269	200	0.46428
1298	0.02	0.56	0.48	0.9269	300	0.32645
1299	0.02	0.56	0.48	0.9269	400	0.25365
1300	0.02	0.68	0.12	0.83265	1	672.99
1301	0.02	0.68	0.12	0.83265	10	67.063
1302	0.02	0.68	0.12	0.83265	15	44.82
1303	0.02	0.68	0.12	0.83265	25	26.964
1304	0.02	0.68	0.12	0.83265	35	19.292
1305	0.02	0.68	0.12	0.83265	50	13.534
1306	0.02	0.68	0.12	0.83265	75	9.0598
1307	0.02	0.68	0.12	0.83265	100	6.8339
1308	0.02	0.68	0.12	0.83265	150	4.6082
1309	0.02	0.68	0.12	0.83265	200	3.5089
1310	0.02	0.68	0.12	0.83265	300	2.4037
1311	0.02	0.68	0.12	0.83265	400	1.8605
1312	0.02	0.68	0.12	0.83265	600	1.3084
1313	0.02	0.68	0.16	0.86349	1	388.07
1314	0.02	0.68	0.16	0.86349	10	38.712
1315	0.02	0.68	0.16	0.86349	15	25.862
1316	0.02	0.68	0.16	0.86349	25	15.559
1317	0.02	0.68	0.16	0.86349	35	11.138
1318	0.02	0.68	0.16	0.86349	50	7.8269
1319	0.02	0.68	0.16	0.86349	75	5.2546
1320	0.02	0.68	0.16	0.86349	100	3.9766
1321	0.02	0.68	0.16	0.86349	150	2.7053
1322	0.02	0.68	0.16	0.86349	200	2.0732
1323	0.02	0.68	0.16	0.86349	300	1.4397
1324	0.02	0.68	0.16	0.86349	400	1.1286
1325	0.02	0.68	0.16	0.86349	600	0.80829
1326	0.02	0.68	0.2	0.88312	1	257.84
1327	0.02	0.68	0.2	0.88312	10	25.74
1328	0.02	0.68	0.2	0.88312	15	17.195
1329	0.02	0.68	0.2	0.88312	25	10.35
1330	0.02	0.68	0.2	0.88312	35	7.4166
1331	0.02	0.68	0.2	0.88312	50	5.2206
1332	0.02	0.68	0.2	0.88312	75	3.5204
1333	0.02	0.68	0.2	0.88312	100	2.6757
1334	0.02	0.68	0.2	0.88312	150	1.8375
1335	0.02	0.68	0.2	0.88312	200	1.418
1336	0.02	0.68	0.2	0.88312	300	1.0022
1337	0.02	0.68	0.2	0.88312	400	0.79169
1338	0.02	0.68	0.2	0.88312	600	0.57264
1339	0.02	0.68	0.24	0.8967	1	187.17
1340	0.02	0.68	0.24	0.8967	10	18.698
1341	0.02	0.68	0.24	0.8967	15	12.493
1342	0.02	0.68	0.24	0.8967	25	7.5266
1343	0.02	0.68	0.24	0.8967	35	5.4009
1344	0.02	0.68	0.24	0.8967	50	3.8119
1345	0.02	0.68	0.24	0.8967	75	2.5836
1346	0.02	0.68	0.24	0.8967	100	1.9738
1347	0.02	0.68	0.24	0.8967	150	1.3685
1348	0.02	0.68	0.24	0.8967	200	1.0661
1349	0.02	0.68	0.24	0.8967	300	0.76107
1350	0.02	0.68	0.24	0.8967	400	0.60261
1351	0.02	0.68	0.24	0.8967	600	0.43675
1352	0.02	0.68	0.28	0.90667	1	142.58
1353	0.02	0.68	0.28	0.90667	10	14.431
1354	0.02	0.68	0.28	0.90667	15	9.645
1355	0.02	0.68	0.28	0.90667	25	5.8179
1356	0.02	0.68	0.28	0.90667	35	4.1821
1357	0.02	0.68	0.28	0.90667	50	2.961
1358	0.02	0.68	0.28	0.90667	75	2.0183
1359	0.02	0.68	0.28	0.90667	100	1.5504
1360	0.02	0.68	0.28	0.90667	150	1.0847

	t/l	h/l	s/l	ϵ	Re_l	f_{unit}
1361	0.02	0.68	0.28	0.90667	200	0.84974
1362	0.02	0.68	0.28	0.90667	300	0.61086
1363	0.02	0.68	0.28	0.90667	400	0.48454
1364	0.02	0.68	0.28	0.90667	600	0.34827
1365	0.02	0.68	0.32	0.91429	1	115.07
1366	0.02	0.68	0.32	0.91429	10	11.638
1367	0.02	0.68	0.32	0.91429	15	7.7818
1368	0.02	0.68	0.32	0.91429	25	4.7012
1369	0.02	0.68	0			

	t/l	h/l	s/l	ϵ	Re_l	f_{unit}
1441	0.02	1.0	0.2	0.89127	600	0.53725
1442	0.02	1.0	0.24	0.90498	1	172.05
1443	0.02	1.0	0.24	0.90498	10	17.178
1444	0.02	1.0	0.24	0.90498	15	11.479
1445	0.02	1.0	0.24	0.90498	25	6.9162
1446	0.02	1.0	0.24	0.90498	35	4.9626
1447	0.02	1.0	0.24	0.90498	50	3.5019
1448	0.02	1.0	0.24	0.90498	75	2.3727
1449	0.02	1.0	0.24	0.90498	100	1.8124
1450	0.02	1.0	0.24	0.90498	150	1.2572
1451	0.02	1.0	0.24	0.90498	200	0.97839
1452	0.02	1.0	0.24	0.90498	300	0.69903
1453	0.02	1.0	0.24	0.90498	400	0.55578
1454	0.02	1.0	0.24	0.90498	600	0.40412
1455	0.02	1.0	0.28	0.91503	1	128.99
1456	0.02	1.0	0.28	0.91503	10	13.073
1457	0.02	1.0	0.28	0.91503	15	8.7383
1458	0.02	1.0	0.28	0.91503	25	5.2712
1459	0.02	1.0	0.28	0.91503	35	3.7889
1460	0.02	1.0	0.28	0.91503	50	2.6822
1461	0.02	1.0	0.28	0.91503	75	1.828
1462	0.02	1.0	0.28	0.91503	100	1.4044
1463	0.02	1.0	0.28	0.91503	150	0.98378
1464	0.02	1.0	0.28	0.91503	200	0.77258
1465	0.02	1.0	0.28	0.91503	300	0.5566
1466	0.02	1.0	0.28	0.91503	400	0.4415
1467	0.02	1.0	0.28	0.91503	600	0.31907
1468	0.02	1.0	0.32	0.92272	1	102.6
1469	0.02	1.0	0.32	0.92272	10	10.391
1470	0.02	1.0	0.32	0.92272	15	6.9487
1471	0.02	1.0	0.32	0.92272	25	4.1982
1472	0.02	1.0	0.32	0.92272	35	3.024
1473	0.02	1.0	0.32	0.92272	50	2.1485
1474	0.02	1.0	0.32	0.92272	75	1.4736
1475	0.02	1.0	0.32	0.92272	100	1.1387
1476	0.02	1.0	0.32	0.92272	150	0.80411
1477	0.02	1.0	0.32	0.92272	200	0.63504
1478	0.02	1.0	0.32	0.92272	300	0.45714
1479	0.02	1.0	0.32	0.92272	400	0.3634
1480	0.02	1.0	0.32	0.92272	600	0.26085
1481	0.02	1.0	0.4	0.93371	1	71.073
1482	0.02	1.0	0.4	0.93371	10	7.1947
1483	0.02	1.0	0.4	0.93371	15	4.818
1484	0.02	1.0	0.4	0.93371	25	2.9229
1485	0.02	1.0	0.4	0.93371	35	2.1162
1486	0.02	1.0	0.4	0.93371	50	1.5159
1487	0.02	1.0	0.4	0.93371	75	1.0531
1488	0.02	1.0	0.4	0.93371	100	0.82186
1489	0.02	1.0	0.4	0.93371	150	0.58639
1490	0.02	1.0	0.4	0.93371	200	0.46349
1491	0.02	1.0	0.4	0.93371	300	0.33195
1492	0.02	1.0	0.4	0.93371	400	0.2615
1493	0.02	1.0	0.4	0.93371	600	0.18441
1494	0.02	1.0	0.48	0.94118	1	53.511
1495	0.02	1.0	0.48	0.94118	10	5.4201
1496	0.02	1.0	0.48	0.94118	15	3.6364
1497	0.02	1.0	0.48	0.94118	25	2.2174
1498	0.02	1.0	0.48	0.94118	35	1.6147
1499	0.02	1.0	0.48	0.94118	50	1.1664
1500	0.02	1.0	0.48	0.94118	75	0.81861
1501	0.02	1.0	0.48	0.94118	100	0.64204
1502	0.02	1.0	0.48	0.94118	150	0.45804
1503	0.02	1.0	0.48	0.94118	200	0.36013
1504	0.02	1.0	0.48	0.94118	300	0.25444
1505	0.02	1.0	0.48	0.94118	400	0.19572
1506	0.04	0.12	0.12	0.5625	1	2254
1507	0.04	0.12	0.12	0.5625	10	225.54
1508	0.04	0.12	0.12	0.5625	15	150.51
1509	0.04	0.12	0.12	0.5625	25	90.494
1510	0.04	0.12	0.12	0.5625	35	64.817
1511	0.04	0.12	0.12	0.5625	50	45.616
1512	0.04	0.12	0.12	0.5625	75	30.76
1513	0.04	0.12	0.12	0.5625	100	24.024
1514	0.04	0.12	0.12	0.5625	150	16.055
1515	0.04	0.12	0.12	0.5625	200	12.418
1516	0.04	0.12	0.12	0.5625	300	8.7961
1517	0.04	0.12	0.12	0.5625	400	6.9972
1518	0.04	0.12	0.12	0.5625	600	5.2663
1519	0.04	0.12	0.16	0.6	1	1570
1520	0.04	0.12	0.16	0.6	10	157.1

	t/l	h/l	s/l	ϵ	Re_l	f_{unit}
1521	0.04	0.12	0.16	0.6	15	104.82
1522	0.04	0.12	0.16	0.6	25	63.036
1523	0.04	0.12	0.16	0.6	35	45.162
1524	0.04	0.12	0.16	0.6	50	31.795
1525	0.04	0.12	0.16	0.6	75	21.445
1526	0.04	0.12	0.16	0.6	100	16.295
1527	0.04	0.12	0.16	0.6	150	11.164
1528	0.04	0.12	0.16	0.6	200	8.6056
1529	0.04	0.12	0.16	0.6	300	6.0531
1530	0.04	0.12	0.16	0.6	400	4.7835
1531	0.04	0.12	0.16	0.6	600	3.5323
1532	0.04	0.12	0.2	0.625	1	1263.4
1533	0.04	0.12	0.2	0.625	10	126.42
1534	0.04	0.12	0.2	0.625	15	84.354
1535	0.04	0.12	0.2	0.625	25	50.73
1536	0.04	0.12	0.2	0.625	35	36.348
1537	0.04	0.12	0.2	0.625	50	25.59
1538	0.04	0.12	0.2	0.625	75	17.255
1539	0.04	0.12	0.2	0.625	100	13.101
1540	0.04	0.12	0.2	0.625	150	8.9573
1541	0.04	0.12	0.2	0.625	200	6.888
1542	0.04	0.12	0.2	0.625	300	4.8207
1543	0.04	0.12	0.2	0.625	400	3.79
1544	0.04	0.12	0.2	0.625	600	2.7692
1545	0.04	0.12	0.24	0.64286	1	1096.8
1546	0.04	0.12	0.24	0.64286	10	109.75
1547	0.04	0.12	0.24	0.64286	15	73.226
1548	0.04	0.12	0.24	0.64286	25	44.036
1549	0.04	0.12	0.24	0.64286	35	31.55
1550	0.04	0.12	0.24	0.64286	50	22.207
1551	0.04	0.12	0.24	0.64286	75	14.963
1552	0.04	0.12	0.24	0.64286	100	11.351
1553	0.04	0.12	0.24	0.64286	150	7.7439
1554	0.04	0.12	0.24	0.64286	200	5.9411
1555	0.04	0.12	0.24	0.64286	300	4.137
1556	0.04	0.12	0.24	0.64286	400	3.235
1557	0.04	0.12	0.24	0.64286	600	2.339
1558	0.04	0.12	0.28	0.65625	1	994.3
1559	0.04	0.12	0.28	0.65625	10	99.488
1560	0.04	0.12	0.28	0.65625	15	66.379
1561	0.04	0.12	0.28	0.65625	25	39.914
1562	0.04	0.12	0.28	0.65625	35	28.592
1563	0.04	0.12	0.28	0.65625	50	20.118
1564	0.04	0.12	0.28	0.65625	75	13.544
1565	0.04	0.12	0.28	0.65625	100	10.265
1566	0.04	0.12	0.28	0.65625	150	6.9881
1567	0.04	0.12	0.28	0.65625	200	5.3489
1568	0.04	0.12	0.28	0.65625	300	3.7057
1569	0.04	0.12	0.28	0.65625	400	2.8822
1570	0.04	0.12	0.28	0.65625	600	2.0629
1571	0.04	0.12	0.32	0.66667	1	925.66
1572	0.04	0.12	0.32	0.66667	10	92.615
1573	0.04	0.12	0.32	0.66667	15	61.791
1574	0.04	0.12	0.32	0.66667	25	37.15
1575	0.04	0.12	0.32	0.66667	35	26.607
1576	0.04	0.12	0.32	0.66667	50	18.714
1577	0.04	0.12	0.32	0.66667	75	12.589
1578	0.04	0.12	0.32	0.66667	100	9.5316
1579	0.04	0.12	0.32	0.66667	150	6.4762
1580	0.04	0.12	0.32	0.66667	200	4.9464
1581	0.04	0.12	0.32	0.66667	300	3.4109
1582	0.04	0.12	0.32	0.66667	400	2.6401
1583	0.04	0.12	0.32	0.66667	600	1.8716
1584	0.04	0.12	0.4	0.68182	1	840.27
1585	0.04	0.12	0.4	0.68182	10	84.064
1586	0.04	0.12	0.4	0.68182	15	56.081
1587	0.04	0.12	0.4	0.68182	25	33.708
1588	0.04	0.12	0.4	0.68182	35	24.313
1589	0.04	0.12	0.4	0.68182	50	16.96
1590	0.04	0.12	0.4	0.68182	75	11.393
1591	0.04	0.12	0.4	0.68182	100	8.6127
1592	0.04	0.12	0.4	0.68182	150	5.8327
1593	0.04	0.12	0.4	0.68182	200	4.4396
1594	0.04	0.12	0.4	0.68182	300	3.04
1595	0.04	0.12	0.4	0.68182	400	2.3365
1596	0.04	0.12	0.4	0.68182	600	1.6325
1597	0.04	0.12	0.48	0.69231	1	789.62
1598	0.04	0.12	0.48	0.69231	10	78.989
1599	0.04	0.12	0.48	0.69231	15	52.691
1600	0.04	0.12	0.48	0.69231	25	31.662

	t/l	h/l	s/l	ϵ	Re_l	f_{unit}
1601	0.04	0.12	0.48	0.69231	35	22.66
1602	0.04	0.12	0.48	0.69231	50	15.917
1603	0.04	0.12	0.48	0.69231	75	10.68
1604	0.04	0.12	0.48	0.69231	100	8.0648
1605	0.04	0.12	0.48	0.69231	150	5.4488
1606	0.04	0.12	0.48	0.69231	200	4.1379
1607	0.04	0.12	0.48	0.69231	300	2.8212
1608	0.04	0.12	0.48	0.69231	400	2.1592
1609	0.04	0.12	0.48	0.69231	600	1.4953
1610	0.04	0.16	0.12	0.6	1	1693.1
1611	0.04	0.16	0.12	0.6	10	

	<i>t/l</i>	<i>h/l</i>	<i>s/l</i>	ϵ	<i>Re_l</i>	<i>f_{unit}</i>
1681	0.04	0.16	0.32	0.71111	75	7.6139
1682	0.04	0.16	0.32	0.71111	100	5.7875
1683	0.04	0.16	0.32	0.71111	150	3.9616
1684	0.04	0.16	0.32	0.71111	200	3.0462
1685	0.04	0.16	0.32	0.71111	300	2.1248
1686	0.04	0.16	0.32	0.71111	400	1.6597
1687	0.04	0.16	0.32	0.71111	600	1.1895
1688	0.04	0.16	0.4	0.72727	1	487.2
1689	0.04	0.16	0.4	0.72727	10	48.756
1690	0.04	0.16	0.4	0.72727	15	32.539
1691	0.04	0.16	0.4	0.72727	25	19.58
1692	0.04	0.16	0.4	0.72727	35	14.036
1693	0.04	0.16	0.4	0.72727	50	9.8878
1694	0.04	0.16	0.4	0.72727	75	6.6679
1695	0.04	0.16	0.4	0.72727	100	5.0595
1696	0.04	0.16	0.4	0.72727	150	3.4486
1697	0.04	0.16	0.4	0.72727	200	2.6392
1698	0.04	0.16	0.4	0.72727	300	1.8232
1699	0.04	0.16	0.4	0.72727	400	1.4114
1700	0.04	0.16	0.4	0.72727	600	0.99575
1701	0.04	0.16	0.48	0.73846	1	448.16
1702	0.04	0.16	0.48	0.73846	10	44.846
1703	0.04	0.16	0.48	0.73846	15	29.927
1704	0.04	0.16	0.48	0.73846	25	18.003
1705	0.04	0.16	0.48	0.73846	35	12.901
1706	0.04	0.16	0.48	0.73846	50	9.0814
1707	0.04	0.16	0.48	0.73846	75	6.1149
1708	0.04	0.16	0.48	0.73846	100	4.632
1709	0.04	0.16	0.48	0.73846	150	3.1455
1710	0.04	0.16	0.48	0.73846	200	2.3982
1711	0.04	0.16	0.48	0.73846	300	1.6452
1712	0.04	0.16	0.48	0.73846	400	1.2657
1713	0.04	0.16	0.48	0.73846	600	0.8836
1714	0.04	0.2	0.12	0.625	1	1432.4
1715	0.04	0.2	0.12	0.625	10	143.26
1716	0.04	0.2	0.12	0.625	15	95.621
1717	0.04	0.2	0.12	0.625	25	57.488
1718	0.04	0.2	0.12	0.625	35	41.165
1719	0.04	0.2	0.12	0.625	50	28.956
1720	0.04	0.2	0.12	0.625	75	19.51
1721	0.04	0.2	0.12	0.625	100	14.822
1722	0.04	0.2	0.12	0.625	150	10.176
1723	0.04	0.2	0.12	0.625	200	7.8763
1724	0.04	0.2	0.12	0.625	300	5.5887
1725	0.04	0.2	0.12	0.625	400	4.4457
1726	0.04	0.2	0.12	0.625	600	3.3104
1727	0.04	0.2	0.16	0.66667	1	885.05
1728	0.04	0.2	0.16	0.66667	10	88.543
1729	0.04	0.2	0.16	0.66667	15	59.092
1730	0.04	0.2	0.16	0.66667	25	35.542
1731	0.04	0.2	0.16	0.66667	35	25.469
1732	0.04	0.2	0.16	0.66667	50	17.94
1733	0.04	0.2	0.16	0.66667	75	12.115
1734	0.04	0.2	0.16	0.66667	100	9.2225
1735	0.04	0.2	0.16	0.66667	150	6.3483
1736	0.04	0.2	0.16	0.66667	200	4.9183
1737	0.04	0.2	0.16	0.66667	300	3.4908
1738	0.04	0.2	0.16	0.66667	400	2.7756
1739	0.04	0.2	0.16	0.66667	600	2.0595
1740	0.04	0.2	0.2	0.69444	1	645.18
1741	0.04	0.2	0.2	0.69444	10	64.984
1742	0.04	0.2	0.2	0.69444	15	43.09
1743	0.04	0.2	0.2	0.69444	25	25.932
1744	0.04	0.2	0.2	0.69444	35	18.596
1745	0.04	0.2	0.2	0.69444	50	13.114
1746	0.04	0.2	0.2	0.69444	75	8.8736
1747	0.04	0.2	0.2	0.69444	100	6.7657
1748	0.04	0.2	0.2	0.69444	150	4.668
1749	0.04	0.2	0.2	0.69444	200	3.622
1750	0.04	0.2	0.2	0.69444	300	2.5746
1751	0.04	0.2	0.2	0.69444	400	2.0474
1752	0.04	0.2	0.2	0.69444	600	1.5134
1753	0.04	0.2	0.24	0.71429	1	518.21
1754	0.04	0.2	0.24	0.71429	10	51.866
1755	0.04	0.2	0.24	0.71429	15	34.621
1756	0.04	0.2	0.24	0.71429	25	20.844
1757	0.04	0.2	0.24	0.71429	35	14.956
1758	0.04	0.2	0.24	0.71429	50	10.557
1759	0.04	0.2	0.24	0.71429	75	7.1524
1760	0.04	0.2	0.24	0.71429	100	5.4586

	<i>t/l</i>	<i>h/l</i>	<i>s/l</i>	ϵ	<i>Re_l</i>	<i>f_{unit}</i>
1761	0.04	0.2	0.24	0.71429	150	3.7707
1762	0.04	0.2	0.24	0.71429	200	2.9273
1763	0.04	0.2	0.24	0.71429	300	2.0794
1764	0.04	0.2	0.24	0.71429	400	1.6493
1765	0.04	0.2	0.24	0.71429	600	1.2103
1766	0.04	0.2	0.28	0.72917	1	442.27
1767	0.04	0.2	0.28	0.72917	10	44.269
1768	0.04	0.2	0.28	0.72917	15	29.554
1769	0.04	0.2	0.28	0.72917	25	17.8
1770	0.04	0.2	0.28	0.72917	35	12.777
1771	0.04	0.2	0.28	0.72917	50	9.0233
1772	0.04	0.2	0.28	0.72917	75	6.1175
1773	0.04	0.2	0.28	0.72917	100	4.6704
1774	0.04	0.2	0.28	0.72917	150	3.2261
1775	0.04	0.2	0.28	0.72917	200	2.5025
1776	0.04	0.2	0.28	0.72917	300	1.7719
1777	0.04	0.2	0.28	0.72917	400	1.3992
1778	0.04	0.2	0.28	0.72917	600	1.0162
1779	0.04	0.2	0.32	0.74074	1	392.82
1780	0.04	0.2	0.32	0.74074	10	39.322
1781	0.04	0.2	0.32	0.74074	15	26.254
1782	0.04	0.2	0.32	0.74074	25	15.815
1783	0.04	0.2	0.32	0.74074	35	11.355
1784	0.04	0.2	0.32	0.74074	50	8.0211
1785	0.04	0.2	0.32	0.74074	75	5.4387
1786	0.04	0.2	0.32	0.74074	100	4.1514
1787	0.04	0.2	0.32	0.74074	150	2.8644
1788	0.04	0.2	0.32	0.74074	200	2.2177
1789	0.04	0.2	0.32	0.74074	300	1.5626
1790	0.04	0.2	0.32	0.74074	400	1.2276
1791	0.04	0.2	0.32	0.74074	600	0.88239
1792	0.04	0.2	0.4	0.75758	1	333.59
1793	0.04	0.2	0.4	0.75758	10	33.396
1794	0.04	0.2	0.4	0.75758	15	22.298
1795	0.04	0.2	0.4	0.75758	25	13.434
1796	0.04	0.2	0.4	0.75758	35	9.6458
1797	0.04	0.2	0.4	0.75758	50	6.8128
1798	0.04	0.2	0.4	0.75758	75	4.6155
1799	0.04	0.2	0.4	0.75758	100	3.5179
1800	0.04	0.2	0.4	0.75758	150	2.4169
1801	0.04	0.2	0.4	0.75758	200	1.8615
1802	0.04	0.2	0.4	0.75758	300	1.2978
1803	0.04	0.2	0.4	0.75758	400	1.0098
1804	0.04	0.2	0.4	0.75758	600	0.71441
1805	0.04	0.2	0.48	0.76923	1	300.09
1806	0.04	0.2	0.48	0.76923	10	30.041
1807	0.04	0.2	0.48	0.76923	15	20.057
1808	0.04	0.2	0.48	0.76923	25	12.082
1809	0.04	0.2	0.48	0.76923	35	8.673
1810	0.04	0.2	0.48	0.76923	50	6.1218
1811	0.04	0.2	0.48	0.76923	75	4.1408
1812	0.04	0.2	0.48	0.76923	100	3.1495
1813	0.04	0.2	0.48	0.76923	150	2.1532
1814	0.04	0.2	0.48	0.76923	200	1.6502
1815	0.04	0.2	0.48	0.76923	300	1.1406
1816	0.04	0.2	0.48	0.76923	400	0.8814
1817	0.04	0.2	0.48	0.76923	600	0.61744
1818	0.04	0.24	0.12	0.64286	1	1286.2
1819	0.04	0.24	0.12	0.64286	10	128.61
1820	0.04	0.24	0.12	0.64286	15	85.849
1821	0.04	0.24	0.12	0.64286	25	51.612
1822	0.04	0.24	0.12	0.64286	35	36.953
1823	0.04	0.24	0.12	0.64286	50	25.987
1824	0.04	0.24	0.12	0.64286	75	17.502
1825	0.04	0.24	0.12	0.64286	100	13.291
1826	0.04	0.24	0.12	0.64286	150	9.1203
1827	0.04	0.24	0.12	0.64286	200	7.0533
1828	0.04	0.24	0.12	0.64286	300	5.0021
1829	0.04	0.24	0.12	0.64286	400	3.9822
1830	0.04	0.24	0.12	0.64286	600	2.9626
1831	0.04	0.24	0.16	0.68571	1	769.06
1832	0.04	0.24	0.16	0.68571	10	76.93
1833	0.04	0.24	0.16	0.68571	15	51.345
1834	0.04	0.24	0.16	0.68571	25	30.883
1835	0.04	0.24	0.16	0.68571	35	22.131
1836	0.04	0.24	0.16	0.68571	50	15.588
1837	0.04	0.24	0.16	0.68571	75	10.528
1838	0.04	0.24	0.16	0.68571	100	8.0154
1839	0.04	0.24	0.16	0.68571	150	5.521
1840	0.04	0.24	0.16	0.68571	200	4.2802

	<i>t/l</i>	<i>h/l</i>	<i>s/l</i>	ϵ	<i>Re_l</i>	<i>f_{unit}</i>
1841	0.04	0.24	0.16	0.68571	300	3.0405
1842	0.04	0.24	0.16	0.68571	400	2.4202
1843	0.04	0.24	0.16	0.68571	600	1.7952
1844	0.04	0.24	0.2	0.71429	1	543.24
1845	0.04	0.24	0.2	0.71429	10	54.357
1846	0.04	0.24	0.2	0.71429	15	36.284
1847	0.04	0.24	0.2	0.71429	25	21.838
1848	0.04	0.24	0.2	0.71429	35	15.664
1849	0.04	0.24	0.2	0.71429	50	11.05
1850	0.04	0.24	0.2	0.71429	75	7.4833
1851</						

	<i>t/l</i>	<i>h/l</i>	<i>s/l</i>	ϵ	<i>Re_l</i>	<i>f_{unit}</i>
1921	0.04	0.24	0.48	0.79121	600	0.4762
1922	0.04	0.28	0.12	0.65625	1	1193.7
1923	0.04	0.28	0.12	0.65625	10	119.35
1924	0.04	0.28	0.12	0.65625	15	79.669
1925	0.04	0.28	0.12	0.65625	25	47.896
1926	0.04	0.28	0.12	0.65625	35	34.29
1927	0.04	0.28	0.12	0.65625	50	24.109
1928	0.04	0.28	0.12	0.65625	75	16.231
1929	0.04	0.28	0.12	0.65625	100	12.321
1930	0.04	0.28	0.12	0.65625	150	8.4476
1931	0.04	0.28	0.12	0.65625	200	6.5335
1932	0.04	0.28	0.12	0.65625	300	4.6288
1933	0.04	0.28	0.12	0.65625	400	3.6809
1934	0.04	0.28	0.12	0.65625	600	2.7347
1935	0.04	0.28	0.16	0.7	1	697.72
1936	0.04	0.28	0.16	0.7	10	69.79
1937	0.04	0.28	0.16	0.7	15	46.581
1938	0.04	0.28	0.16	0.7	25	28.017
1939	0.04	0.28	0.16	0.7	35	20.077
1940	0.04	0.28	0.16	0.7	50	14.139
1941	0.04	0.28	0.16	0.7	75	9.5486
1942	0.04	0.28	0.16	0.7	100	7.2698
1943	0.04	0.28	0.16	0.7	150	5.0081
1944	0.04	0.28	0.16	0.7	200	3.8833
1945	0.04	0.28	0.16	0.7	300	2.7598
1946	0.04	0.28	0.16	0.7	400	2.1963
1947	0.04	0.28	0.16	0.7	600	1.6296
1948	0.04	0.28	0.2	0.72917	1	481.67
1949	0.04	0.28	0.2	0.72917	10	48.185
1950	0.04	0.28	0.2	0.72917	15	32.166
1951	0.04	0.28	0.2	0.72917	25	19.362
1952	0.04	0.28	0.2	0.72917	35	13.888
1953	0.04	0.28	0.2	0.72917	50	9.7995
1954	0.04	0.28	0.2	0.72917	75	6.6393
1955	0.04	0.28	0.2	0.72917	100	5.0705
1956	0.04	0.28	0.2	0.72917	150	3.5108
1957	0.04	0.28	0.2	0.72917	200	2.7331
1958	0.04	0.28	0.2	0.72917	300	1.9525
1959	0.04	0.28	0.2	0.72917	400	1.5574
1960	0.04	0.28	0.2	0.72917	600	1.1528
1961	0.04	0.28	0.24	0.75	1	367.92
1962	0.04	0.28	0.24	0.75	10	36.823
1963	0.04	0.28	0.24	0.75	15	24.587
1964	0.04	0.28	0.24	0.75	25	14.811
1965	0.04	0.28	0.24	0.75	35	10.635
1966	0.04	0.28	0.24	0.75	50	7.5175
1967	0.04	0.28	0.24	0.75	75	5.1087
1968	0.04	0.28	0.24	0.75	100	3.9124
1969	0.04	0.28	0.24	0.75	150	2.721
1970	0.04	0.28	0.24	0.75	200	2.1248
1971	0.04	0.28	0.24	0.75	300	1.5223
1972	0.04	0.28	0.24	0.75	400	1.2131
1973	0.04	0.28	0.24	0.75	600	0.89201
1974	0.04	0.28	0.28	0.76563	1	300.46
1975	0.04	0.28	0.28	0.76563	10	30.08
1976	0.04	0.28	0.28	0.76563	15	20.089
1977	0.04	0.28	0.28	0.76563	25	12.111
1978	0.04	0.28	0.28	0.76563	35	8.7047
1979	0.04	0.28	0.28	0.76563	50	6.1625
1980	0.04	0.28	0.28	0.76563	75	4.1986
1981	0.04	0.28	0.28	0.76563	100	3.2223
1982	0.04	0.28	0.28	0.76563	150	2.2479
1983	0.04	0.28	0.28	0.76563	200	1.758
1984	0.04	0.28	0.28	0.76563	300	1.2581
1985	0.04	0.28	0.28	0.76563	400	0.99873
1986	0.04	0.28	0.28	0.76563	600	0.72693
1987	0.04	0.28	0.32	0.77778	1	255.05
1988	0.04	0.28	0.32	0.77778	10	25.726
1989	0.04	0.28	0.32	0.77778	15	17.185
1990	0.04	0.28	0.32	0.77778	25	10.367
1991	0.04	0.28	0.32	0.77778	35	7.4578
1992	0.04	0.28	0.32	0.77778	50	5.2867
1993	0.04	0.28	0.32	0.77778	75	3.6087
1994	0.04	0.28	0.32	0.77778	100	2.7735
1995	0.04	0.28	0.32	0.77778	150	1.9375
1996	0.04	0.28	0.32	0.77778	200	1.5144
1997	0.04	0.28	0.32	0.77778	300	1.0795
1998	0.04	0.28	0.32	0.77778	400	0.85248
1999	0.04	0.28	0.32	0.77778	600	0.61457
2000	0.04	0.28	0.4	0.79545	1	204.29

	<i>t/l</i>	<i>h/l</i>	<i>s/l</i>	ϵ	<i>Re_l</i>	<i>f_{unit}</i>
2001	0.04	0.28	0.4	0.79545	10	20.583
2002	0.04	0.28	0.4	0.79545	15	13.755
2003	0.04	0.28	0.4	0.79545	25	8.3066
2004	0.04	0.28	0.4	0.79545	35	5.9825
2005	0.04	0.28	0.4	0.79545	50	4.2474
2006	0.04	0.28	0.4	0.79545	75	2.9042
2007	0.04	0.28	0.4	0.79545	100	2.2331
2008	0.04	0.28	0.4	0.79545	150	1.5565
2009	0.04	0.28	0.4	0.79545	200	1.2111
2010	0.04	0.28	0.4	0.79545	300	0.85374
2011	0.04	0.28	0.4	0.79545	400	0.66736
2012	0.04	0.28	0.4	0.79545	600	0.47396
2013	0.04	0.28	0.48	0.80769	1	176.16
2014	0.04	0.28	0.48	0.80769	10	17.733
2015	0.04	0.28	0.48	0.80769	15	11.853
2016	0.04	0.28	0.48	0.80769	25	7.1619
2017	0.04	0.28	0.48	0.80769	35	5.1604
2018	0.04	0.28	0.48	0.80769	50	3.6651
2019	0.04	0.28	0.48	0.80769	75	2.5045
2020	0.04	0.28	0.48	0.80769	100	1.9221
2021	0.04	0.28	0.48	0.80769	150	1.3323
2022	0.04	0.28	0.48	0.80769	200	1.0304
2023	0.04	0.28	0.48	0.80769	300	0.71901
2024	0.04	0.28	0.48	0.80769	400	0.55797
2025	0.04	0.28	0.48	0.80769	600	0.39226
2026	0.04	0.32	0.12	0.66667	1	1130.3
2027	0.04	0.32	0.12	0.66667	10	112.98
2028	0.04	0.32	0.12	0.66667	15	75.43
2029	0.04	0.32	0.12	0.66667	25	45.347
2030	0.04	0.32	0.12	0.66667	35	32.462
2031	0.04	0.32	0.12	0.66667	50	22.821
2032	0.04	0.32	0.12	0.66667	75	15.36
2033	0.04	0.32	0.12	0.66667	100	11.654
2034	0.04	0.32	0.12	0.66667	150	7.9857
2035	0.04	0.32	0.12	0.66667	200	6.1732
2036	0.04	0.32	0.12	0.66667	300	4.3728
2037	0.04	0.32	0.12	0.66667	400	3.4743
2038	0.04	0.32	0.12	0.66667	600	2.5821
2039	0.04	0.32	0.16	0.71111	1	649.99
2040	0.04	0.32	0.16	0.71111	10	65.005
2041	0.04	0.32	0.16	0.71111	15	43.391
2042	0.04	0.32	0.16	0.71111	25	26.099
2043	0.04	0.32	0.16	0.71111	35	18.701
2044	0.04	0.32	0.16	0.71111	50	13.169
2045	0.04	0.32	0.16	0.71111	75	8.892
2046	0.04	0.32	0.16	0.71111	100	6.769
2047	0.04	0.32	0.16	0.71111	150	4.6623
2048	0.04	0.32	0.16	0.71111	200	3.6152
2049	0.04	0.32	0.16	0.71111	300	2.5695
2050	0.04	0.32	0.16	0.71111	400	2.0451
2051	0.04	0.32	0.16	0.71111	600	1.5162
2052	0.04	0.32	0.2	0.74074	1	441.01
2053	0.04	0.32	0.2	0.74074	10	44.123
2054	0.04	0.32	0.2	0.74074	15	29.456
2055	0.04	0.32	0.2	0.74074	25	17.731
2056	0.04	0.32	0.2	0.74074	35	12.719
2057	0.04	0.32	0.2	0.74074	50	8.9752
2058	0.04	0.32	0.2	0.74074	75	6.0819
2059	0.04	0.32	0.2	0.74074	100	4.646
2060	0.04	0.32	0.2	0.74074	150	3.2189
2061	0.04	0.32	0.2	0.74074	200	2.5074
2062	0.04	0.32	0.2	0.74074	300	1.7938
2063	0.04	0.32	0.2	0.74074	400	1.4321
2064	0.04	0.32	0.2	0.74074	600	1.06
2065	0.04	0.32	0.24	0.7619	1	331.28
2066	0.04	0.32	0.24	0.7619	10	33.154
2067	0.04	0.32	0.24	0.7619	15	22.138
2068	0.04	0.32	0.24	0.7619	25	13.338
2069	0.04	0.32	0.24	0.7619	35	9.5795
2070	0.04	0.32	0.24	0.7619	50	6.7736
2071	0.04	0.32	0.24	0.7619	75	4.6066
2072	0.04	0.32	0.24	0.7619	100	3.5309
2073	0.04	0.32	0.24	0.7619	150	2.4597
2074	0.04	0.32	0.24	0.7619	200	1.9235
2075	0.04	0.32	0.24	0.7619	300	1.381
2076	0.04	0.32	0.24	0.7619	400	1.1018
2077	0.04	0.32	0.24	0.7619	600	0.80988
2078	0.04	0.32	0.28	0.77778	1	263.77
2079	0.04	0.32	0.28	0.77778	10	26.654
2080	0.04	0.32	0.28	0.77778	15	17.803

	<i>t/l</i>	<i>h/l</i>	<i>s/l</i>	ϵ	<i>Re_l</i>	<i>f_{unit}</i>
2081	0.04	0.32	0.28	0.77778	25	10.736
2082	0.04	0.32	0.28	0.77778	35	7.7202
2083	0.04	0.32	0.28	0.77778	50	5.4694
2084	0.04	0.32	0.28	0.77778	75	3.7323
2085	0.04	0.32	0.28	0.77778	100	2.8686
2086	0.04	0.32	0.28	0.77778	150	2.0068
2087	0.04	0.32	0.28	0.77778	200	1.5729
2088	0.04	0.32	0.28	0.77778	300	1.129
2089	0.04	0.32	0.28	0.77778	400	0.89761
2090	0.04	0.32	0.28			

	<i>t/l</i>	<i>h/l</i>	<i>s/l</i>	ϵ	<i>Re_l</i>	<i>f_{unit}</i>
2161	0.04	0.4	0.2	0.75758	50	7.971
2162	0.04	0.4	0.2	0.75758	75	5.4014
2163	0.04	0.4	0.2	0.75758	100	4.1262
2164	0.04	0.4	0.2	0.75758	150	2.8595
2165	0.04	0.4	0.2	0.75758	200	2.2286
2166	0.04	0.4	0.2	0.75758	300	1.5953
2167	0.04	0.4	0.2	0.75758	400	1.2752
2168	0.04	0.4	0.2	0.75758	600	0.9441
2169	0.04	0.4	0.24	0.77922	1	287.39
2170	0.04	0.4	0.24	0.77922	10	28.761
2171	0.04	0.4	0.24	0.77922	15	19.207
2172	0.04	0.4	0.24	0.77922	25	11.574
2173	0.04	0.4	0.24	0.77922	35	8.3137
2174	0.04	0.4	0.24	0.77922	50	5.8804
2175	0.04	0.4	0.24	0.77922	75	4.0018
2176	0.04	0.4	0.24	0.77922	100	3.0695
2177	0.04	0.4	0.24	0.77922	150	2.1417
2178	0.04	0.4	0.24	0.77922	200	1.6774
2179	0.04	0.4	0.24	0.77922	300	1.2073
2180	0.04	0.4	0.24	0.77922	400	0.96482
2181	0.04	0.4	0.24	0.77922	600	0.71026
2182	0.04	0.4	0.28	0.79545	1	222.86
2183	0.04	0.4	0.28	0.79545	10	22.594
2184	0.04	0.4	0.28	0.79545	15	15.094
2185	0.04	0.4	0.28	0.79545	25	9.1057
2186	0.04	0.4	0.28	0.79545	35	6.5505
2187	0.04	0.4	0.28	0.79545	50	4.645
2188	0.04	0.4	0.28	0.79545	75	3.1747
2189	0.04	0.4	0.28	0.79545	100	2.4444
2190	0.04	0.4	0.28	0.79545	150	1.7155
2191	0.04	0.4	0.28	0.79545	200	1.3482
2192	0.04	0.4	0.28	0.79545	300	0.97136
2193	0.04	0.4	0.28	0.79545	400	0.77392
2194	0.04	0.4	0.28	0.79545	600	0.56435
2195	0.04	0.4	0.32	0.80808	1	184.06
2196	0.04	0.4	0.32	0.80808	10	18.628
2197	0.04	0.4	0.32	0.80808	15	12.449
2198	0.04	0.4	0.32	0.80808	25	7.5195
2199	0.04	0.4	0.32	0.80808	35	5.4173
2200	0.04	0.4	0.32	0.80808	50	3.8511
2201	0.04	0.4	0.32	0.80808	75	2.6425
2202	0.04	0.4	0.32	0.80808	100	2.0414
2203	0.04	0.4	0.32	0.80808	150	1.4386
2204	0.04	0.4	0.32	0.80808	200	1.1318
2205	0.04	0.4	0.32	0.80808	300	0.81317
2206	0.04	0.4	0.32	0.80808	400	0.64477
2207	0.04	0.4	0.32	0.80808	600	0.4661
2208	0.04	0.4	0.4	0.82645	1	138.3
2209	0.04	0.4	0.4	0.82645	10	13.973
2210	0.04	0.4	0.4	0.82645	15	9.3456
2211	0.04	0.4	0.4	0.82645	25	5.6582
2212	0.04	0.4	0.4	0.82645	35	4.0883
2213	0.04	0.4	0.4	0.82645	50	2.9189
2214	0.04	0.4	0.4	0.82645	75	2.0149
2215	0.04	0.4	0.4	0.82645	100	1.5624
2216	0.04	0.4	0.4	0.82645	150	1.1028
2217	0.04	0.4	0.4	0.82645	200	0.86475
2218	0.04	0.4	0.4	0.82645	300	0.61249
2219	0.04	0.4	0.4	0.82645	400	0.48269
2220	0.04	0.4	0.4	0.82645	600	0.34444
2221	0.04	0.4	0.48	0.83916	1	113.14
2222	0.04	0.4	0.48	0.83916	10	11.421
2223	0.04	0.4	0.48	0.83916	15	7.6452
2224	0.04	0.4	0.48	0.83916	25	4.6382
2225	0.04	0.4	0.48	0.83916	35	3.3586
2226	0.04	0.4	0.48	0.83916	50	2.4046
2227	0.04	0.4	0.48	0.83916	75	1.664
2228	0.04	0.4	0.48	0.83916	100	1.2902
2229	0.04	0.4	0.48	0.83916	150	0.90623
2230	0.04	0.4	0.48	0.83916	200	0.70604
2231	0.04	0.4	0.48	0.83916	300	0.49667
2232	0.04	0.4	0.48	0.83916	400	0.38728
2233	0.04	0.4	0.48	0.83916	600	0.27397
2234	0.04	0.48	0.12	0.69231	1	999.54
2235	0.04	0.48	0.12	0.69231	10	99.85
2236	0.04	0.48	0.12	0.69231	15	66.684
2237	0.04	0.48	0.12	0.69231	25	40.089
2238	0.04	0.48	0.12	0.69231	35	28.694
2239	0.04	0.48	0.12	0.69231	50	20.163
2240	0.04	0.48	0.12	0.69231	75	13.557

	<i>t/l</i>	<i>h/l</i>	<i>s/l</i>	ϵ	<i>Re_l</i>	<i>f_{unit}</i>
2241	0.04	0.48	0.12	0.69231	100	10.277
2242	0.04	0.48	0.12	0.69231	150	7.0296
2243	0.04	0.48	0.12	0.69231	200	5.4262
2244	0.04	0.48	0.12	0.69231	300	3.8354
2245	0.04	0.48	0.12	0.69231	400	3.0448
2246	0.04	0.48	0.12	0.69231	600	2.255
2247	0.04	0.48	0.16	0.73846	1	555.54
2248	0.04	0.48	0.16	0.73846	10	55.54
2249	0.04	0.48	0.16	0.73846	15	37.078
2250	0.04	0.48	0.16	0.73846	25	22.3
2251	0.04	0.48	0.16	0.73846	35	15.976
2252	0.04	0.48	0.16	0.73846	50	11.246
2253	0.04	0.48	0.16	0.73846	75	7.587
2254	0.04	0.48	0.16	0.73846	100	5.7712
2255	0.04	0.48	0.16	0.73846	150	3.9704
2256	0.04	0.48	0.16	0.73846	200	3.0764
2257	0.04	0.48	0.16	0.73846	300	2.1859
2258	0.04	0.48	0.16	0.73846	400	1.7392
2259	0.04	0.48	0.16	0.73846	600	1.2884
2260	0.04	0.48	0.2	0.76923	1	363.24
2261	0.04	0.48	0.2	0.76923	10	36.332
2262	0.04	0.48	0.2	0.76923	15	24.258
2263	0.04	0.48	0.2	0.76923	25	14.602
2264	0.04	0.48	0.2	0.76923	35	10.474
2265	0.04	0.48	0.2	0.76923	50	7.3893
2266	0.04	0.48	0.2	0.76923	75	5.0058
2267	0.04	0.48	0.2	0.76923	100	3.8233
2268	0.04	0.48	0.2	0.76923	150	2.6491
2269	0.04	0.48	0.2	0.76923	200	2.0646
2270	0.04	0.48	0.2	0.76923	300	1.479
2271	0.04	0.48	0.2	0.76923	400	1.1825
2272	0.04	0.48	0.2	0.76923	600	0.8756
2273	0.04	0.48	0.24	0.79121	1	262.57
2274	0.04	0.48	0.24	0.79121	10	26.275
2275	0.04	0.48	0.24	0.79121	15	17.548
2276	0.04	0.48	0.24	0.79121	25	10.575
2277	0.04	0.48	0.24	0.79121	35	7.596
2278	0.04	0.48	0.24	0.79121	50	5.3728
2279	0.04	0.48	0.24	0.79121	75	3.6566
2280	0.04	0.48	0.24	0.79121	100	2.8051
2281	0.04	0.48	0.24	0.79121	150	1.9583
2282	0.04	0.48	0.24	0.79121	200	1.5349
2283	0.04	0.48	0.24	0.79121	300	1.1062
2284	0.04	0.48	0.24	0.79121	400	0.88496
2285	0.04	0.48	0.24	0.79121	600	0.65169
2286	0.04	0.48	0.28	0.80769	1	200.32
2287	0.04	0.48	0.28	0.80769	10	20.331
2288	0.04	0.48	0.28	0.80769	15	13.583
2289	0.04	0.48	0.28	0.80769	25	8.1958
2290	0.04	0.48	0.28	0.80769	35	5.897
2291	0.04	0.48	0.28	0.80769	50	4.1829
2292	0.04	0.48	0.28	0.80769	75	2.8605
2293	0.04	0.48	0.28	0.80769	100	2.2041
2294	0.04	0.48	0.28	0.80769	150	1.5493
2295	0.04	0.48	0.28	0.80769	200	1.2193
2296	0.04	0.48	0.28	0.80769	300	0.88042
2297	0.04	0.48	0.28	0.80769	400	0.70241
2298	0.04	0.48	0.28	0.80769	600	0.51264
2299	0.04	0.48	0.32	0.82051	1	162.95
2300	0.04	0.48	0.32	0.82051	10	16.511
2301	0.04	0.48	0.32	0.82051	15	11.036
2302	0.04	0.48	0.32	0.82051	25	6.6681
2303	0.04	0.48	0.32	0.82051	35	4.8064
2304	0.04	0.48	0.32	0.82051	50	3.4194
2305	0.04	0.48	0.32	0.82051	75	2.3496
2306	0.04	0.48	0.32	0.82051	100	1.8176
2307	0.04	0.48	0.32	0.82051	150	1.2842
2308	0.04	0.48	0.32	0.82051	200	1.0125
2309	0.04	0.48	0.32	0.82051	300	0.72957
2310	0.04	0.48	0.32	0.82051	400	0.5794
2311	0.04	0.48	0.32	0.82051	600	0.41928
2312	0.04	0.48	0.4	0.83916	1	118.97
2313	0.04	0.48	0.4	0.83916	10	12.034
2314	0.04	0.48	0.4	0.83916	15	8.052
2315	0.04	0.48	0.4	0.83916	25	4.8799
2316	0.04	0.48	0.4	0.83916	35	3.5303
2317	0.04	0.48	0.4	0.83916	50	2.5257
2318	0.04	0.48	0.4	0.83916	75	1.7493
2319	0.04	0.48	0.4	0.83916	100	1.3605
2320	0.04	0.48	0.4	0.83916	150	0.96452

	<i>t/l</i>	<i>h/l</i>	<i>s/l</i>	ϵ	<i>Re_l</i>	<i>f_{unit}</i>
2321	0.04	0.48	0.4	0.83916	200	0.75852
2322	0.04	0.48	0.4	0.83916	300	0.5411
2323	0.04	0.48	0.4	0.83916	400	0.42574
2324	0.04	0.48	0.4	0.83916	600	0.30425
2325	0.04	0.48	0.48	0.85207	1	94.835
2326	0.04	0.48	0.48	0.85207	10	9.5868
2327	0.04	0.48	0.48	0.85207	15	6.4218
2328	0.04	0.48	0.48	0.85207	25	3.9034
2329	0.04	0.48	0.48	0.85207	35	2.833

	<i>t/l</i>	<i>h/l</i>	<i>s/l</i>	ϵ	<i>Re_l</i>	<i>f_{unit}</i>
2401	0.04	0.56	0.28	0.81667	600	0.47934
2402	0.04	0.56	0.32	0.82963	1	149.85
2403	0.04	0.56	0.32	0.82963	10	15.198
2404	0.04	0.56	0.32	0.82963	15	10.16
2405	0.04	0.56	0.32	0.82963	25	6.1397
2406	0.04	0.56	0.32	0.82963	35	4.4263
2407	0.04	0.56	0.32	0.82963	50	3.1499
2408	0.04	0.56	0.32	0.82963	75	2.1657
2409	0.04	0.56	0.32	0.82963	100	1.6766
2410	0.04	0.56	0.32	0.82963	150	1.1863
2411	0.04	0.56	0.32	0.82963	200	0.93659
2412	0.04	0.56	0.32	0.82963	300	0.67619
2413	0.04	0.56	0.32	0.82963	400	0.53761
2414	0.04	0.56	0.32	0.82963	600	0.38932
2415	0.04	0.56	0.4	0.84848	1	107.16
2416	0.04	0.56	0.4	0.84848	10	10.849
2417	0.04	0.56	0.4	0.84848	15	7.2612
2418	0.04	0.56	0.4	0.84848	25	4.4034
2419	0.04	0.56	0.4	0.84848	35	3.1878
2420	0.04	0.56	0.4	0.84848	50	2.2832
2421	0.04	0.56	0.4	0.84848	75	1.5845
2422	0.04	0.56	0.4	0.84848	100	1.2346
2423	0.04	0.56	0.4	0.84848	150	0.87775
2424	0.04	0.56	0.4	0.84848	200	0.69168
2425	0.04	0.56	0.4	0.84848	300	0.49463
2426	0.04	0.56	0.4	0.84848	400	0.38969
2427	0.04	0.56	0.4	0.84848	600	0.27857
2428	0.04	0.56	0.48	0.86154	1	83.748
2429	0.04	0.56	0.48	0.86154	10	8.4753
2430	0.04	0.56	0.48	0.86154	15	5.6801
2431	0.04	0.56	0.48	0.86154	25	3.4571
2432	0.04	0.56	0.48	0.86154	35	2.5128
2433	0.04	0.56	0.48	0.86154	50	1.8097
2434	0.04	0.56	0.48	0.86154	75	1.2633
2435	0.04	0.56	0.48	0.86154	100	0.98609
2436	0.04	0.56	0.48	0.86154	150	0.69854
2437	0.04	0.56	0.48	0.86154	200	0.54731
2438	0.04	0.56	0.48	0.86154	300	0.38746
2439	0.04	0.56	0.48	0.86154	400	0.30329
2440	0.04	0.68	0.12	0.70833	1	932.18
2441	0.04	0.68	0.12	0.70833	10	93.072
2442	0.04	0.68	0.12	0.70833	15	62.178
2443	0.04	0.68	0.12	0.70833	25	37.381
2444	0.04	0.68	0.12	0.70833	35	26.752
2445	0.04	0.68	0.12	0.70833	50	18.794
2446	0.04	0.68	0.12	0.70833	75	12.63
2447	0.04	0.68	0.12	0.70833	100	9.5677
2448	0.04	0.68	0.12	0.70833	150	6.5367
2449	0.04	0.68	0.12	0.70833	200	5.0403
2450	0.04	0.68	0.12	0.70833	300	3.555
2451	0.04	0.68	0.12	0.70833	400	2.8206
2452	0.04	0.68	0.12	0.70833	600	2.0866
2453	0.04	0.68	0.16	0.75556	1	509.27
2454	0.04	0.68	0.16	0.75556	10	50.897
2455	0.04	0.68	0.16	0.75556	15	33.983
2456	0.04	0.68	0.16	0.75556	25	20.438
2457	0.04	0.68	0.16	0.75556	35	14.639
2458	0.04	0.68	0.16	0.75556	50	10.301
2459	0.04	0.68	0.16	0.75556	75	6.9449
2460	0.04	0.68	0.16	0.75556	100	5.2791
2461	0.04	0.68	0.16	0.75556	150	3.6277
2462	0.04	0.68	0.16	0.75556	200	2.8086
2463	0.04	0.68	0.16	0.75556	300	1.9926
2464	0.04	0.68	0.16	0.75556	400	1.5854
2465	0.04	0.68	0.16	0.75556	600	1.1741
2466	0.04	0.68	0.2	0.78704	1	326.88
2467	0.04	0.68	0.2	0.78704	10	32.686
2468	0.04	0.68	0.2	0.78704	15	21.825
2469	0.04	0.68	0.2	0.78704	25	13.137
2470	0.04	0.68	0.2	0.78704	35	9.4205
2471	0.04	0.68	0.2	0.78704	50	6.6436
2472	0.04	0.68	0.2	0.78704	75	4.4975
2473	0.04	0.68	0.2	0.78704	100	3.4329
2474	0.04	0.68	0.2	0.78704	150	2.3767
2475	0.04	0.68	0.2	0.78704	200	1.8517
2476	0.04	0.68	0.2	0.78704	300	1.3264
2477	0.04	0.68	0.2	0.78704	400	1.0598
2478	0.04	0.68	0.2	0.78704	600	0.78549
2479	0.04	0.68	0.24	0.80952	1	226.71
2480	0.04	0.68	0.24	0.80952	10	23.18

	<i>t/l</i>	<i>h/l</i>	<i>s/l</i>	ϵ	<i>Re_l</i>	<i>f_{unit}</i>
2481	0.04	0.68	0.24	0.80952	15	15.482
2482	0.04	0.68	0.24	0.80952	25	9.3286
2483	0.04	0.68	0.24	0.80952	35	6.6988
2484	0.04	0.68	0.24	0.80952	50	4.7373
2485	0.04	0.68	0.24	0.80952	75	3.2224
2486	0.04	0.68	0.24	0.80952	100	2.4713
2487	0.04	0.68	0.24	0.80952	150	1.7252
2488	0.04	0.68	0.24	0.80952	200	1.3529
2489	0.04	0.68	0.24	0.80952	300	0.97645
2490	0.04	0.68	0.24	0.80952	400	0.78239
2491	0.04	0.68	0.24	0.80952	600	0.57644
2492	0.04	0.68	0.28	0.82639	1	172.67
2493	0.04	0.68	0.28	0.82639	10	17.572
2494	0.04	0.68	0.28	0.82639	15	11.741
2495	0.04	0.68	0.28	0.82639	25	7.0845
2496	0.04	0.68	0.28	0.82639	35	5.0971
2497	0.04	0.68	0.28	0.82639	50	3.6152
2498	0.04	0.68	0.28	0.82639	75	2.4723
2499	0.04	0.68	0.28	0.82639	100	1.9055
2500	0.04	0.68	0.28	0.82639	150	1.341
2501	0.04	0.68	0.28	0.82639	200	1.057
2502	0.04	0.68	0.28	0.82639	300	0.76579
2503	0.04	0.68	0.28	0.82639	400	0.61188
2504	0.04	0.68	0.28	0.82639	600	0.44724
2505	0.04	0.68	0.32	0.83951	1	137.59
2506	0.04	0.68	0.32	0.83951	10	13.975
2507	0.04	0.68	0.32	0.83951	15	9.3422
2508	0.04	0.68	0.32	0.83951	25	5.646
2509	0.04	0.68	0.32	0.83951	35	4.0705
2510	0.04	0.68	0.32	0.83951	50	2.8968
2511	0.04	0.68	0.32	0.83951	75	1.9922
2512	0.04	0.68	0.32	0.83951	100	1.543
2513	0.04	0.68	0.32	0.83951	150	1.0931
2514	0.04	0.68	0.32	0.83951	200	0.8641
2515	0.04	0.68	0.32	0.83951	300	0.62508
2516	0.04	0.68	0.32	0.83951	400	0.49756
2517	0.04	0.68	0.32	0.83951	600	0.36065
2518	0.04	0.68	0.4	0.85859	1	96.327
2519	0.04	0.68	0.4	0.85859	10	9.7647
2520	0.04	0.68	0.4	0.85859	15	6.5367
2521	0.04	0.68	0.4	0.85859	25	3.9658
2522	0.04	0.68	0.4	0.85859	35	2.8723
2523	0.04	0.68	0.4	0.85859	50	2.0589
2524	0.04	0.68	0.4	0.85859	75	1.431
2525	0.04	0.68	0.4	0.85859	100	1.1167
2526	0.04	0.68	0.4	0.85859	150	0.79612
2527	0.04	0.68	0.4	0.85859	200	0.62864
2528	0.04	0.68	0.4	0.85859	300	0.45069
2529	0.04	0.68	0.4	0.85859	400	0.3555
2530	0.04	0.68	0.4	0.85859	600	0.25422
2531	0.04	0.68	0.48	0.87179	1	73.709
2532	0.04	0.68	0.48	0.87179	10	7.4691
2533	0.04	0.68	0.48	0.87179	15	5.0081
2534	0.04	0.68	0.48	0.87179	25	3.0515
2535	0.04	0.68	0.48	0.87179	35	2.2208
2536	0.04	0.68	0.48	0.87179	50	1.6026
2537	0.04	0.68	0.48	0.87179	75	1.1222
2538	0.04	0.68	0.48	0.87179	100	0.87816
2539	0.04	0.68	0.48	0.87179	150	0.62453
2540	0.04	0.68	0.48	0.87179	200	0.49037
2541	0.04	0.68	0.48	0.87179	300	0.34813
2542	0.04	0.68	0.48	0.87179	400	0.273
2543	0.04	1.0	0.12	0.72115	1	884.5
2544	0.04	1.0	0.12	0.72115	10	88.266
2545	0.04	1.0	0.12	0.72115	15	58.985
2546	0.04	1.0	0.12	0.72115	25	35.464
2547	0.04	1.0	0.12	0.72115	35	25.379
2548	0.04	1.0	0.12	0.72115	50	17.826
2549	0.04	1.0	0.12	0.72115	75	11.974
2550	0.04	1.0	0.12	0.72115	100	9.0711
2551	0.04	1.0	0.12	0.72115	150	6.192
2552	0.04	1.0	0.12	0.72115	200	4.7646
2553	0.04	1.0	0.12	0.72115	300	3.3592
2554	0.04	1.0	0.12	0.72115	400	2.6613
2555	0.04	1.0	0.12	0.72115	600	1.966
2556	0.04	1.0	0.16	0.76923	1	477.5
2557	0.04	1.0	0.16	0.76923	10	47.705
2558	0.04	1.0	0.16	0.76923	15	31.857
2559	0.04	1.0	0.16	0.76923	25	19.158
2560	0.04	1.0	0.16	0.76923	35	13.72

	<i>t/l</i>	<i>h/l</i>	<i>s/l</i>	ϵ	<i>Re_l</i>	<i>f_{unit}</i>
2561	0.04	1.0	0.16	0.76923	50	9.6518
2562	0.04	1.0	0.16	0.76923	75	6.5033
2563	0.04	1.0	0.16	0.76923	100	4.9404
2564	0.04	1.0	0.16	0.76923	150	3.3913
2565	0.04	1.0	0.16	0.76923	200	2.6236
2566	0.04	1.0	0.16	0.76923	300	1.8613
2567	0.04	1.0	0.16	0.76923	400	1.4786
2568	0.04	1.0	0.16	0.76923	600	1.0944
2569						

	t/l	h/l	s/l	ϵ	Re_l	f_{unit}
2641	0.04	1.0	0.48	0.88757	100	0.74381
2642	0.04	1.0	0.48	0.88757	150	0.53166
2643	0.04	1.0	0.48	0.88757	200	0.41886
2644	0.04	1.0	0.48	0.88757	300	0.2984
2645	0.04	1.0	0.48	0.88757	400	0.23533
2646	0.06	0.12	0.12	0.44444	1	3792
2647	0.06	0.12	0.12	0.44444	10	385.36
2648	0.06	0.12	0.12	0.44444	15	253.94
2649	0.06	0.12	0.12	0.44444	25	153.48
2650	0.06	0.12	0.12	0.44444	35	110.71
2651	0.06	0.12	0.12	0.44444	50	78.909
2652	0.06	0.12	0.12	0.44444	75	54.496
2653	0.06	0.12	0.12	0.44444	100	42.972
2654	0.06	0.12	0.12	0.44444	150	30.656
2655	0.06	0.12	0.12	0.44444	200	24.97
2656	0.06	0.12	0.12	0.44444	300	19.281
2657	0.06	0.12	0.12	0.44444	400	16.572
2658	0.06	0.12	0.12	0.44444	600	13.987
2659	0.06	0.12	0.16	0.48485	600	7.2389
2660	0.06	0.12	0.24	0.53333	1	1469.8
2661	0.06	0.12	0.24	0.53333	10	147.24
2662	0.06	0.12	0.24	0.53333	15	98.374
2663	0.06	0.12	0.24	0.53333	25	59.373
2664	0.06	0.12	0.24	0.53333	35	42.725
2665	0.06	0.12	0.24	0.53333	50	30.295
2666	0.06	0.12	0.24	0.53333	75	20.677
2667	0.06	0.12	0.24	0.53333	100	15.886
2668	0.06	0.12	0.24	0.53333	150	11.105
2669	0.06	0.12	0.24	0.53333	200	8.7194
2670	0.06	0.12	0.24	0.53333	300	6.3535
2671	0.06	0.12	0.24	0.53333	400	5.1854
2672	0.06	0.12	0.24	0.53333	600	3.9926
2673	0.06	0.12	0.48	0.59259	1	1001.1
2674	0.06	0.12	0.48	0.59259	10	100.65
2675	0.06	0.12	0.48	0.59259	15	67.184
2676	0.06	0.12	0.48	0.59259	25	40.451
2677	0.06	0.12	0.48	0.59259	35	29.02
2678	0.06	0.12	0.48	0.59259	50	20.377
2679	0.06	0.12	0.48	0.59259	75	13.825
2680	0.06	0.12	0.48	0.59259	100	10.507
2681	0.06	0.12	0.48	0.59259	150	7.1765
2682	0.06	0.12	0.48	0.59259	200	5.5187
2683	0.06	0.12	0.48	0.59259	300	3.8496
2684	0.06	0.12	0.48	0.59259	400	3.0115
2685	0.06	0.12	0.48	0.59259	600	2.1501
2686	0.06	0.16	0.12	0.48485	600	9.7097
2687	0.06	0.2	0.12	0.51282	600	7.6919
2688	0.06	0.24	0.12	0.53333	1	1972
2689	0.06	0.24	0.12	0.53333	10	211.02
2690	0.06	0.24	0.12	0.53333	15	140.89
2691	0.06	0.24	0.12	0.53333	25	84.913
2692	0.06	0.24	0.12	0.53333	35	61.028
2693	0.06	0.24	0.12	0.53333	50	43.226
2694	0.06	0.24	0.12	0.53333	75	29.527
2695	0.06	0.24	0.12	0.53333	100	22.775
2696	0.06	0.24	0.12	0.53333	150	16.143
2697	0.06	0.24	0.12	0.53333	200	12.895
2698	0.06	0.24	0.12	0.53333	300	9.7049
2699	0.06	0.24	0.12	0.53333	400	8.1488
2700	0.06	0.24	0.12	0.53333	600	6.6691
2701	0.06	0.24	0.24	0.64	1	544.57
2702	0.06	0.24	0.24	0.64	10	54.561
2703	0.06	0.24	0.24	0.64	15	36.709
2704	0.06	0.24	0.24	0.64	25	22.17
2705	0.06	0.24	0.24	0.64	35	15.967
2706	0.06	0.24	0.24	0.64	50	11.339
2707	0.06	0.24	0.24	0.64	75	7.7627
2708	0.06	0.24	0.24	0.64	100	5.9854
2709	0.06	0.24	0.24	0.64	150	4.2147
2710	0.06	0.24	0.24	0.64	200	3.3297
2711	0.06	0.24	0.24	0.64	300	2.4721
2712	0.06	0.24	0.24	0.64	400	2.0351
2713	0.06	0.24	0.24	0.64	600	1.6062
2714	0.06	0.24	0.48	0.71111	1	263.06
2715	0.06	0.24	0.48	0.71111	10	26.455
2716	0.06	0.24	0.48	0.71111	15	17.69
2717	0.06	0.24	0.48	0.71111	25	10.701
2718	0.06	0.24	0.48	0.71111	35	7.7186
2719	0.06	0.24	0.48	0.71111	50	5.4889
2720	0.06	0.24	0.48	0.71111	75	3.7569

	t/l	h/l	s/l	ϵ	Re_l	f_{unit}
2721	0.06	0.24	0.48	0.71111	100	2.8882
2722	0.06	0.24	0.48	0.71111	150	2.0121
2723	0.06	0.24	0.48	0.71111	200	1.5677
2724	0.06	0.24	0.48	0.71111	300	1.114
2725	0.06	0.24	0.48	0.71111	400	0.87983
2726	0.06	0.24	0.48	0.71111	600	0.63787
2727	0.06	0.48	0.12	0.59259	1	1492.5
2728	0.06	0.48	0.12	0.59259	10	160.53
2729	0.06	0.48	0.12	0.59259	15	107.14
2730	0.06	0.48	0.12	0.59259	25	64.492
2731	0.06	0.48	0.12	0.59259	35	46.276
2732	0.06	0.48	0.12	0.59259	50	32.682
2733	0.06	0.48	0.12	0.59259	75	22.203
2734	0.06	0.48	0.12	0.59259	100	17.029
2735	0.06	0.48	0.12	0.59259	150	11.941
2736	0.06	0.48	0.12	0.59259	200	9.4502
2737	0.06	0.48	0.12	0.59259	300	7.0072
2738	0.06	0.48	0.12	0.59259	400	5.8072
2739	0.06	0.48	0.12	0.59259	600	4.6323
2740	0.06	0.48	0.24	0.71111	1	325.79
2741	0.06	0.48	0.24	0.71111	10	33.113
2742	0.06	0.48	0.24	0.71111	15	22.131
2743	0.06	0.48	0.24	0.71111	25	13.364
2744	0.06	0.48	0.24	0.71111	35	9.6233
2745	0.06	0.48	0.24	0.71111	50	6.836
2746	0.06	0.48	0.24	0.71111	75	4.688
2747	0.06	0.48	0.24	0.71111	100	3.624
2748	0.06	0.48	0.24	0.71111	150	2.5665
2749	0.06	0.48	0.24	0.71111	200	2.0377
2750	0.06	0.48	0.24	0.71111	300	1.5028
2751	0.06	0.48	0.24	0.71111	400	1.2286
2752	0.06	0.48	0.24	0.71111	600	0.94486
2753	0.06	0.48	0.48	0.79012	1	110.26
2754	0.06	0.48	0.48	0.79012	10	11.138
2755	0.06	0.48	0.48	0.79012	15	7.468
2756	0.06	0.48	0.48	0.79012	25	4.5498
2757	0.06	0.48	0.48	0.79012	35	3.3101
2758	0.06	0.48	0.48	0.79012	50	2.3867
2759	0.06	0.48	0.48	0.79012	75	1.6689
2760	0.06	0.48	0.48	0.79012	100	1.3047
2761	0.06	0.48	0.48	0.79012	150	0.92762
2762	0.06	0.48	0.48	0.79012	200	0.72952
2763	0.06	0.48	0.48	0.79012	300	0.52108
2764	0.06	0.48	0.48	0.79012	400	0.41175
2765	0.06	0.48	0.48	0.79012	600	0.29545

REFERENCES

- ¹S. Kandlikar, S. Garimella, D. Li, S. Colin, and M. R. King, *Heat transfer and fluid flow in minichannels and microchannels* (elsevier, 2005).
- ²W. A. Khan, J. Culham, and M. Yovanovich, “The role of fin geometry in heat sink performance,” *Journal of Electronic Packaging* **128**, 324–330 (2006).
- ³T. İzci, M. Koz, and A. Koşar, “The effect of micro pin-fin shape on thermal and hydraulic performance of micro pin-fin heat sinks,” *Heat Transfer Engineering* **36**, 1447–1457 (2015).
- ⁴D. Yang, Z. Jin, Y. Wang, G. Ding, and G. Wang, “Heat removal capacity of laminar coolant flow in a micro channel heat sink with different pin fins,” *International Journal of Heat and Mass Transfer* **113**, 366–372 (2017).
- ⁵A. V. Bapat and S. G. Kandlikar, “Thermohydraulic performance analysis of offset strip fin microchannel heat exchangers,” in *International Conference on Nanochannels, Microchannels, and Minichannels*, Vol. 47608 (ASME, 2006) pp. 347–353.
- ⁶C.-Y. Yang, C.-T. Yeh, W.-C. Liu, and B.-C. Yang, “Advanced micro-heat exchangers for high heat flux,” *Heat transfer engineering* **28**, 788–794 (2007).
- ⁷F. Hong and P. Cheng, “Three dimensional numerical analyses and optimization of offset strip-fin microchannel heat sinks,” *International Communications in Heat and Mass Transfer* **36**, 651–656 (2009).
- ⁸K. H. Do, B.-I. Choi, Y.-S. Han, and T. Kim, “Experimental investigation on the pressure drop and heat transfer characteristics of a recuperator with offset strip fins for a micro gas turbine,” *International Journal of Heat and Mass Transfer* **103**, 457–467 (2016).
- ⁹T. Nagasaki, R. Tokue, S. Kashima, and Y. Ito, “Conceptual design of recuperator for ultramicro gas turbine,” in *Proceedings of the International Gas Turbine Congress* (Citeseer, 2003) pp. 2–7.
- ¹⁰Y. Yang, Y. Li, B. Si, and J. Zheng, “Heat transfer performances of cryogenic fluids in offset strip fin-channels considering the effect of fin efficiency,” *International Journal of Heat and Mass Transfer* **114**, 1114–1125 (2017).
- ¹¹Q. Jiang, M. Zhuang, Z. Zhu, and J. Shen, “Thermal hydraulic characteristics of cryogenic offset-strip fin heat exchangers,” *Applied Thermal Engineering* **150**, 88–98 (2019).
- ¹²M. Yang, X. Yang, X. Li, Z. Wang, and P. Wang, “Design and optimization of a solar air heater with offset strip fin absorber plate,” *Applied Energy* **113**, 1349–1362 (2014).
- ¹³K. Pottler, C. M. Sippel, A. Beck, and J. Fricke, “Optimized finned absorber geometries for

- solar air heating collectors,” *Solar Energy* **67**, 35–52 (1999).
- ¹⁴D. B. Tuckerman and R. F. W. Pease, “High-performance heat sinking for vlsi,” *IEEE Electron device letters* **2**, 126–129 (1981).
- ¹⁵A. Bartolini, M. Cacciari, A. Tilli, and L. Benini, “Thermal and energy management of high-performance multicores: Distributed and self-calibrating model-predictive controller,” *IEEE Transactions on Parallel and Distributed Systems* **24**, 170–183 (2012).
- ¹⁶M. Zargartalebi, A. M. Benneker, and J. Azaiez, “The impact of heterogeneous pin based microstructures on flow dynamics and heat transfer in micro-scale heat exchangers,” *Physics of Fluids* **32**, 052007 (2020).
- ¹⁷D. S. Gluzdov and E. Y. Gatapova, “Friction reduction by inlet temperature variation in microchannel flow,” *Physics of Fluids* **33**, 062003 (2021).
- ¹⁸H. M. Joshi and R. L. Webb, “Heat transfer and friction in the offset stripfin heat exchanger,” *International Journal of Heat and Mass Transfer* **30**, 69–84 (1987).
- ¹⁹S. Mochizuki, Y. Yagi, and W.-J. Yang, “Flow pattern and turbulence intensity in stacks of interrupted parallel-plate surfaces,” *Experimental Thermal and Fluid Science* **1**, 51–57 (1988).
- ²⁰N. DeJong and A. Jacobi, “An experimental study of flow and heat transfer in parallel-plate arrays: local, row-by-row and surface average behavior,” *International Journal of Heat and Mass Transfer* **40**, 1365–1378 (1997).
- ²¹A. Renfer, M. K. Tiwari, T. Brunswiler, B. Michel, and D. Poulikakos, “Experimental investigation into vortex structure and pressure drop across microcavities in 3d integrated electronics,” *Experiments in fluids* **51**, 731–741 (2011).
- ²²F. Xu, Z. Pan, and H. Wu, “Experimental investigation on the flow transition in different pin-fin arranged microchannels,” *Microfluidics and Nanofluidics* **22**, 11 (2018).
- ²³R. M. Manglik and A. E. Bergles, “Heat transfer and pressure drop correlations for the rectangular offset strip fin compact heat exchanger,” *Experimental Thermal and Fluid Science* **10**, 171–180 (1995).
- ²⁴J. Dong, J. Chen, Z. Chen, and Y. Zhou, “Air-side thermal hydraulic performance of offset strip fin aluminum heat exchangers,” *Applied Thermal Engineering* **27**, 306–313 (2007).
- ²⁵M.-S. Kim, J. Lee, S.-J. Yook, and K.-S. Lee, “Correlations and optimization of a heat exchanger with offset-strip fins,” *International Journal of Heat and Mass Transfer* **54**, 2073–2079 (2011).
- ²⁶W. M. Kays and A. L. London, *Compact heat exchangers* (McGraw-Hill, New York, NY, 1984).
- ²⁷S. Manson, “Correlations of heat transfer data and of friction data for interrupted plate fins

- staggered in successive rows, naca tech,” Tech. Rep. (Note 2237, National Advisory Committee for Aeronautics, Washington, DC, 1950).
- ²⁸A. R. Wieting, “Empirical correlations for heat transfer and flow friction characteristics of rectangular offset-fin plate-fin heat exchangers,” *Journal of Heat Transfer* **79**, 488–490 (1975).
- ²⁹L. Guo, F. Qin, J. Chen, and Z. Chen, “Lubricant side thermal–hydraulic characteristics of steel offset strip fins with different flow angles,” *Applied thermal engineering* **28**, 907–914 (2008).
- ³⁰S. D. Jadhav, L. R. Goossens, Y. Kinds, B. Van Hooreweder, and K. Vanmeensel, “Laser-based powder bed fusion additive manufacturing of pure copper,” *Additive Manufacturing* **42**, 101990 (2021).
- ³¹F. Walters, “Hypersonic research engine project-phase iia, category i test report on fin heat transfer and pressure drop testing, data item no. 63.02, airesearch manufacturing co. doc,” AiResearch Manufacturing Co., Torrance, CA, USA, Doc. AP-69-5348 (1969).
- ³²R. K. Shah and A. L. London, “Offset rectangular plate-fin surfaces–heat transfer and flow friction characteristics.” Tech. Rep. 66 (Stanford University, California, Department of Mechanical Engineering, 1967).
- ³³Y. S. Muzychka and M. M. Yovanovich, “Modeling the f and j characteristics for transverse flow through an offset strip fin at low reynolds number,” *Journal of enhanced heat transfer* **8** (2001).
- ³⁴X. Zhang, Y. Wang, Z. Yu, and D. Zhao, “Numerical analysis of thermal-hydraulic characteristics on serrated fins with different attack angles and wavelength to fin length ratio,” *Applied Thermal Engineering* **91**, 126–137 (2015).
- ³⁵P.-S. Lee, S. V. Garimella, and D. Liu, “Investigation of heat transfer in rectangular microchannels,” *International journal of heat and mass transfer* **48**, 1688–1704 (2005).
- ³⁶S. Patankar, C. Liu, and E. Sparrow, “Fully developed flow and heat transfer in ducts having streamwise-periodic variations of cross-sectional area,” *Journal of Heat Transfer—Transactions of the ASME* **99**, 180–186 (1977).
- ³⁷G. Buckinx and M. Baelmans, “Multi-scale modelling of flow in periodic solid structures through spatial averaging,” *Journal of Computational Physics* **291**, 34–51 (2015).
- ³⁸M. S. Alnæs, J. Blechta, J. Hake, A. Johansson, B. Kehlet, A. Logg, C. Richardson, J. Ring, M. E. Rognes, and G. N. Wells, “The fenics project version 1.5,” *Archive of Numerical Software* **3** (2015), 10.11588/ans.2015.100.20553.
- ³⁹M. Mortensen and K. Valen-Sendstad, “Oasis: A high-level/high-performance open source navier–stokes solver,” *Computer physics communications* **188**, 177–188 (2015).

- ⁴⁰L. F. Richardson, “Ix. the approximate arithmetical solution by finite differences of physical problems involving differential equations, with an application to the stresses in a masonry dam,” *Philosophical Transactions of the Royal Society of London. Series A, Containing Papers of a Mathematical or Physical Character* **210**, 307–357 (1911).
- ⁴¹P. J. Roache, “Perspective: a method for uniform reporting of grid refinement studies,” (1994).
- ⁴²P. Forchheimer, “Wasserbewegung durch boden,” *Z. Ver. Deutsch, Ing.* **45**, 1782–1788 (1901).
- ⁴³S. Ergun, “Fluid flow through packed columns,” *Chem. Eng. Prog.* **48**, 89–94 (1952).
- ⁴⁴C. K. Ghaddar, “On the permeability of unidirectional fibrous media: a parallel computational approach,” *Physics of Fluids* **7**, 2563–2586 (1995).
- ⁴⁵B. Markicevic and T. Papathanasiou, “On the apparent permeability of regular arrays of nonuniform fibers,” *Physics of Fluids* **14**, 3347–3349 (2002).
- ⁴⁶Y. Matsumura and T. Jackson, “Numerical simulation of fluid flow through random packs of cylinders using immersed boundary method,” *Physics of Fluids* **26**, 043602 (2014).
- ⁴⁷D. L. Koch and A. J. Ladd, “Moderate reynolds number flows through periodic and random arrays of aligned cylinders,” *Journal of Fluid Mechanics* **349**, 31–66 (1997).
- ⁴⁸D. Lasseux, A. A. Abbasian Arani, and A. Ahmadi, “On the stationary macroscopic inertial effects for one phase flow in ordered and disordered porous media,” *Physics of fluids* **23**, 073103 (2011).
- ⁴⁹S. P. Suter and R. Skalak, “The history of poiseuille’s law,” *Annual review of fluid mechanics* **25**, 1–20 (1993).
- ⁵⁰C. Mei and J.-L. Auriault, “The effect of weak inertia on flow through a porous medium,” *Journal of Fluid Mechanics* **222**, 647–663 (1991).
- ⁵¹H. P. Amaral Souto and C. Moyne, “Dispersion in two-dimensional periodic porous media. part i. hydrodynamics,” *Physics of Fluids* **9**, 2243–2252 (1997).
- ⁵²R. J. Hill and D. L. Koch, “Moderate-reynolds-number flow in a wall-bounded porous medium,” *Journal of Fluid Mechanics* **453**, 315 (2002).
- ⁵³P. Virtanen, R. Gommers, T. E. Oliphant, M. Haberland, T. Reddy, D. Cournapeau, E. Burovski, P. Peterson, W. Weckesser, J. Bright, S. J. van der Walt, M. Brett, J. Wilson, K. J. Millman, N. Mayorov, A. R. J. Nelson, E. Jones, R. Kern, E. Larson, C. J. Carey, Í. Polat, Y. Feng, E. W. Moore, J. VanderPlas, D. Laxalde, J. Perktold, R. Cimrman, I. Henriksen, E. A. Quintero, C. R. Harris, A. M. Archibald, A. H. Ribeiro, F. Pedregosa, P. van Mulbregt, and SciPy 1.0 Contributors, “SciPy 1.0: Fundamental Algorithms for Scientific Computing in Python,”

Nature Methods **17**, 261–272 (2020).

⁵⁴R. De Wolf, R. Coosemans, W. Dekeyser, and M. Baelmans, “Bayesian approach to parameter estimation and model validation for nuclear fusion reactor mean-field edge turbulence modelling,” Nuclear Fusion (2021).